Draft version February 10, 2009
Preprint typeset using LaTeX style emulateapj v. 26/01/00

H I SPECTRA AND COLUMN DENSITIES TOWARD HVC AND IVC PROBES

B.P. Wakker
Department of Astronomy, University of Wisconsin
475 N Charter St, Madison, WI 53706, USA
wakker@astro.wisc.edu
P.M.W. Kalberla
Radio-astronomisches Institut Universität Bonn
D-53121 Bonn, Germany
kalberla@astro.uni-bonn.de
H. van Woerden
Rijks Universiteit Groningen
Postbus 800, 9700 AV, Groningen, The Netherlands
hugo@astro.rug.nl
K.S. de Boer
Sternwarte Universität Bonn
D-53121 Bonn, Germany
deboer@astro.uni-bonn.de
M.E. Putman
Research School of Astronomy & Astrophysics, Australian National University
Weston Creek P.O., Weston, ACT 2611 Australia
mary.putman@atnf.csiro.au

Draft version February 10, 2009

ABSTRACT

We show 21-cm line profiles in the direction of stars and extragalactic objects, lying projected on high- and intermediate-velocity clouds (HVCs and IVCs). About half of these are from new data obtained with the Effelsberg 100-m telescope, about a quarter are extracted from the Leiden-Dwingeloo Survey (LDS) and the remaining quarter were observed with other single-dish telescopes. H I column densities were determined for each HVC/IVC. Wakker (2001) (Paper I) uses these in combination with optical and ultraviolet high-resolution measurements to derive abundances. Here, an analysis is given of the difference and ratio of N(H I) as observed with a $9'$ versus a $35'$ beam. For HVCs and IVCs the ratio N(H I-$9'$)/N(H I-$35'$) lies in the range 0.2−2.5. For low-velocity gas this ratio ranges from 0.75 to 1.3 (the observed ratio is 0.85−1.4, but it appears that the correction for stray radiation is slightly off). The smaller range for the low-velocity gas may be caused by confusion in the line of sight, so that a low ratio in one component can be compensated by a high ratio in another − for 11 low-velocity clouds fit by one component the distribution of ratios has a larger dispersion. Comparison with higher angular resolution data is possible for sixteen sightlines. Eight sightlines with H I data at $1'-2'$ resolution show a range of 0.75−1.25 for N(H I-$2'$)/N(H I-$9'$), while in eight other sightlines N(H I-Lyα)/N(H I-$9'$) ranges from 0.74 to 0.98.

Subject headings: ISM: clouds, Galaxy: halo, radio lines: ISM,

1. INTRODUCTION

A description of progress in understanding distances and metallicities of high- and intermediate-velocity neutral hydrogen (HVCs and IVCs) is given by Wakker (2001), who lists all published data concerning ionic absorption lines in such clouds. This paper is referred to below as "Paper I". The present paper offers a (re)analysis of 21-cm H I data that were used to derive ion/H I ratios. The H I data are important for two reasons: a) if absorption lines due to the HVC or IVC are present, they allow one to derive an ion abundance for the cloud and b) if such absorption is absent, the H I data are required to derive the expected optical line strength, in order to interpret the absence of absorption as a lower distance limit or showing the need for deeper integrations. This is explained more fully in Paper I (see description of Col. 18 in that paper).

Previous experience has suggested that a measurement with the smallest possible beam is required. A few HVC cores have been observed at high angular resolution (2 arcmin or better; Schwarz & Oort 1981, Wakker & Schwarz 1991, Wakker et al. 1996, Braun & Burton 2000). From these studies it is clear that these cores contain much fine structure, with column density contrasts up to a factor 5 at arcminute scales. Outside cores, however, the contrast seems to be less (Wakker et al. 1996, Schwarz & Wakker 2001). Also, the factor 5 represents the extreme contrast. For any randomly chosen direction within a field, the contrast is closer to a factor 2 over arcminute scales.

It is not known whether similar contrast would occur if observations with even smaller beams could be made. A possible way of studying this is to compare N(H I) as observed at 21-cm with N(H I) derived from Lyα absorption toward extra-galactic background sources. A preliminary analysis of this kind by Savage et al. (2000) suggests that N(H I-Lyα) usually lies in the range 0.6−1 times N(H I-21-cm). However, with this method it is not possible to separately measure N(H I) for different components. For further discussion see Sect. 6.

Interferometer maps (1−2 arcmin beam) clearly are necessary to get accurate abundances for important background probes, but it is impractical to observe every probe that way. The next-best estimate requires a large single-dish telescope. For probes with declinations between about 0 and +38 degrees, Arecibo (3 arcmin beam) is preferable, though data are rarely available. We used the 100-m Effelsberg telescope (9 arcmin beam) for probes with declinations above about −30 degrees. In the future the 100-m GBT (Green Bank Telescope) may also prove useful.

Effelsberg data were obtained for about half of the 269 probes listed in Paper I (excluding the 52 stars in the LMC). For about a quarter of these probes, other good single-dish data exist, obtained with the telescopes at Arecibo (3 arcmin beam), Jodrell Bank (12 arcmin beam), Parkes (15 arcmin beam), Green Bank (21 arcmin beam) and Hat Creek (36 arcmin beam, but 0.0015 K rms). For the remaining quarter we needed to use the Leiden-Dwingeloo Survey (LDS) of Hartmann & Burton (1997), which has a 35 arcmin beam. The Effelsberg data allow us for the first time to systematically analyze the difference of N(H I) observed with a $9'$ beam vs a $35'$ beam, as LDS data are available for every direction north of declination $-35°$.

Section 2 gives a description of the Effelsberg observations, which have not been presented elsewhere. Section 3 summarizes the characteristics of the other data. Section 4 describes the procedure used to derive N(H I) for the HVC and IVC components, and Sect. 5 describes the spectra shown in Fig. 1. That figure presents an H I spectrum for each of the probes for which absorption line measurements are listed in Paper I. Finally, in Sect. 6 we make a preliminary analysis of the difference between N(H I) as observed at Effelsberg vs N(H I) in the same direction as extracted from the LDS.

2. EFFELSBERG OBSERVATIONS

2.1. *Summary of runs*

Observations were done on 19 dates: 12 Jan 1995, 24 Jan 1995, 26 Aug 1995, 10 Sep 1995, 11−12 Aug 1996, 13−14 Sep 1996, 27 Jun 1999, 12−14 Jul 1999, 3 Mar 2000, 25−26 Mar 2000, 3−4 Apr 2000, 3−4 May 2000. The large gap between 1996 and 1999 is caused by a problem with interference that is most probably due to Digital Audio Broadcasting (DAB).

The DAB transmission at a frequency near 1452 MHz was variable in intensity and strongly polarized. The nearest transmitter at a distance of 30 km caused interference which was received through the backlobes of the telescope, even under the most favorable circumstances. This interference caused spurious lines and partly a saturation of the receiver, resulting in strongly variable baseline ripples which made a proper data reduction for weak lines impossible. Fortunately, DAB turned out to be of little commercial interest, and it was switched off. Further interference was found to be caused by local equipment (workstations and active components). Most of the interference from such components was removed either by shielding or switching off the devices.

Data taken before Sep 1996 generally are of good quality, with baselines that were relatively easy to determine and not affected by interference. The Sep 1996 data vary in quality, as during some times of the day interference popped up. Many spectra were unusable because of interference spikes at frequencies of interest or because interference caused bad baselines. About 50% of the June/July 1999 data are generally usable, though some caution is needed. Baselines may show strong curvature, and S-shaped interference spikes can be seen in many spectra (see e.g. those of BD+10 2179, HD 83206, Mrk 279, PG 0804+761 and PKS 0837−12). In contrast with earlier runs, the spectra from the two receivers (one for each polarization) were separately reduced, as in about 20% of the cases only one of the two was corrupted. Spectra taken in 2000 tend to show less interference and are of slightly higher quality than the 1999 set. However, again only about 50% are usable.

In the 1995 and 1996 runs, a total of 469 spectra were taken, toward 173 different probes. Directions were selected in three ways. For about 40 probes high-resolution absorption line data already existed. For about 130 probes high-resolution absorption line data were anticipated or hoped for (about 50 of these have now indeed been observed). The corresponding H I data will be published together with the absorption-line data. Finally, for 12 probes

high-angular resolution (1−2 arcmin) Westerbork data existed, and a 3×3 grid of positions was observed.

During the 1999 and 2000 runs 247 spectra were taken of 105 different probes. All of these were selected because high-resolution absorption line data existed (see Paper I). For this set the results for each polarization were separately reduced, effectively leading to 494 spectra. Further, integration times for individual spectra were limited to 5 minutes, even if the total on the target could be up to 30 minutes. Each of these spectra was judged individually, and if interference clearly posed a problem the spectrum was eliminated. The remaining spectra were averaged (a few times also adding in a spectrum with shorter integration time from 1995 or 1996) to form the final spectrum toward a target.

Because of some overlap between the two sets of runs (for targets where the earlier spectra were not good or deep enough), a total of 249 probes has been observed. Of these, 91 have high-resolution absorption data. The H I column densities for these are included in the table in Paper I − the spectra are shown here.

2.2. *Data reduction and calibration*

The data processing has been performed using the standard reduction programs of the Max-Planck-Institut für Radioastronomie and the Radioastronomical Institute of the University Bonn. The antenna temperature of the observed spectra has been calibrated against IAU standard position S7 (Kalberla et al. 1982). Afterwards the stray radiation from the sidelobes of the antenna diagram was removed (Kalberla et al. 1980).

The instrumental baseline was removed after fitting a third order polynomial to those channels which were free of line emission. A number of observations were seriously affected by baseline ripples and a polynomial of order 5 to 7 had to be used. This was the case for e.g. the spectra of HD 12323, HD 12993 and PG 1519+640, where a residual ripple can be seen. In cases such as these, the brightness temperatures for the low-velocity gas are unreliable, but the baseline under the HVC is still acceptable for determining N(H I) to within ∼25%. If this is the case and if the star is not critical for determining a lower distance limit to a cloud, the spectrum is still included in the sample.

The spectra were taken with two HEMT receivers for two independent branches with different circular polarization. The data processing was independent for both channels. After the reduction we intercompared and averaged both spectra. Interference and instrumental problems usually resulted in discrepant spectra. Such data have been rejected except for those cases in which obviously only a single channel was affected.

The final rms noise varies with the integration time and also somewhat between runs. A typical value is 0.055 K in 10 minutes for the 1995/1996 data. For the 1999/2000 data interference and baseline problems cause the measured noise to vary by a factor up to 1.5 for a given integration time, although the average value still is typically 0.055 K in 10 minutes.

3. OTHER OBSERVATIONS

3.1. *Overview*

For slightly over half of the probes in Paper I, N(H I) is based on data from a telescope other than Effelsberg. This can be for one of four reasons. a) Higher-angular resolution data are available (23 probes; sometimes these were combined with the Effelsberg spectrum). b) Higher-quality (i.e. higher signal-to-noise ratio or less interference) single-dish spectra are available (44 probes). c) The probe is in the southern sky (14 probes). d) No directed single-dish data are available (67 probes). In the latter case the data in the Leiden-Dwingeloo Survey (LDS, Hartmann & Burton 1997) were used. This gives spectra at each half-degree point in longitude and latitude. A weighted average was constructed from the four spectra surrounding the target direction, with weights $\max(0,0.5-\sqrt{\Delta l^2+\Delta b^2})$ (with Δl and Δb in degrees).

Special cases are posed by 31 targets for which Effelsberg data were used to derive N(H I), even though Fig. 1 does not show the Effelsberg spectrum in the direction of the probe. First, for the 22 stars in M 15 for which absorption-line data exist, the final value of N(H I) is based on an interpolation between nine Effelsberg spectra that are positioned on a 3×3 grid with $5'$ spacing. Only the central position is shown in Fig. 1. Second, for 9 probes the published value is based on an Effelsberg spectrum, but the original data were lost. This pertains to 3 probes of complex A observed by Lilienthal et al. (1990), and to 6 probes of complexes C, H and K observed by Centurión et al. (1994). For these targets, Fig. 1 shows a spectrum based on the Leiden-Dwingeloo Survey (see below), but the best final value of N(H I) is based on the published spectrum.

There are also a number of cases where a probe was observed at Arecibo or with an interferometer as well as at Effelsberg, but we do not have the high-angular resolution spectrum available in digital form. Then the Effelsberg spectrum is shown in Fig. 1, but the label contains, e.g., "Use Arecibo" as a warning that the column density used in Paper I was derived from the better data.

A final special case is presented by SN 1993 J. Two spectra are shown in Fig. 1. First, the actual spectrum from de Boer et al. (1993), which includes emission from M 81 between velocities of −250 and +150 km s^{-1}. Second, a spectrum in which M 81 was removed by means of a third-order polynomial fit.

3.2. *Spectra with angular resolution $<9'$*

For 9 probes the Effelsberg spectrum is complemented by data taken with the Westerbork Synthesis Radio Telescope (WSRT): 0159+625 from Wakker & Schwarz (1991), PG 0832+675 from Schwarz et al. (1995), Mrk 106, PG 0859+593, PG 0906+597 from Wakker et al. (1996), HD 135485 and 4 Lac from Stoppelenburg et al. (1998), Mrk 290 from Wakker et al. (1999) and Mrk 205 from Braun & Burton (2000). In this case Fig. 1 shows the Effelsberg spectrum, but Paper I uses the value of N(H I) derived from the combination of WSRT and Effelsberg data, as indicated in the label (see e.g. the plot for 0159+625).

For two probes (NGC 3783 and HD 101274) Paper I gives N(H I) from a combination of data from the Australia Telescope Compact Array (*ATCA*) and the Parkes telescope (Wakker et al. 2001). Fig. 1 shows the Parkes spectrum.

For the 10 stars that have been observed in M 13 (Shaw et al. 1996), Paper I gives N(H I) based on a combination of data from Jodrell Bank (12′ beam) and the Dominion Radio Astronomy Observatory (*DRAO*, 1′ beam). Fig. 1 shows a spectrum based on the Leiden-Dwingeloo Survey.

Payne et al. (1978, 1980) and Colgan et al. (1990) used Arecibo (3′ beam) to derive values for N(H I) in the direction of seventeen 21-cm radio continuum sources, in whose spectrum they searched for H I absorption. Arecibo was also used by Tamanaha (1996) to derive N(H I) toward the probes in core AC0. For these targets, Fig. 1 shows the LDS spectrum, but the Arecibo value for N(H I) is used in Paper I, as indicated in the label (see e.g. 3C 78).

3.3. *Higher-quality single-dish spectra*

High-quality spectra for a number of probes of complex A, M and the IV-arch were obtained by Ryans et al. (1997a, 1997b) using the Jodrell Bank telescope (12′ beam). For most of these an Effelsberg spectrum was also obtained, except for PG 1213+456 and H.O.+41B. Further, for BD+38 2182, HD 93521, HD 203664 and HD 205556 the Effelsberg data are of much lesser quality than the Jodrell Bank spectrum. For the latter two, Fig. 1 shows the Effelsberg spectrum, but for the other four probes, Fig. 1 shows the Jodrell Bank spectrum, courtesy of R. Ryans. For all six targets the value of N(H I) derived from the Jodrell Bank spectrum is used in Paper I.

In 1992, at our request, C. Heiles used the Hat Creek telescope (36′ beam) to make an especially deep observation (24 hours integration time) of the direction toward SN 1991 T. In this direction Meyer & Roth (1991) had detected weak Ca II absorption at velocities of +215 and $+263\,\mathrm{km\,s^{-1}}$. Even though the Hat Creek H I spectrum has a detection limit of $3\times10^{17}\,\mathrm{cm^{-2}}$, no emission is seen at these velocities. Fig. 1 shows the Hat Creek spectrum.

Green Bank 140-ft data (21′ beam) were used by Danly et al. (1992) and Albert et al. (1993) in their absorption-line studies of IVCs. Paper I includes 16 of their stars, for 10 of which an improved spectrum was obtained using Westerbork, Effelsberg or Jodrell Bank; for 4 stars the LDS spectrum is used instead of the Green Bank data. HD 86248 lies at too low a declination for both northern telescopes, but the Parkes data are not yet properly reduced to improve on the Green Bank spectrum. Further, for the $+73\,\mathrm{km\,s^{-1}}$ component toward HD 100340 and the $-43\,\mathrm{km\,s^{-1}}$ component toward HD 137569, the published column density limit based on the Green Bank spectrum is better than the limit based on the LDS spectrum.

Savage et al. (2000) used previously unpublished data obtained by Murphy with the Green Bank 140-ft telescope in the direction of many AGNs that were also observed using the Faint Object Spectrograph on the Hubble Space Telescope. These spectra are of very high quality and have noise levels of about 0.015 K. For a few probes a high-quality Effelsberg spectrum also exists (3C 351.0, H 1821+643, HS 0624+6907, PKS 1136−13 and PG 1116+215). The first of these samples the edge of an HVC, which is detected in the larger Green Bank beam, but not in the smaller Effelsberg beam. For the other four Savage et al. (2000) do not list the HVC component separately, but only mention that the H I spectrum has a high-velocity tail. Thus, for these five probes the value of (or limit for) N(H I) is derived from the Effelsberg spectrum, while for the remaining AGNs discussed by Savage et al. (2000) Paper I uses the values for N(H I) and velocity derived from the Green Bank spectrum. In Fig. 1 the Effelsberg spectrum is shown for 3 of these, while the LDS spectrum is shown for the 10 others.

3.4. *Southern targets*

Sixteen HVC/IVC probes lie below declination −35°, the limit of the Leiden-Dwingeloo Survey. For two of these an *ATCA* spectrum was obtained (NGC 3783 and HD 101274, see above). For the remaining probes, spectra were extracted from observations made with the 64-m Parkes radio telescope equipped with a 21-cm multibeam receiver (Staveley-Smith 1997). For ten of these, high-velocity resolution data ($0.8\,\mathrm{km\,s^{-1}}$) were available via observations made with the narrow-band multi-feed facility (Haynes et al. 1999; Brüns et al. 2001). The narrow-band system utilizes the central 7 beams of the 13-beam multibeam receiver with two orthogonal polarizations and a bandwidth of 8 MHz. Narrow-band data were unavailable for three of the sources, and the spectra were therefore taken from the HVC-reduced (Putman et al. 2001) "H I Parkes All-Sky Survey" (*HIPASS*; Barnes et al. 2001). The standard *HIPASS* reduction method filters out emission which extends over more than 2° in declination, while the HVC method recovers the emission unless it completely fills an 8° scan. After Hanning smoothing, these data have a velocity resolution of $26\,\mathrm{km\,s^{-1}}$ and this low resolution makes it difficult to discern the weak HVC (and especially IVC) components. At 21-cm the Parkes telescope has a beamwidth of 14′, but the gridding process which combines the individual scans increases the spatial resolution to 15.′5±1′. The spectra were extracted from the gridded data at the pixel closest to the coordinates of the probe.

4. COMPONENT FITTING

To derive column densities for the HVC and IVC components in the spectra, a decomposition into gaussians was made. The fitting procedure requires an estimate of the rms noise and a set of initial estimates. Since the purpose of the fitting is to determine N(H I) and v_{LSR} for the HVCs and IVCs, no great effort was made to obtain perfect fits to the peak near $0\,\mathrm{km\,s^{-1}}$ that is present in all spectra. Still, that component is often fitted quite well, although in a few cases line wings were not fitted. For the HVC and IVC components, however, extra care was always taken. For probes near the Galactic plane (in HVC complex H), the low-velocity gas was not fitted, as the structure is very complex and components can easily be artificial superpositions in the line of sight.

The rms was estimated from a spectral region free from H I emission. Wherever possible the region between -400 and $-200\,\mathrm{km\,s^{-1}}$ ($-250\,\mathrm{km\,s^{-1}}$ when necessary) was used. However, for a substantial fraction (33%) of spectra there is either an HVC component (10% of the 33% lie in the Magellanic Stream) or interference at those velocities, in which case an alternative range is used. See Fig. 1 for the actual selected velocity range for each target.

For about half of the spectra it was possible to make an initial estimate automatically. For the other half, it was necessary to help the fit along by giving a fairly good estimate of the amplitude, velocity and width. Care was taken

to make sure that in general the final fitted components were no broader than about $40\,\mathrm{km\,s^{-1}}$. However, there are a few exceptional cases where the HVC or IVC profile is fitted just as well by a single component as by two components (e.g. for I Zw 18). Larger widths were then allowed.

In 40% of the cases the fit was made piecewise, i.e. two spectral regions were fit separately. This mostly happens when the HVC component is weak. Then the formal fit for the low-velocity component can usually be improved by adding one (or more) components, even if these are not clearly seen by eye. The fitting procedure then tends to ignore the weak HVC component, unless an unrealistic total number of components is used. Sometimes piecewise fits were also needed if the central component has broad wings. Free fitting then tends to create components with unrealistic FWHMs of $80\,\mathrm{km\,s^{-1}}$ or more, which then absorb the HVC/IVC component. By restricting the velocity range of the fit this problem can usually be avoided. This procedure works well in most cases, but a few times some artifacts remain visible in the fit for the low-velocity gas (e.g. for 3C 395, HD 32641, HD 45315 and Mrk 509).

5. RESULTS

Figure 1 shows the spectra and the fits. All probes in Table 2 of Paper I are shown. The order is alphabetical, rather than by cloud, as about a third of the sightlines goes through more than one cloud.

For each target the H I spectrum is shown with two vertical scales. The top scale emphasizes the low-velocity gas, the bottom scale gives the clearest view of the HVC or IVC component. In both cases the gaussian fit is superposed on the actual spectrum. The velocity range used to estimate the rms noise is shown as a horizontal bar in the top spectrum. A label is included too, which gives on the first line the probe name and on the second line the galactic longitude and latitude. The third line gives some information about the observations. For spectra obtained using Effelsberg, the date of observation is given in the format "yymmdd", as is the integration time, in minutes. If the final N(H I) values used in Paper I were obtained from another telescope this is indicated too, by a label such as "Use Arecibo". The fourth label line shows the velocity resolution and rms noise. The velocity resolution is $1.28\,\mathrm{km\,s^{-1}}$ for Effelsberg data, $1.21\,\mathrm{km\,s^{-1}}$ for Jodrell Bank data, $0.82\,\mathrm{km\,s^{-1}}$ for Parkes data and $1.03\,\mathrm{km\,s^{-1}}$ for spectra extracted from the LDS. For all these the label gives "1 km/s". For Parkes *HIPASS* data the velocity resolution is $26\,\mathrm{km\,s^{-1}}$. In a number of cases it was necessary to smooth to 2, 4 or even $8\,\mathrm{km\,s^{-1}}$ to be able to fit a weak HVC component. The lower resolution data are then shown on the plot.

Below the two spectra a list of components is given. This gives for each component the central velocity (in $\mathrm{km\,s^{-1}}$), the amplitude (in K), the FWHM (in $\mathrm{km\,s^{-1}}$) and the derived column density with its error (in units of $10^{18}\,\mathrm{cm^{-2}}$). The final column gives (for HVC and IVC components) the cloud name with which the component is identified, based on the catalogues of Wakker & van Woerden (1991) and Kuntz & Danly (1996) and some new definitions given in Paper I. In a few cases the text "Other IVC" is given, which refers to an unnamed IVC listed in the set of "Other negative/positive IVCs" in Table 2 of Paper I. Notes in square brackets, such as "[WSRT: −199 190]" give the telescope, velocity and column density for HVC and IVC components if the final value was based on better data than the Effelsberg or LDS spectrum that is shown. In a few cases, such a note is not associated with a fitted component, indicating the existence of an absorption without associated H I, or the existence of an H I component fainter than what is visible in the displayed spectrum.

For a number of spectra the listed component has a large systematic error (i.e. much larger than the listed statistical error). There can be various reasons for this. The most important of these cases are individually described below.

1) 3C 351.0, complex C component at $-130\,\mathrm{km\,s^{-1}}$. The fits give N(H I)=$4.5\pm0.6\times10^{18}\,\mathrm{cm^{-2}}$ for the 35′ LDS beam (see Fig. 2a for the spectrum), $2.8\pm0.1\times10^{18}\,\mathrm{cm^{-2}}$ for the 21′ Green Bank beam (see Lockman & Savage 1995 for the spectrum) and $4.2\pm0.3\times10^{18}\,\mathrm{cm^{-2}}$ for the 9′ Effelsberg beam (see Fig. 2a and Fig. 1b). In the LDS spectrum this component looks particularly noisy and the fitted width may be too large. Similarly, in the Green Bank spectrum, the component is particularly faint, and is not a nice easy-to-fit gaussian. Finally, the Effelsberg spectrum may have been affected by interference. Thus, the systematic errors are large. We estimate them to be $\sim1.5\times10^{18}\,\mathrm{cm^{-2}}$. Nevertheless, it also may be the case that there is much structure in the cloud. In the neighbouring LDS profiles the $-130\,\mathrm{km\,s^{-1}}$ component varies by a factor of 2. Thus, The Effelsberg beam might be picking up a brighter spot, which is beam diluted in the Green Bank beam, whereas multiple bright spots are seen in the LDS beam. Better data is needed to settle this question.

2) For 3C 418 six components are needed to fit the profile between −150 and $-50\,\mathrm{km\,s^{-1}}$. However, they are badly blended and probably incorrect in detail. The combined N(H I) for the three Outer Arm components is probably OK to within 20%, however.

3) The complex G component at $-107\,\mathrm{km\,s^{-1}}$ fitted for the 4 Lac sightline is rather wide, not symmetrical and probably a blend.

4) The parameters of the two IVCs at −79 and $-42\,\mathrm{km\,s^{-1}}$ fitted to BT Dra are rather uncertain, as they blend with the HVC and the low-velocity gas. The systematic error is estimated to be $\sim2\times10^{18}\,\mathrm{cm^{-2}}$, or 50%.

5) Toward H 1821+643, there are substantial differences between the LDS, Effelsberg and Green Bank spectra. In the LDS spectrum (Fig. 2b) emission at velocities $<-80\,\mathrm{km\,s^{-1}}$ is barely discernable (total column density estimated at $\sim1.2\times10^{18}\,\mathrm{cm^{-2}}$). In the Green Bank spectrum (Lockman & Savage 1995) there is a broad component running from −140 to $-80\,\mathrm{km\,s^{-1}}$, with total column density $\sim14.5\times10^{18}\,\mathrm{cm^{-2}}$, while the Effelsberg spectrum clearly shows two components at −128 and $-87\,\mathrm{km\,s^{-1}}$ with a total column density of $11.8\times10^{18}\,\mathrm{cm^{-2}}$. A larger-scale look at the LDS data reveals that H 1821+643 sits in a hole in the large area of emission associated with the Outer Arm. Apparently there is a small patch of bright H I right around H 1821+643, which is picked up by the Green Bank and Effelsberg telescopes, but beam-diluted in the LDS beam. However, the maximum dilution factor between the 21′ Green Bank and the 35′ LDS beam is only a factor 3, so some of the discrepancy must be due to a baseline error or just too low an S/N ratio in the LDS

spectrum.

6) The $-70\,\mathrm{km\,s^{-1}}$ IV spur component toward HD 103400 blends with the lower-velocity gas. The real uncertainty in the column density is probably twice the given statistical error.

7) The $-100\,\mathrm{km\,s^{-1}}$ complex L component toward HD 135485 is four times weaker in the $1'$ beam combined WSRT and Jodrell Bank data than in the LDS data. This is probably related to the fact that the surrounding cloud is fairly small and shows much structure.

8) The $+80\,\mathrm{km\,s^{-1}}$ component toward HD 203664 is very weak, and blends in with the gas at less positive velocities. In the Jodrell Bank spectrum (Ryans et al. 1996; N(H I)=$2.2\pm0.4\times10^{18}\,\mathrm{cm^{-2}}$) it is more clearly seen than in the Effelsberg spectrum (Fig. 1; N(H I)=$1.1\pm1.5\times10^{18}\,\mathrm{cm^{-2}}$). Thus, this component is clearly present, but its column density could be anywhere in the range 0.5 to $2.5\times10^{18}\,\mathrm{cm^{-2}}$. The fits toward the nearby stars HD 203699 and HD 205556 (probing the same IVC) also suffer from problems with blending.

9) The spectrum toward Mrk 279 was fitted by 8 components, all of which can be identified with continuous structures in the surrounding area. In this case the fitted values appear fairly reliable, in spite of the blending.

10) PKS 2345−67, Magellanic Stream component at $-174\,\mathrm{km\,s^{-1}}$. The listed component is a fit to the left wing of the profile. At neighbouring positions two separate components are seen at −190 and $-130\,\mathrm{km\,s^{-1}}$, so the profile may show a particularly bad blend of interpolated components.

11) The parameters of the IVC fitted to the H I spectrum toward SN 1981 D are rather uncertain since the spectral resolution is just $26\,\mathrm{km\,s^{-1}}$.

12) The VHVC fit to the H I spectrum toward SN 1986 G is vary narrow. This may or may not be realistic. Better data are needed to tell.

13) For SN 1993 J, the contribution of M 81 was removed by fitting a third order polynomial to the velocity ranges −120 to −80 and +30 to $+70\,\mathrm{km\,s^{-1}}$. The LLIV and low-velocity component were then fitted. However, it is not clear how much of the emission near $-25\,\mathrm{km\,s^{-1}}$ is associated with M 81. Including the velocity range −35 to $-20\,\mathrm{km\,s^{-1}}$ in the baseline reduces the column density of the LLIV component from 80 to $60\times10^{18}\,\mathrm{cm^{-2}}$. The final value used in Paper I thus is $70\pm10\times10^{18}\,\mathrm{cm^{-2}}$.

6. ANALYSIS

6.1. *Comparison of Leiden-Dwingeloo Survey and Effelsberg column densities*

For each of the directions in which an Effelsberg spectrum was available, we also extracted a spectrum from the LDS in the manner described in Sect. 3.1. A gaussian fit was made to this spectrum, in almost all cases using the same initial estimates as for the Effelsberg spectrum. In a few cases subtle differences required an extra low-velocity component for one of the two, or other small adaptations.

Figure 2 shows some examples of the differences observed in the profiles with a 9.1 and a 35 arcmin beam. These examples were chosen to illustrate some of the more extreme differences. The $-181\,\mathrm{km\,s^{-1}}$ component toward 3C 351.0 illustrates that some faint HVC components can be clearly visible in a 35 arcmin beam, but disappear at higher angular resolution. This spectrum also illustrates structure in the low-velocity gas, which has N(H I)=$157\times10^{18}\,\mathrm{cm^{-2}}$ at 35 arcmin, but $177\times10^{18}\,\mathrm{cm^{-2}}$ at 9 arcmin. The spectrum of BD+63 985 illustrates fine structure in the IV arch (core IV21). Toward BS16079-0017 the column density of the low-velocity gas increases by 30% when going from a 35 arcmin to a 9 arcmin beam. The spectrum toward H 1821+643 shows that high-velocity components can also appear, rather than disappear, at higher angular resolution. HD 83206 illustrates that components can appear separated at low angular resolution, but blended at higher angular resolution. The spectrum toward M 15 shows that small-scale structure also occurs at positive velocities. Mrk 106 illustrates another case of varying relative strength of low- and intermediate-velocity gas. Toward Mrk 116 the low-velocity component at $+7\,\mathrm{km\,s^{-1}}$ is 60% weaker at lower angular resolution. The 9 arcmin Effelsberg spectrum of Mrk 279 shows 8 identified components, all of which are present in the LDS spectrum, but with different relative strengths. PG 1259+593 illustrates how the high-velocity component differs by a factor 2 in column density; this is near a core of HVC complex C.

Using all of the gaussian fits, a table was made of N(H I) observed at either telescope, separately for the high-, intermediate- and low-velocity components. The low-velocity peak usually had to be fit with 2 or 3 components, once with 4, once with 5, while in 14% of the cases 1 component was sufficient. For the comparison, all low-velocity components were combined, as the exact decomposition depends on the details of the profile rather than on the real physical origin of the components.

Figures 3 and 4 present the results in graphical form. In Fig. 3 the left panels show the ratio as function of log N(H I-Eff), separately for high-, intermediate- and low-velocity gas. The right panels show the histogram of ratios for the three kinds of gas. Figure 4 shows the scatter plot and histogram of column density differences.

6.2. *Results for HVCs and IVCs*

For high- and intermediate-velocity clouds the ratio, R, of N(H I) measured with a 9 vs a 35 arcmin beam lies in the range 0.25−2.5 (0.3−2.1 when excluding the three most extreme points at either end). The full range is seen in most of the individual HVCs and IVCs, suggesting that the small-scale structure has similar characteristics in each of these. In one case (PG 0229+064, next to the Cohen Stream) the ratio is 0, as the HVC is not seen at all in the Effelsberg beam, although the LDS spectrum suggests N(H I)=$20\times10^{18}\,\mathrm{cm^{-2}}$. For HVCs the distribution of ratios peaks at a ratio $R\sim0.7$ (the median is 0.8), and it is slightly skewed towards values of $R<1$ (10 ratios fall between 0 and 0.5, 32 between 0.5 and 1, 18 between 1 and 1.5, and 9 above 1.5). For IVCs the distribution appears more symmetrical (the median is 1.03 and 15 lie between 0.5 and 1, 18 between 1 and 1.5). The skewness for the HVC ratio distribution may be real as bright condensations fill only a fraction <50% of the Dwingeloo beam, and an arbitrary direction will in most cases have smaller N(H I) than the average of a larger area seen in the Dwingeloo beam.

For the HVCs and IVCs, the maximum difference be-

tween the two column density measurements tends to increase with increasing N(H I), and can go either way. The histograms of differences are centered around no difference, with a range of $\pm 30\times10^{18}\,\mathrm{cm}^{-2}$. This width is mostly determined by the directions with high N(H I), as the range of ratios is independent of N(H I).

6.3. *Results for low-velocity gas*

For low-velocity gas, the ratio distribution is much narrower, with a sharp peak and a range of only 0.76−2.0 (0.92−1.4 when excluding the three most extreme points at either end). However, the peak is centered around a ratio of 1.1, not 1. Below we suggest that this offset is an artifact of the stray-radiation correction. If so, the real range of ratios would be 0.85−1.3. This range is smaller than for HVCs and IVCs. The histogram of differences for low-velocity gas is offset from zero by about $15\times10^{18}\,\mathrm{cm}^{-2}$, and positive differences (i.e. N(H I-Eff)>N(H I-LDS)) dominate. This is the same effect as seen in the offset of the average ratio.

There are several possible explanations for the difference between HVCs/IVCs and low-velocity gas in the range of ratios. 1) There is intrinsically less small-scale structure in the nearby low-velocity gas. 2) The relative magnitude of fluctuations may decrease with spatial size, and because the low-velocity gas is closer we are probing smaller absolute scales. 3) This is an artifact because for the low-velocity gas two or more components are mixed together, so that upward fluctuations in one component may be compensated by downward fluctuations in another component. That the third of these effects plays a role is indicated by the histogram of ratios for the 11 sightlines where just one component was fit for the low-velocity gas. That distribution has a larger dispersion than the histogram for all low-velocity gas.

The offset in the average value of N(H I-Eff) and N(H I-LDS) observed for the low-velocity gas is not completely understood. It is unlikely to be due to a calibration (i.e. scaling) error, as then the same offset should have been seen for the HVCs and IVCs. A more likely possibility is that the stray-radiation correction is not completely correct. This correction has been applied to both datasets. The LDS data are used to correct themselves, and the Effelsberg data are corrected using the corrected LDS-data. Apparently there is a slight undercorrection in the latter case, which amounts to about $15\times10^{18}\,\mathrm{cm}^{-2}$ on average. For the high-latitude directions studied here that is on average 10% of N(H I). However, most of the correction is due to higher column density low-latitude directions, so this is no more than ∼1% of the total correction.

Such a problem may indicate that the correction for the far sidelobes is slightly incorrect (about 1 to 2% of the total correction). The Effelsberg antenna pattern was determined by Kalberla et al. (1980) and updated in 1992. After this date some mechanical changes within the telescope surface were made. A problem may arise from spoilers which have been mounted on the feed support legs. The intention was to eliminate baseline ripples due to standing waves at short wavelengths. However, at 21 cm these spoilers are expected to increase the effective cross section for the scattering of waves falling on the feed support legs. We suspect that the stray cones of the antenna diagram due to the feed support legs have been altered by these mechanical modifications. Attempts to improve the quality of the antenna diagram which is used to correct for stray radiation remained unsuccessful.

6.4. *Comparison with column densities measured at high resolution*

Table 1 lists the values measured for N(H I) in the direction of 16 probes of HVCs for which H I data exist at high resolution. There are two groups. First, probes for which 21-cm interferometer data exist, so that individual velocity components can be compared with single-dish data. Second, distant stars or extra-galactic probes for which the integrated H I column density along the line of sight was also measured using Lyα absorption.

This table shows that the ratio N(H I-2′)/N(H I-35′) has the same wide range of 0.25−2.5 as the ratio N(H I-9′)/N(H I-35′). When excluding the extreme value at each end the range is 0.54−2.0. However, the ratio N(H I-2′)/N(H I-9′) lies in the much narrower range 0.74−1.24 (0.75−1.06 when excluding the extreme value at each end). This is consistent with the result described in Sect. 6.2, where we showed that the contrast between a 9 and a 35 arcmin beam is a factor up to 2.5. The difference in ranges suggests that N(H I) derived from a 9′ beam approximates the value obtained at higher resolution to within 25%, and that on average N(H I) tends to be slightly lower at higher resolution.

Measuring N(H I) using Lyα absorption gives the smallest possible beam (<0.1 arcsec). However, only the combined column density in all components can be measured. Still, this may give some indication of structure on scales smaller than the 1′ limit of interferometers, since the integrated column density is usually dominated by the low-velocity components. Effelsberg data exist toward 6 AGNs in the sample of Savage et al. (2000), who measured N(H I-Lyα) using the Faint Object Spectrograph (*FOS*) on the Hubble Space Telescope. Effelsberg data are also available for distant two stars in the sample of Diplas & Savage (1994), who measured N(H I-Lyα) using *IUE*. Excluding the deviant value toward HS 0624+6907, which has a particularly large systematic uncertainty, the ratio N(H I-Lyα)/N(H I-Eff) lies in the range 0.74−0.98. This range is slightly narrower but similar to that found for N(H I-Lyα)/N(H I-Green Bank) (0.63−0.87), but smaller than that for N(H I-Lyα)/N(H I-LDS) (0.69−1.24).

Even though this is a small sample, it suggests that measurements of N(H I) with a 9 arcmin beam are sufficient to obtain reasonable column density estimates, whereas measurements with a 35 arcmin beam are only accurate to a factor of about 2−3.

It would be useful to also compare the Effelsberg 9 arcmin and LDS 35 arcmin column densities with observations with an intermediate beam, such as the 21 arcmin beam provided by the Green Bank 140-ft. The data of Murphy et al. (2000) for AGNs observed with the *FOS* provide numbers for about 190 directions. However, so far only 10 of these have also been observed at Effelsberg, and most do not show well-isolated HVC or IVC component. So, only a limited comparison will be possible.

7. CONCLUSIONS

a) For HVCs and IVCs improving the resolution by a factor $\sim$4 (from $35'$ to $9'$ beam, a factor 15 in area) can change the derived value of N(H I) by a factor up to about 3 either way. In most (two-thirds) of the directions the change is a factor $>$1.5 either way, while in just one-third is the change a factor between 0.5 and 1.5.

b) For HVCs/IVCs where higher resolution data are available, the ratio between N(H I) as observed with a $1'-2'$ beam vs a $9'$ beam (a factor $\sim$20 in area) lies in the range 0.74$-$1.24 whereas comparing $1-2'$ data with $35'$ data (another factor $\sim$20 in area) gives a range 0.25$-$2.5.

c) For sightlines where N(H I-total) was derived from Lyα absorption the ratio N(H I-Lyα) to N(H I-$9'$,total) lies in the range 0.74$-$0.98.

d) Combining b) and c) suggests that a $9'$ beam is sufficient to derive abundances to within about 25%, whereas using a larger beam leads to larger uncertainties, of up to a factor 3.

e) On average the single-dish column densities tend to be slightly higher than the values measured at higher resolution, so that on average ionic abundances tend to be underestimated by 0$-$25%.

The Effelsberg Telescope belongs to the Max Planck Institute for Radio Astronomy in Bonn. We thank Carl Heiles for observing the sightline to SN 1991 T for 24 hours, using the Hat Creek telescope. Finally, we thank Robert Ryans for providing his Jodrell Bank spectra.

REFERENCES

Albert C.E., Blades J.C., Morton D.C., Lockman F.J., Proulx M., Ferrarese L., 1993, ApJS, 88, 81
Barnes D., et al. 2001, MNRAS, in press
Braun R., Burton W.B., 2000, A&A, 354, 853
Brüns C., Kerp J., Staveley-Smith L., 2001, in "Mapping the Hidden Universe", ASP Conf. Ser., in press
Centurión M., Vladilo G., de Boer K.S., Herbstmeier U., Schwarz U.J., 1994, A&A, 292, 261
Colgan S.W.J., Salpeter E.E., Terzian Y., 1990, ApJ, 351, 503
Danly L., Lockman F.J., Meade M.R., Savage B.D., 1992, ApJS, 81, 125
de Boer K.S., Rodriguez-Pascual P., Wamsteker W., Sonneborn G., Fransson C., Bomans D.J., Kirshner R.P., 1993, A&A, 280, L15
Diplas A., Savage B.D., 1994, ApJS, 93, 211
Hartmann D., Burton W.B., 1997, Atlas of Galactic Neutral Hydrogen, Cambridge University Press
Haynes R., Staveley-Smith L., Mebold U., Kalberla P.M.W., Jones K., White G., Jones P., Filipovic M., Dickey J., Green A., 1999, IAU Symp. 190, 108
Kalberla P.M.W., Mebold U., Reich W., 1980, A&A, 82, 175
Kalberla P.M.W., Mebold U., Reif K., 1982, A&A, 106, 190
Kuntz K.D., Danly L., 1996, ApJ, 457, 703
Lilienthal D., Meyerdierks H., de Boer K.S., 1990, A&A, 240, 487
Lockman F.J., Savage B.D., 1995, ApJS, 97, 1
Meyer D.M., Roth K.C., 1991, ApJ, 383, L41
Payne H.E., Dickey J.M., Salpeter E.E., Terzian Y., 1978, ApJ, 221, L95
Payne H.E., Salpeter E.E., Terzian Y., 1980, ApJ, 240, 499
Putman M.E., et al., 2001, in preparation
Ryans R.S.I., Sembach K.R., Keenan F.P., 1996, A&A, 314, 609
Ryans R.S.I., Keenan F.P., Sembach K.R., Davies R.D., 1997a, MNRAS, 289, 83
Ryans R.S.I., Keenan F.P., Sembach K.R., Davies R.D., 1997a, MNRAS, 289, 986
Savage B.D., Wakker B.P., Bahcall J.N., Bergeron J., Boksenberg A., Hartig G.F., Jannuzi B.T., Kirhakos S., Lockman F.J., Murphy E.M., Sargent W.L.W., Schneider D.P., Turnshek D., Weymann R.J., Wolfe A.M., 2000, ApJS, 129, 563
Schwarz U.J., Oort J.H., 1981, A&A, 101, 305
Schwarz U.J., Wakker B.P., van Woerden H., 1995, A&A, 302, 364
Schwarz U.J., Wakker B.P., 2001, in "High-Velocity Clouds", Kluwer Acad. Publ., eds. H. van Woerden, U.J. Schwarz, K.S. de Boer, B.P. Wakker, in preparation
Shaw C.R., Bates B., Kemp S.N., Keenan F.P., Davies R.D., Roger R.S., 1996, ApJ, 473, 849
Staveley Smith L., 1997, Proc. Ast. Soc. Austr., 14, 111
Stoppelenburg P.S., Schwarz U.J., van Woerden H., 1998, A&A, 338, 200
Tamanaha C.M., 1996, ApJS, 104, 81
Wakker B.P., Howk C., van Woerden H., Schwarz U.J., Beers T.C., Wilhelm R., Kalberla P.M.W., Danly L., 1996, ApJ, 473, 834
Wakker B.P., Howk C., Savage B.D., Tufte S.L. Reynolds R.J., van Woerden H., Schwarz U.J., Peletier R.F., Kalberla P.M.W., 1999b, Nature, 400, 388
Wakker B.P., Schwarz U.J., 1991, A&A, 250, 484
Wakker B.P., 2001, Paper I, this Volume
Wakker B.P., Oosterloo T.A., Putman M.E., 2001, submitted to AJ
Wakker B.P., van Woerden H., 1997, ARA&A, 35, 217

TABLE 1

EFFECT OF H I SMALL-SCALE STRUCTURE

Probe	35′ beam[a]	21′ beam[b]	9′ beam[b]	1 or 2′ beam[c]	Lyα[d]
N(H I) in HVC/IVC components					
Mrk 106	36×10^{18}		36×10^{18}	38×10^{18}	
	13×10^{18}		21×10^{18}	26×10^{18}	
Mrk 290	76×10^{18}		123×10^{18}	92×10^{18}	
PG 0832+675	56×10^{18}		40×10^{18}	30×10^{18}	
PG 0859+593	23×10^{18}		32×10^{18}	34×10^{18}	
	63×10^{18}		66×10^{18}	53×10^{18}	
PG 0906+597	28×10^{18}		34×10^{18}	29×10^{18}	
	95×10^{18}		121×10^{18}	110×10^{18}	
NGC 3783	112×10^{18}	120×10^{18}		80×10^{18}	
HD 135485	20×10^{18}		5×10^{18}	5.1×10^{18}	
4 Lac	$<2\times10^{18}$		6.3×10^{18}	5.0×10^{18}	
N(H I) integrated over all velocities					
3C 351	161×10^{18}	203×10^{18}	180×10^{18}		177×10^{18}
HD 93521	110×10^{18}		113×10^{18}		126×10^{18}
HD 203664	368×10^{18}		413×10^{18}		347×10^{18}
HS 0624+6907	581×10^{18}	655×10^{18}	742×10^{18}		302×10^{18}
H 1821+643	306×10^{18}	384×10^{18}	349×10^{18}		259×10^{18}
PG 0953+414	120×10^{18}	112×10^{18}	112×10^{18}		83×10^{18}
PG 1116+215	117×10^{18}	140×10^{18}	112×10^{18}		88×10^{18}
PG 1259+593	105×10^{18}	154×10^{18}	157×10^{18}		130×10^{18}

NOTE.—a: N(H I) as measured in the Leiden-Dwingeloo Survey. b: these colums show result for intermediate beams: 21′ (NRAO 140-foot), 12′ (Jodrell Bank) or 9′ (Effelsberg). c: N(H I) as measured by combining the highest-resolution single-dish data with a Westerbork or ATCA map. d: N(H I) as measured from Lyα absorption, from Savage et al. (2000).

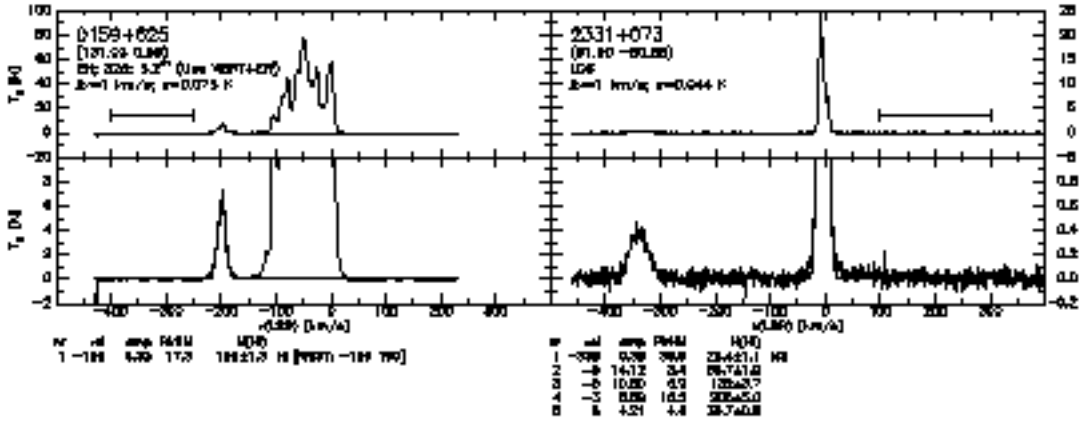
0159+625
2331+073

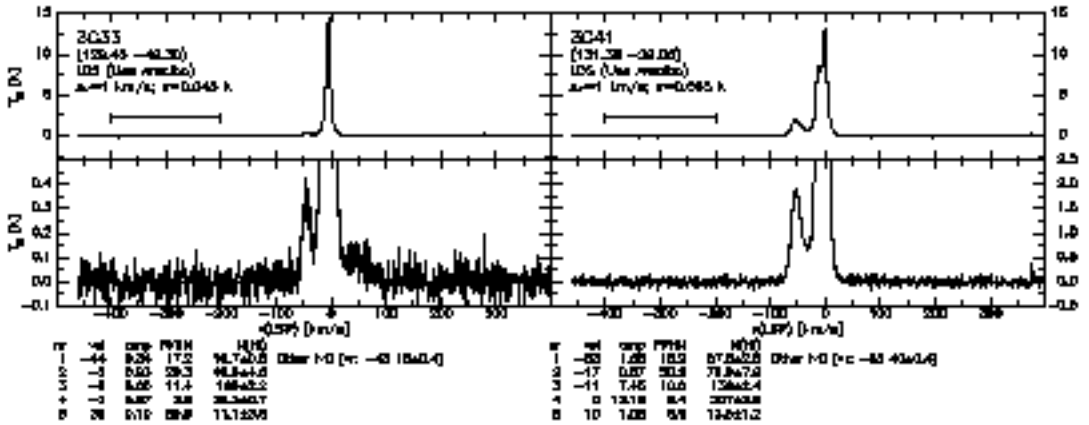
3C33
3C41

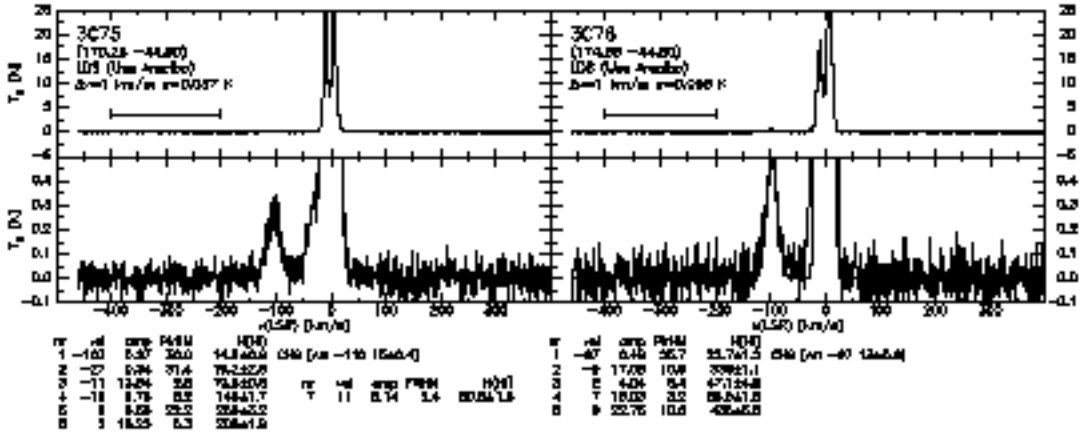
3C75
3C76

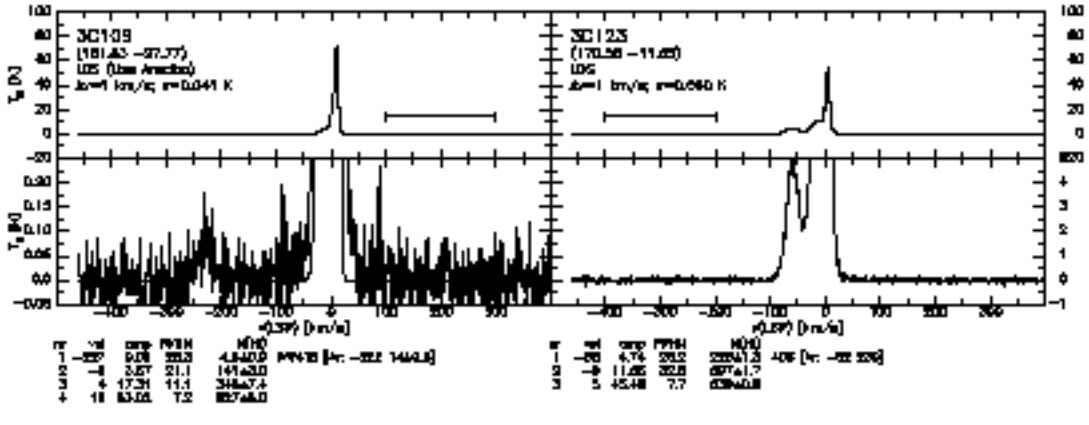
3C109
3C123

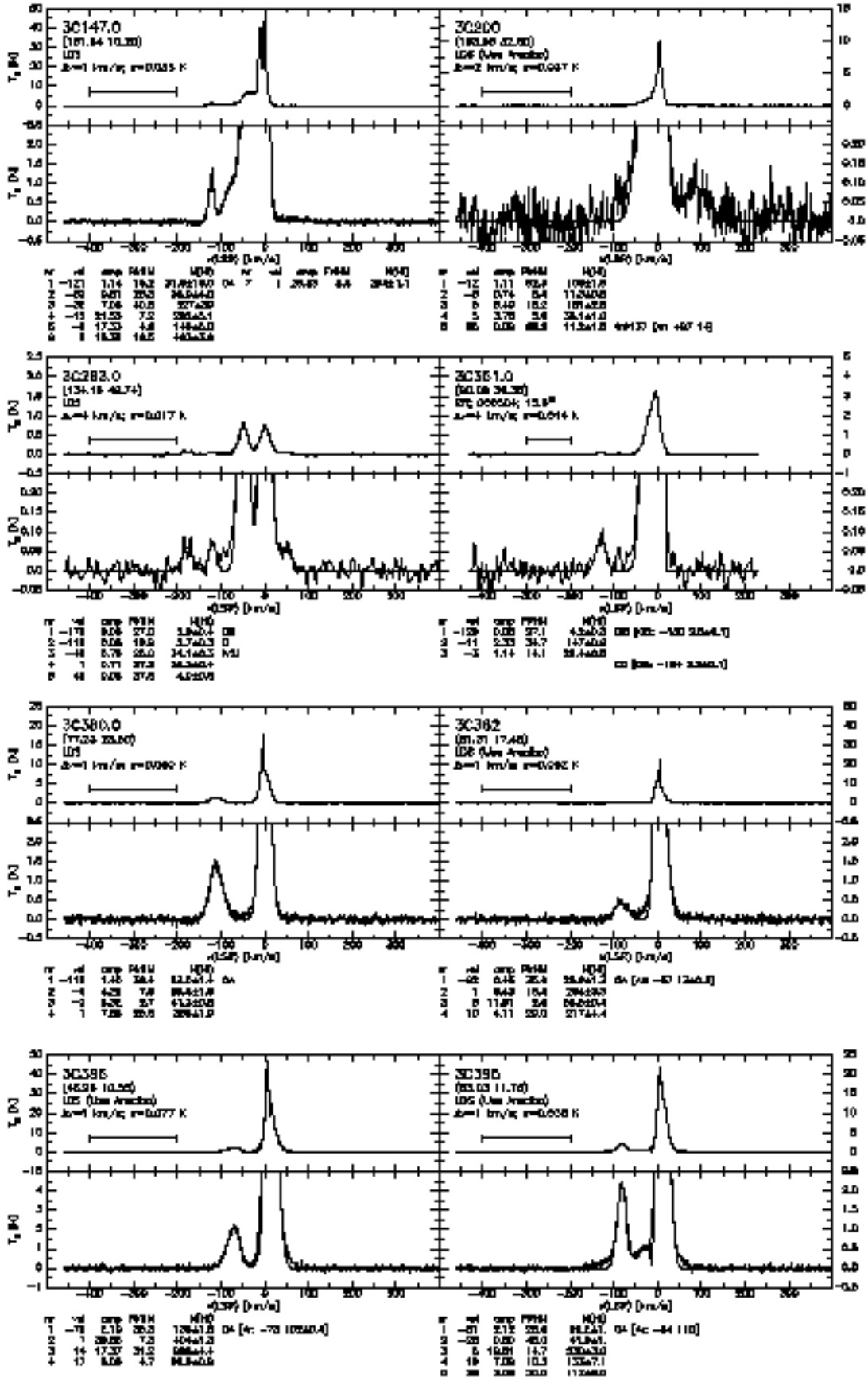
3C147.0
3C200
3C282.0
3C351.0
3C380.0
3C382
3C395
3C395

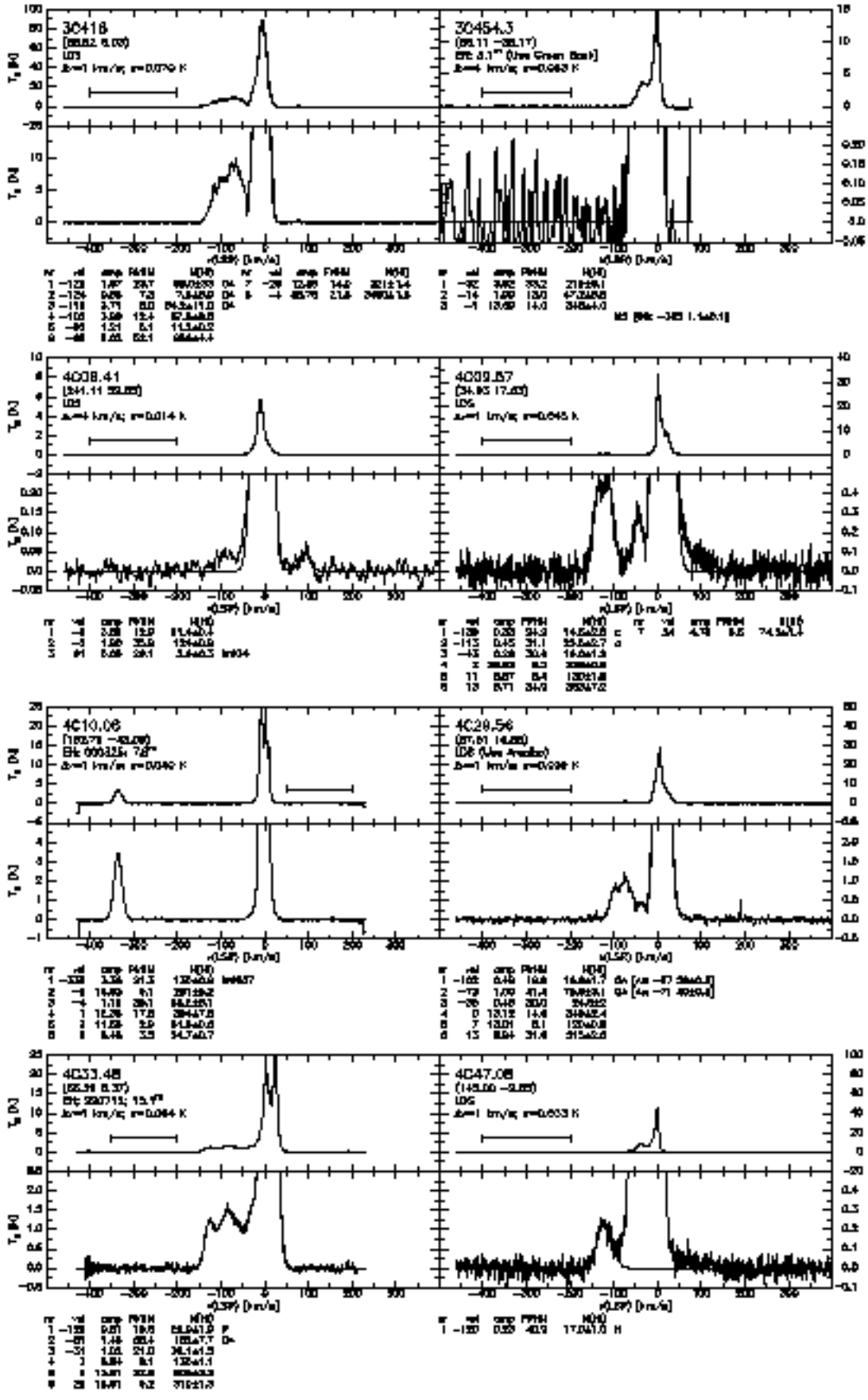
3C418
3C454.3
4C08.41
4C09.57
4C10.06
4C28.56
4C33.48
4C47.08

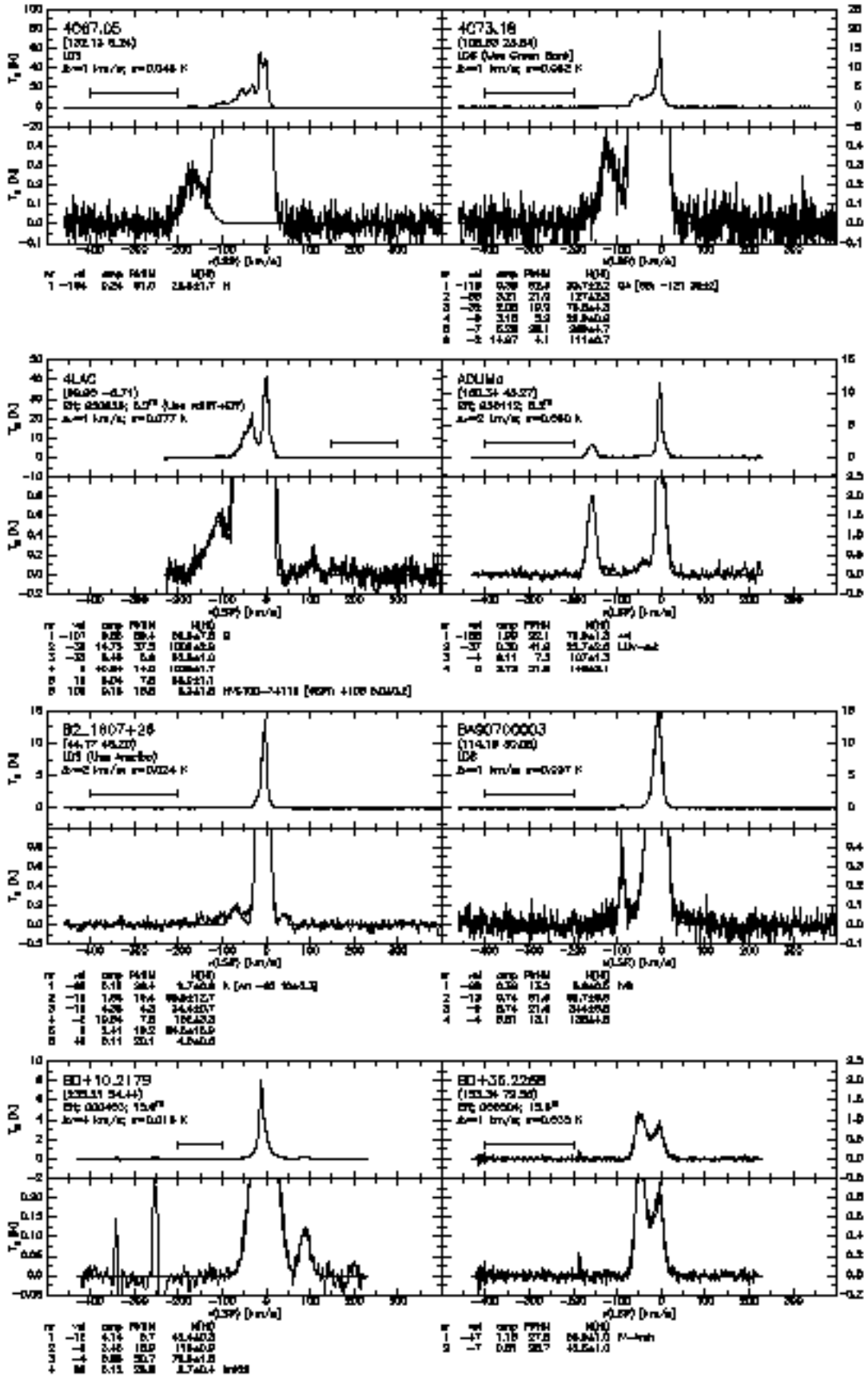

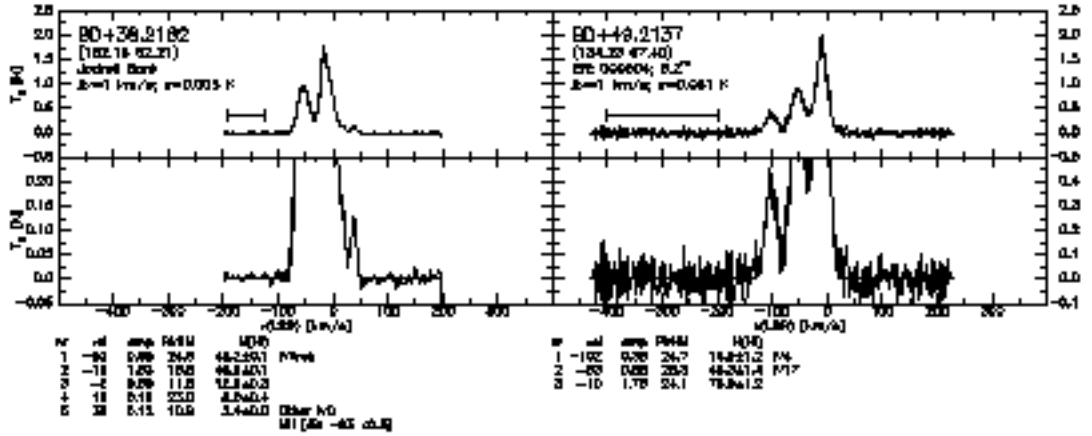
BD+39.2182
BD++49.2137
v(LSR) [km/s]

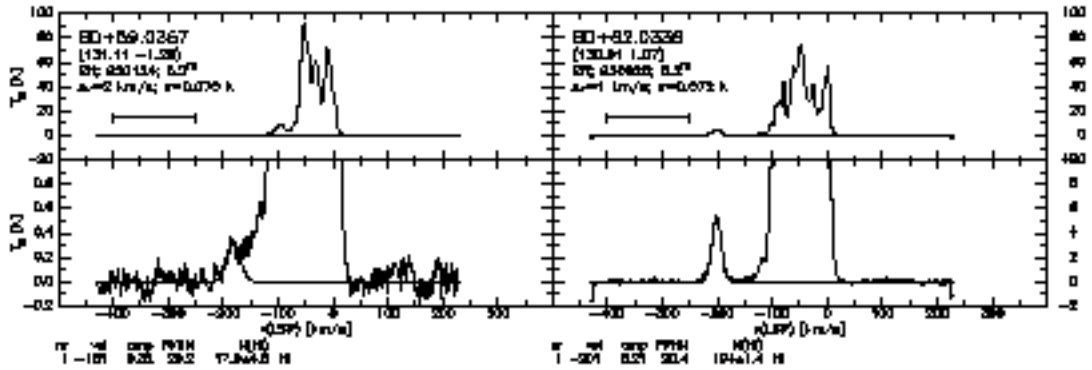
BD+59.0267
BD+62.0338
v(LSR) [km/s]

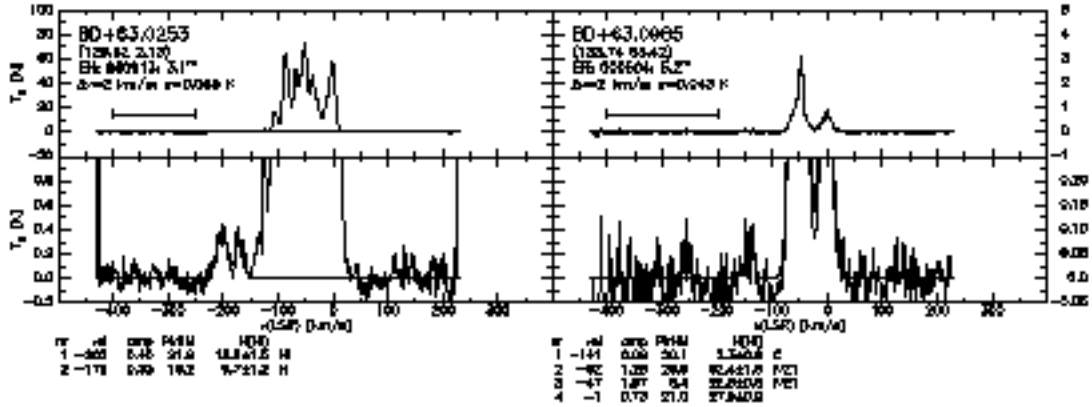
BD+63.0253
BD+63.0965
v(LSR) [km/s]

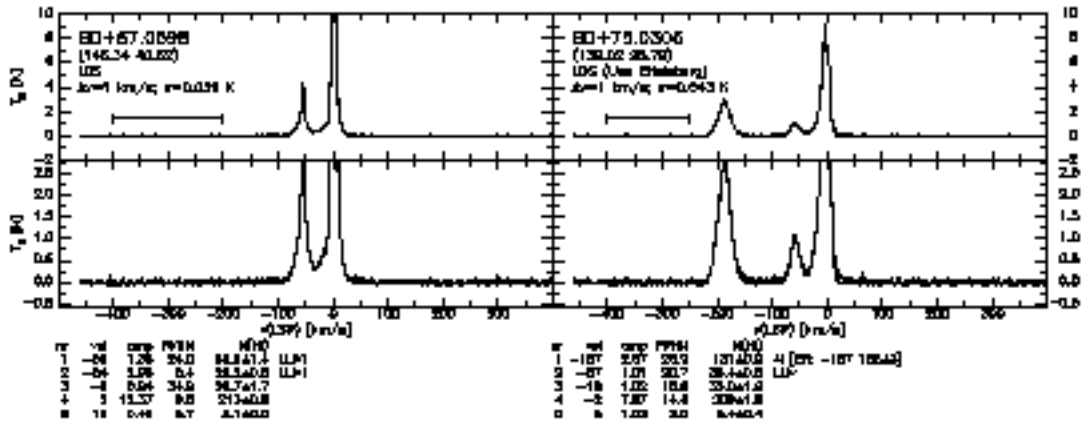
BD+67.0598
BD+75.0306
v(LSR) [km/s]

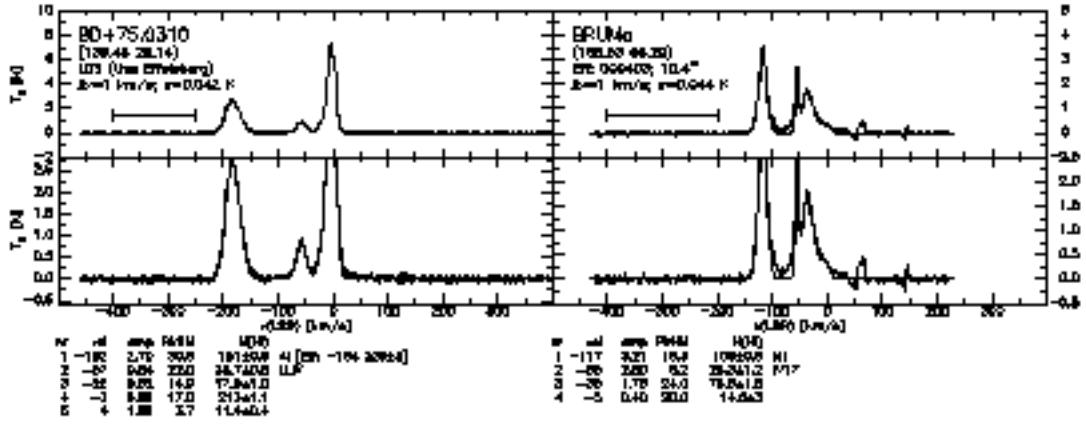
B0+75.0310
BRUN4a

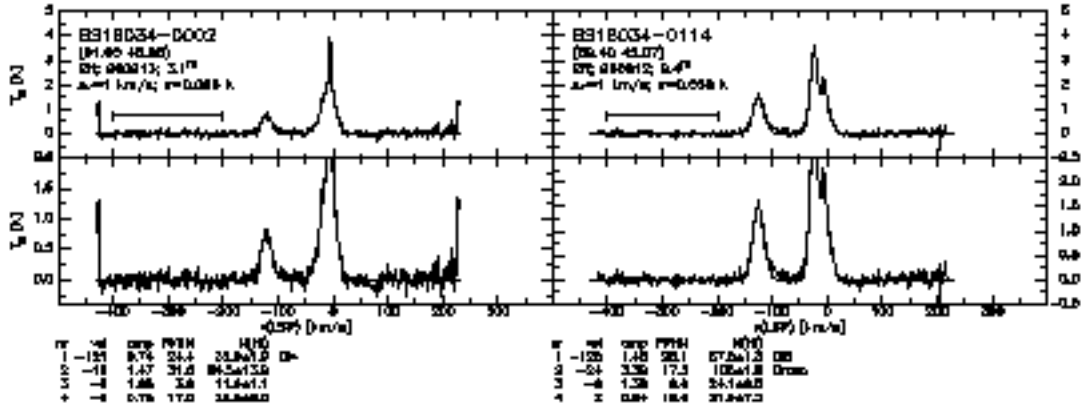
BS18034−0002
BS18034−0114

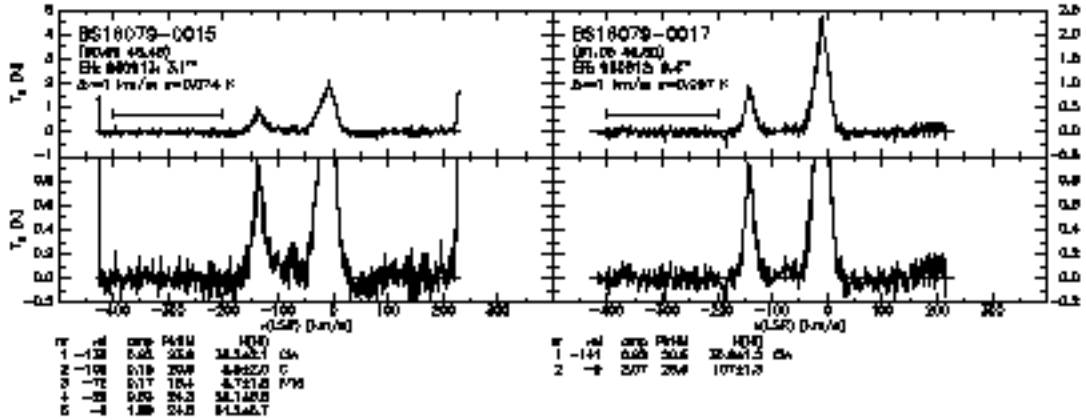
BS18079−0015
BS18079−0017

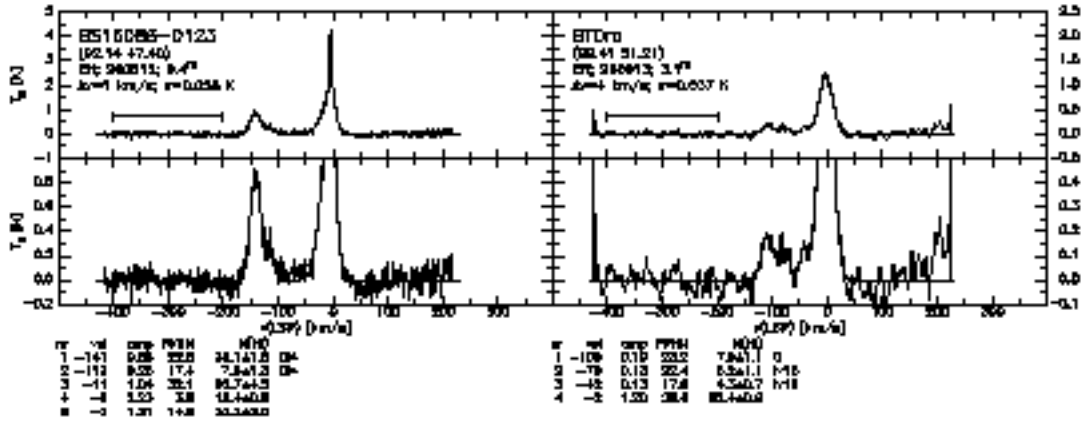
BS18085−0123
BTDra

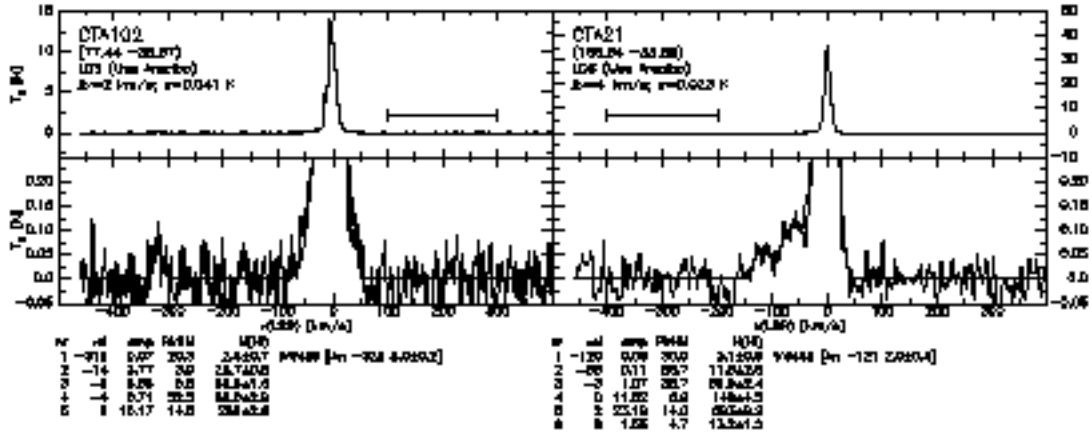
CTA102
CTA21

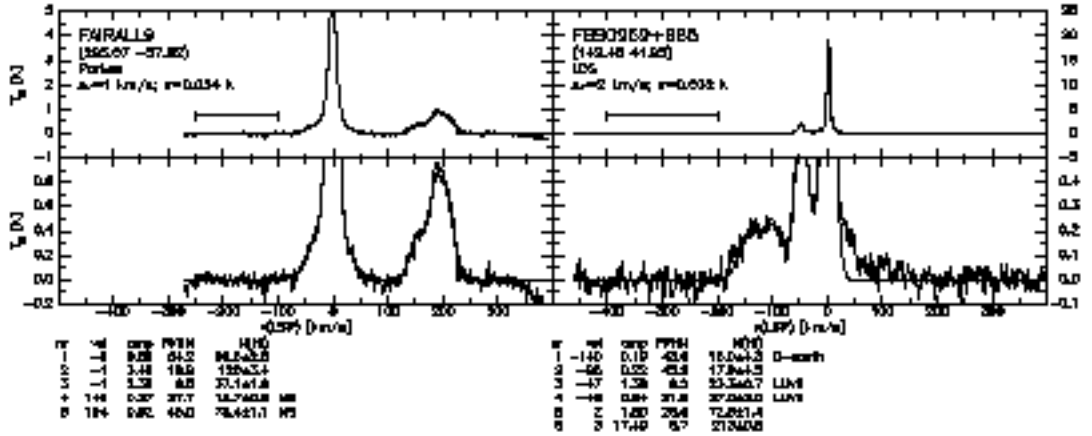
FAIRALL9
FEB0359+855

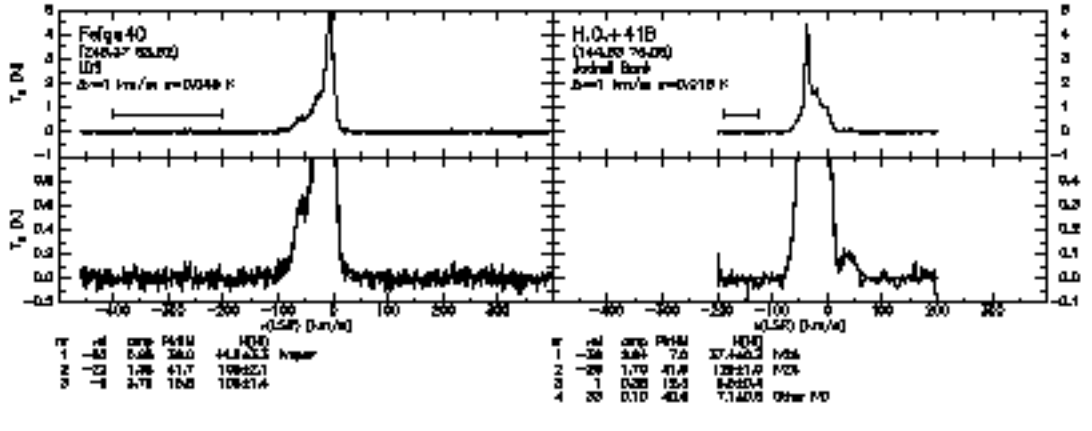
Fe(qs40
H.0.+41B

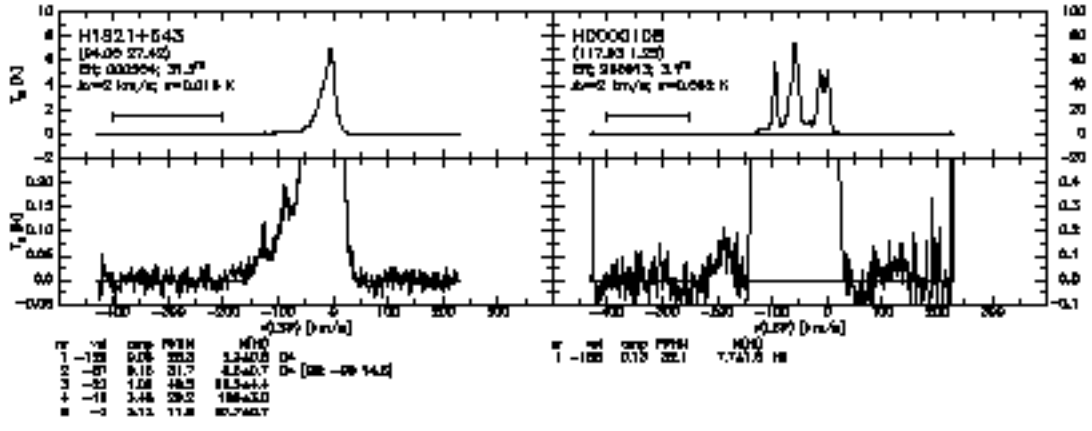
H1821+643
HD00010B

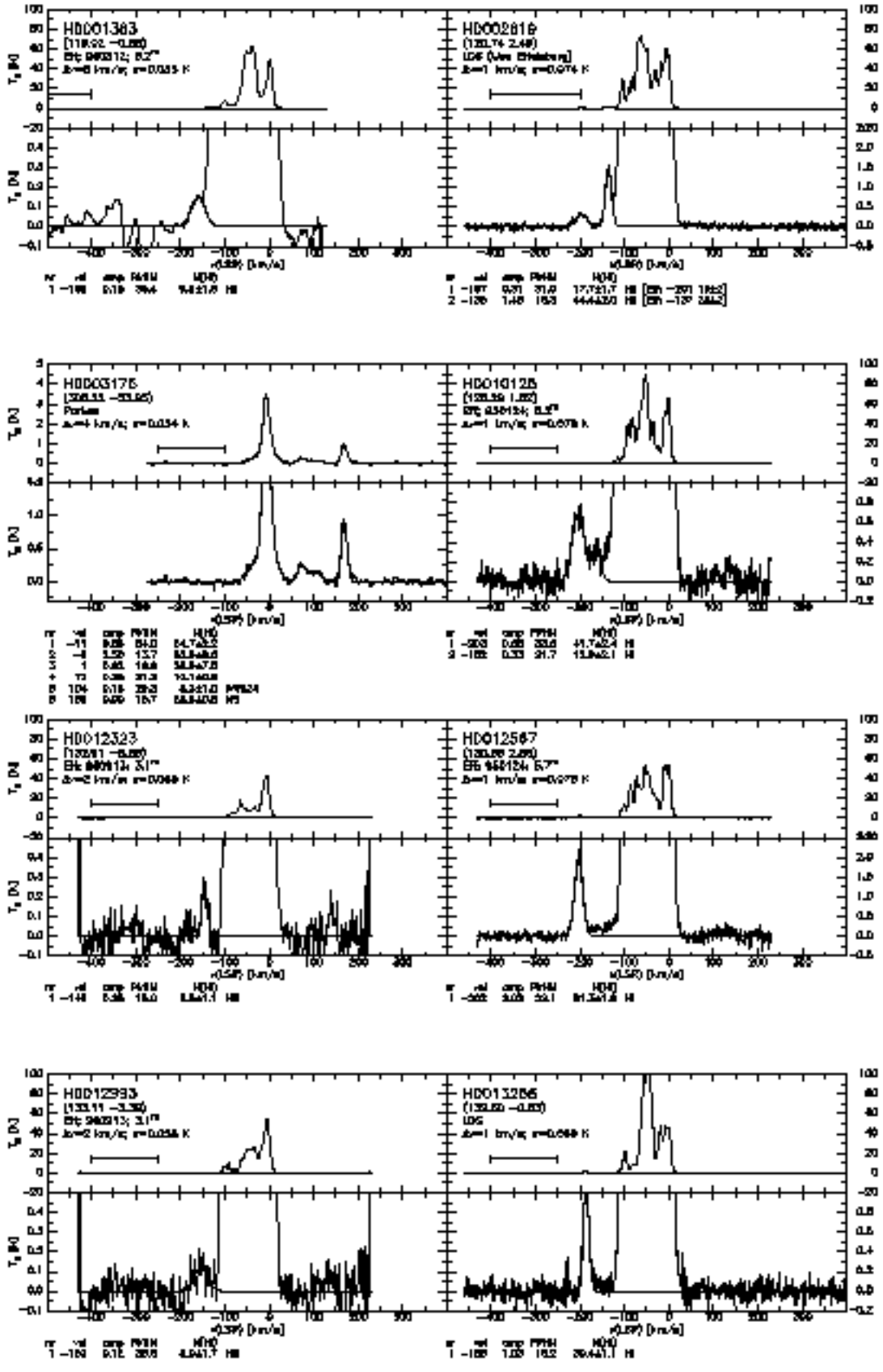

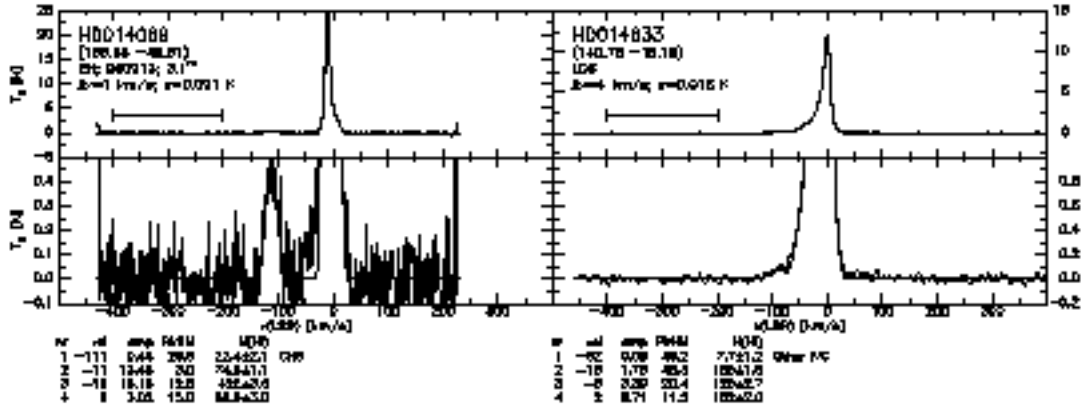
HD014088
HD014833
LDS
T_B [K]
T_B [K]
v(LSR) [km/s]
v(LSR) [km/s]

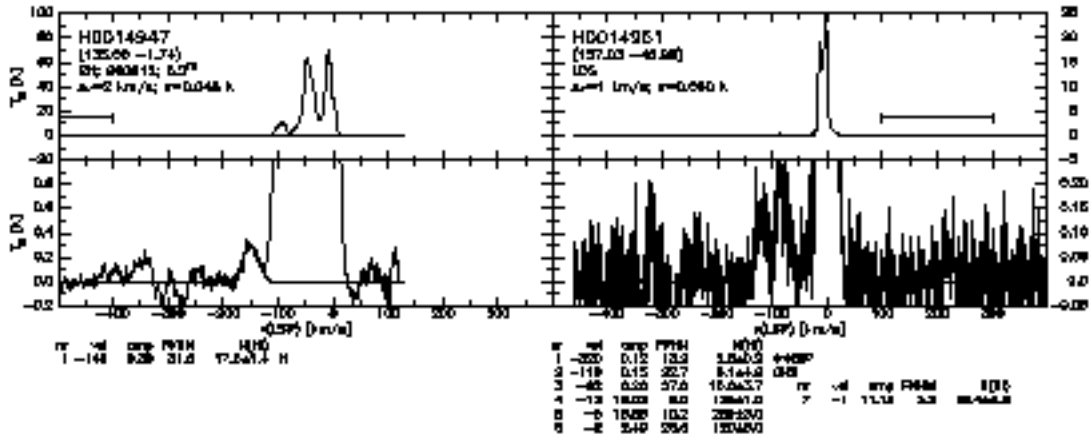
HD014947
HD014951
LDS
T_B [K]
T_B [K]
v(LSR) [km/s]
v(LSR) [km/s]

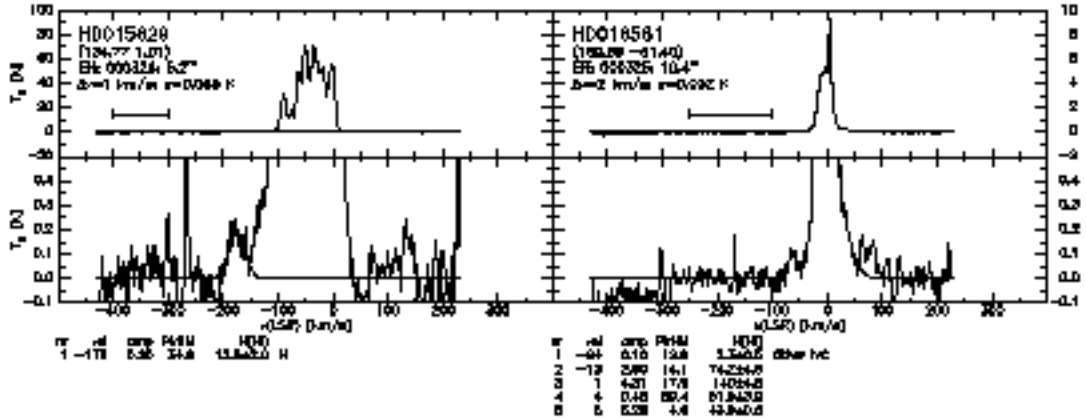
HD015629
HD016561
T_B [K]
T_B [K]
v(LSR) [km/s]
v(LSR) [km/s]

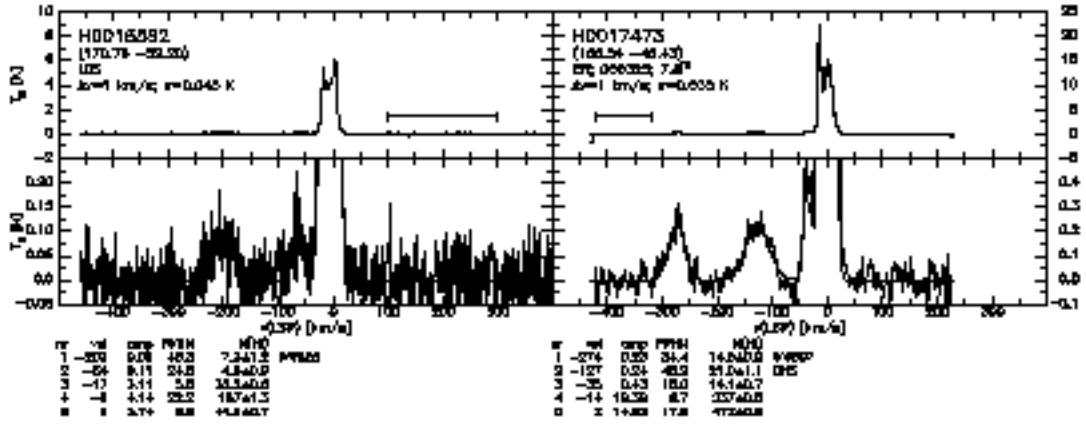
HD016582
HD017475
LDS
T_B [K]
T_B [K]
v(LSR) [km/s]
v(LSR) [km/s]

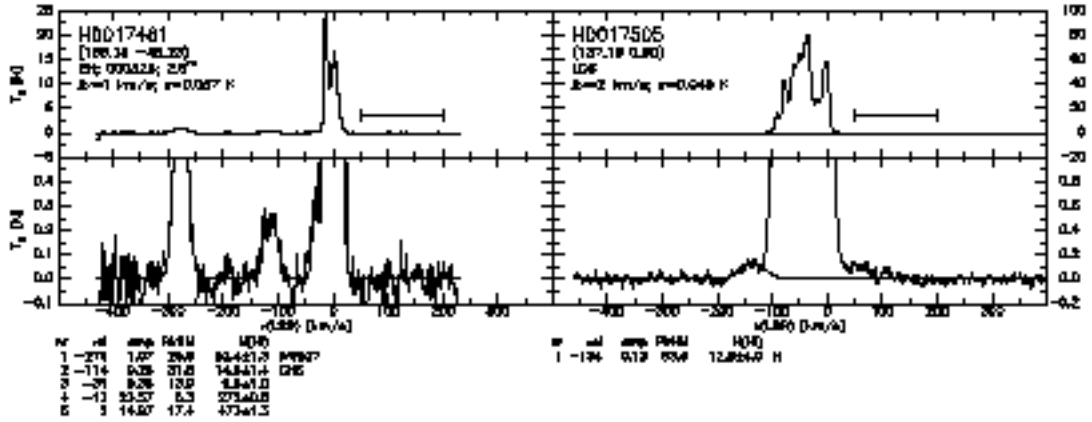
HD017481
HD017505

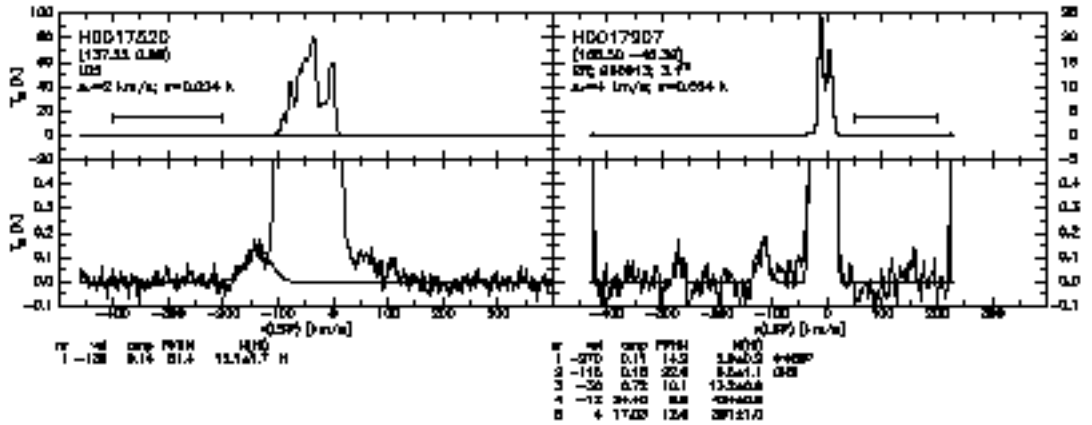
HD017520
HD017907

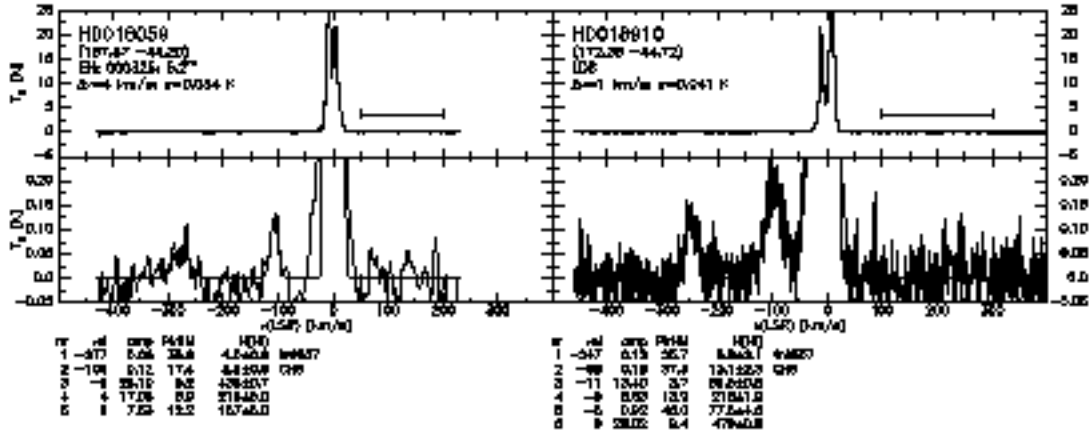
HD018059
HD018910

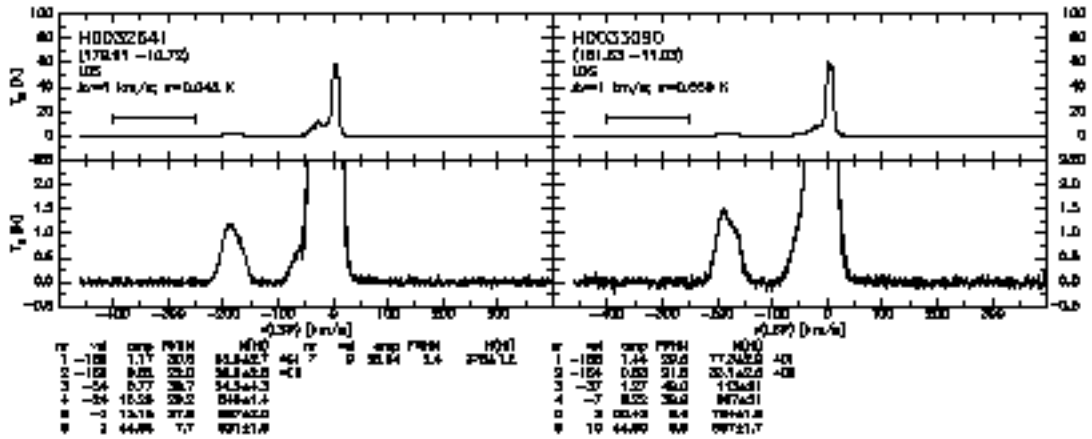
HD032641
HD033090

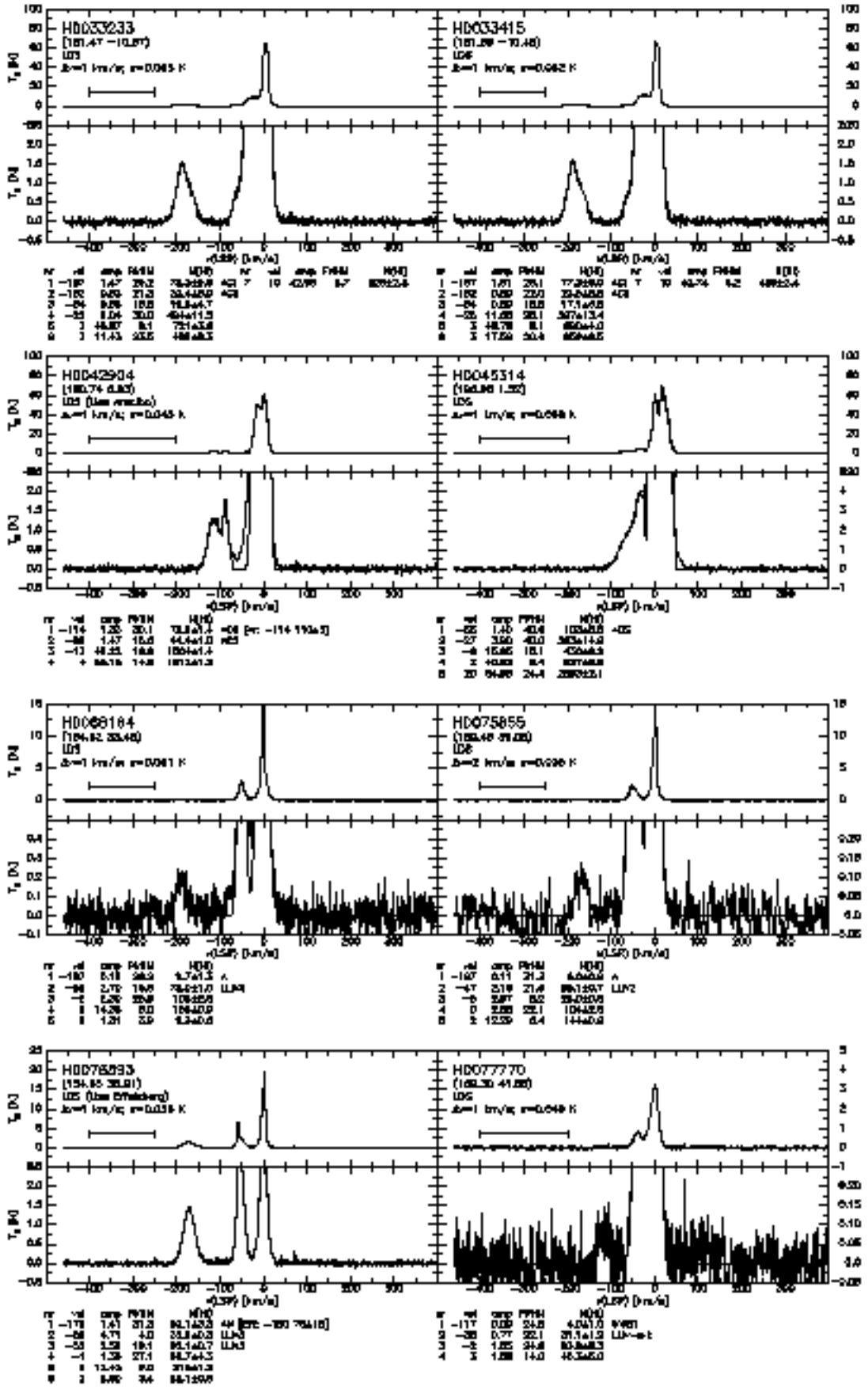
HD033233
HD033415
HD042934
HD045314
HD068164
HD075855
HD076093
HD077770

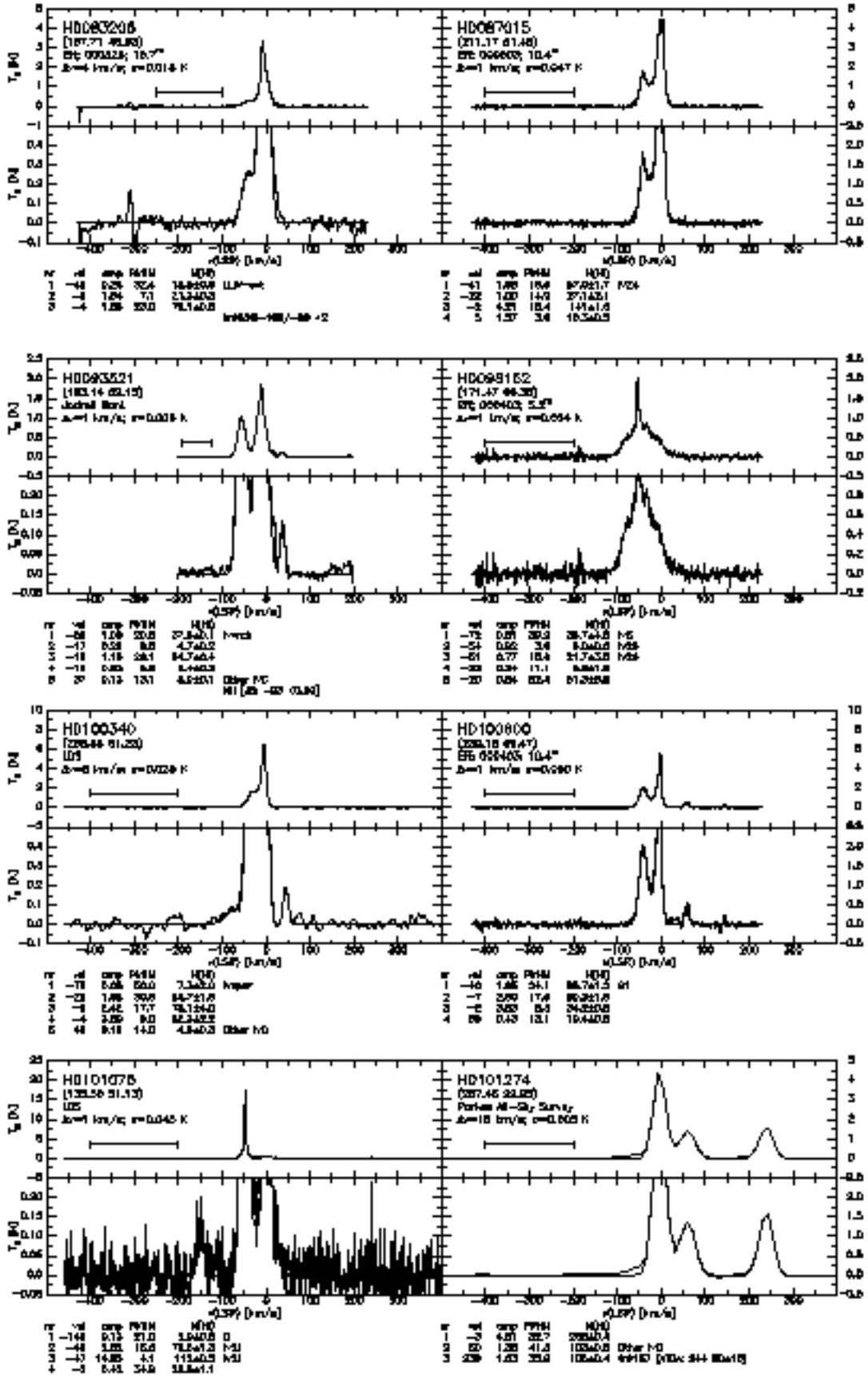
HD083206
HD087015
HD093521
HD093152
HD100340
HD100600
HD101075
HD101274

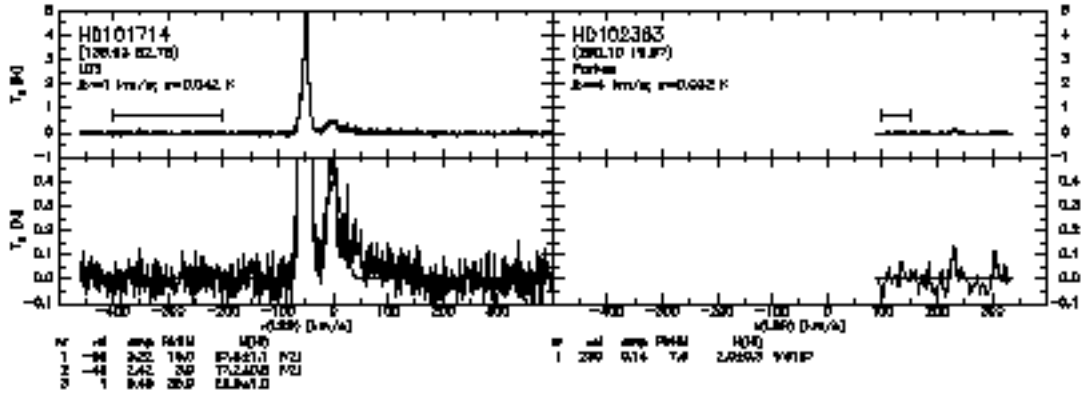
HD101714
HD102383

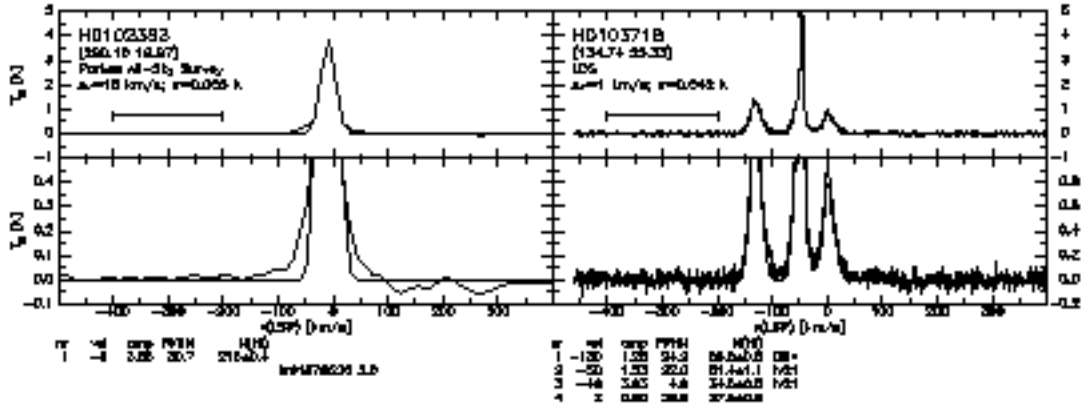
HD102393
HD103718

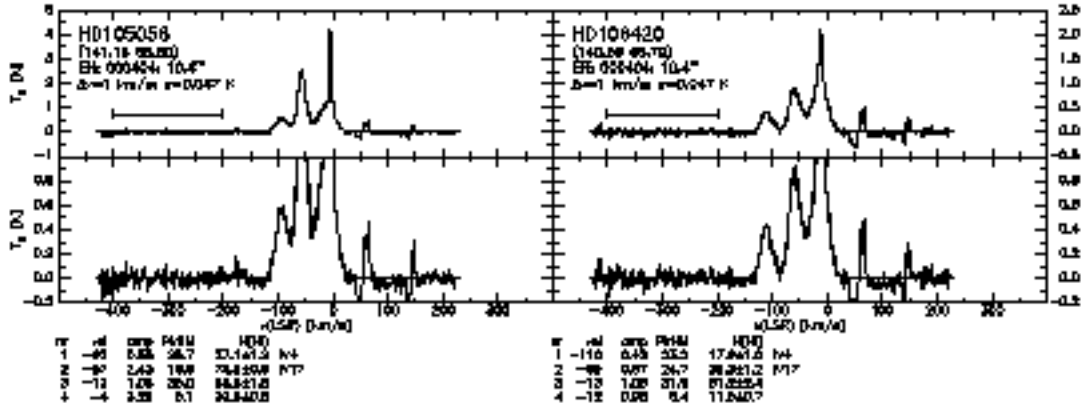
HD105056
HD106420

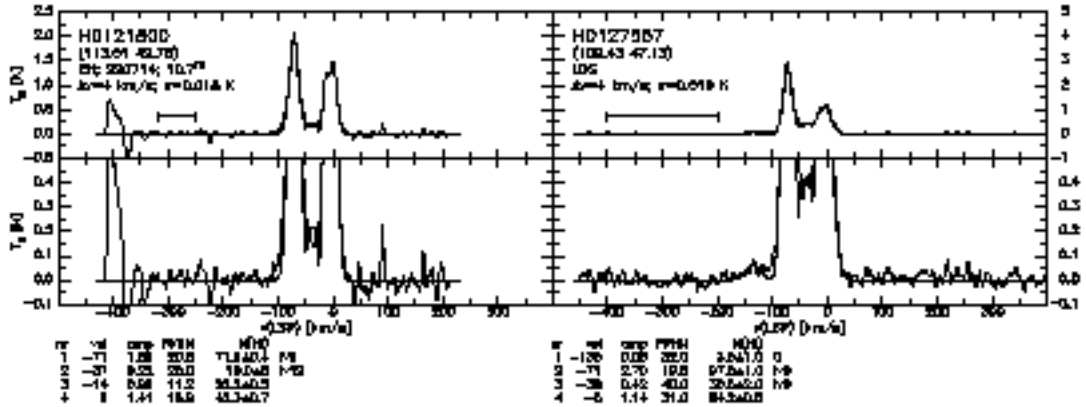
HD121800
HD127567

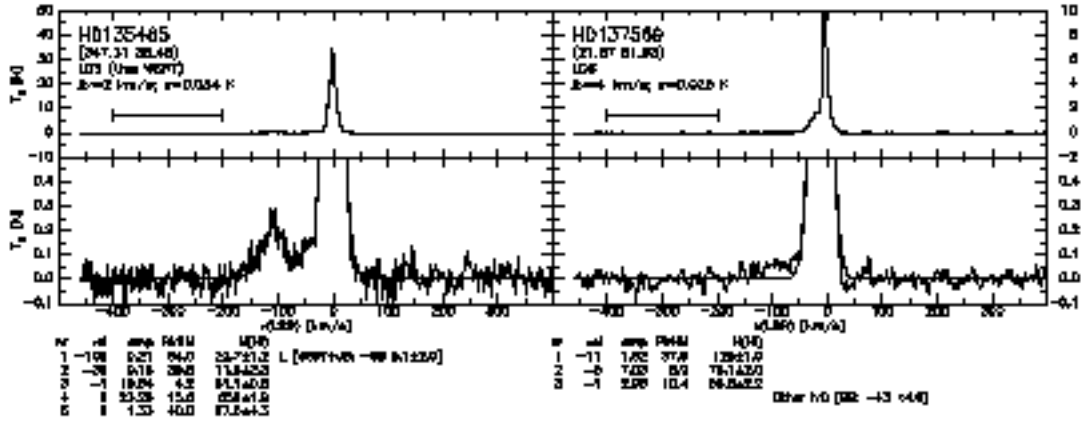
HD135485
HD137569

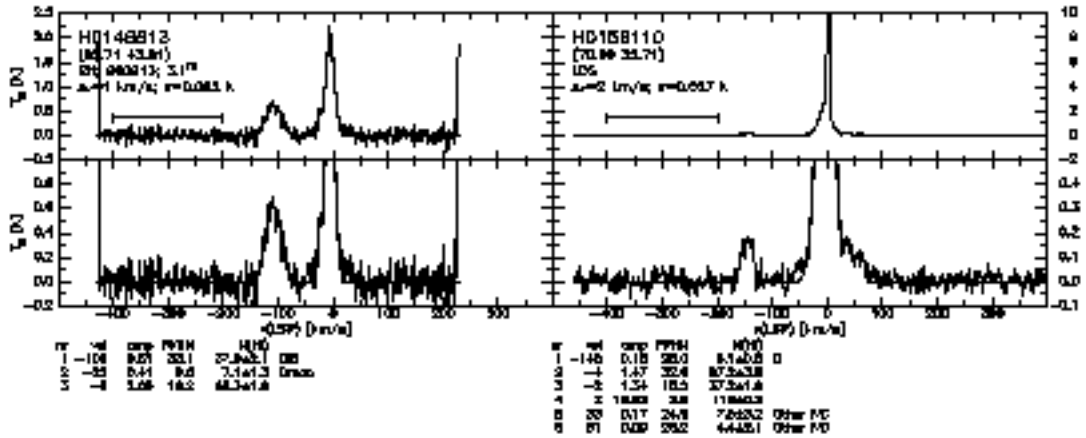
HD148813
HD158110

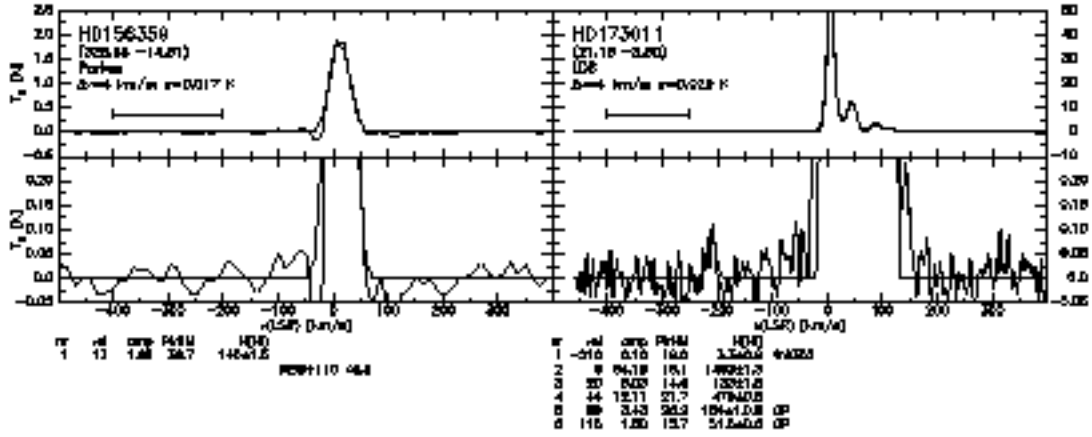
HD156359
HD173011

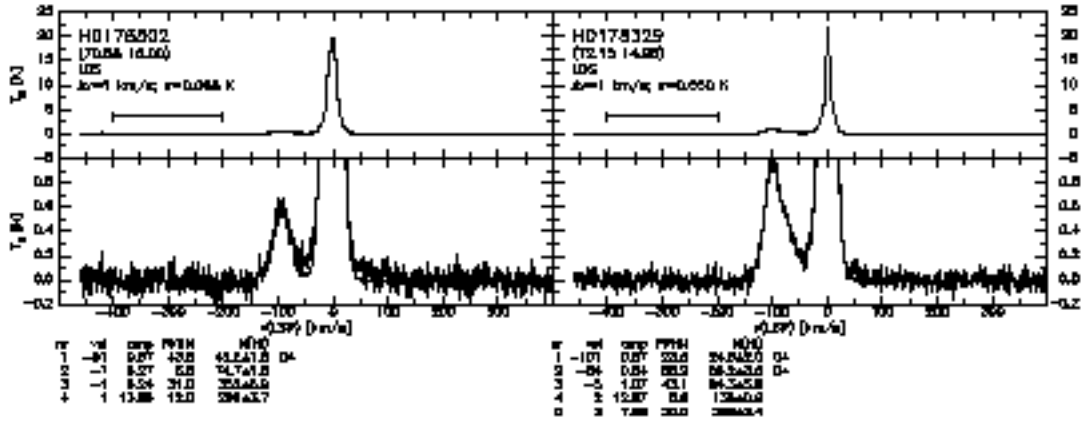
HD176502
HD178329

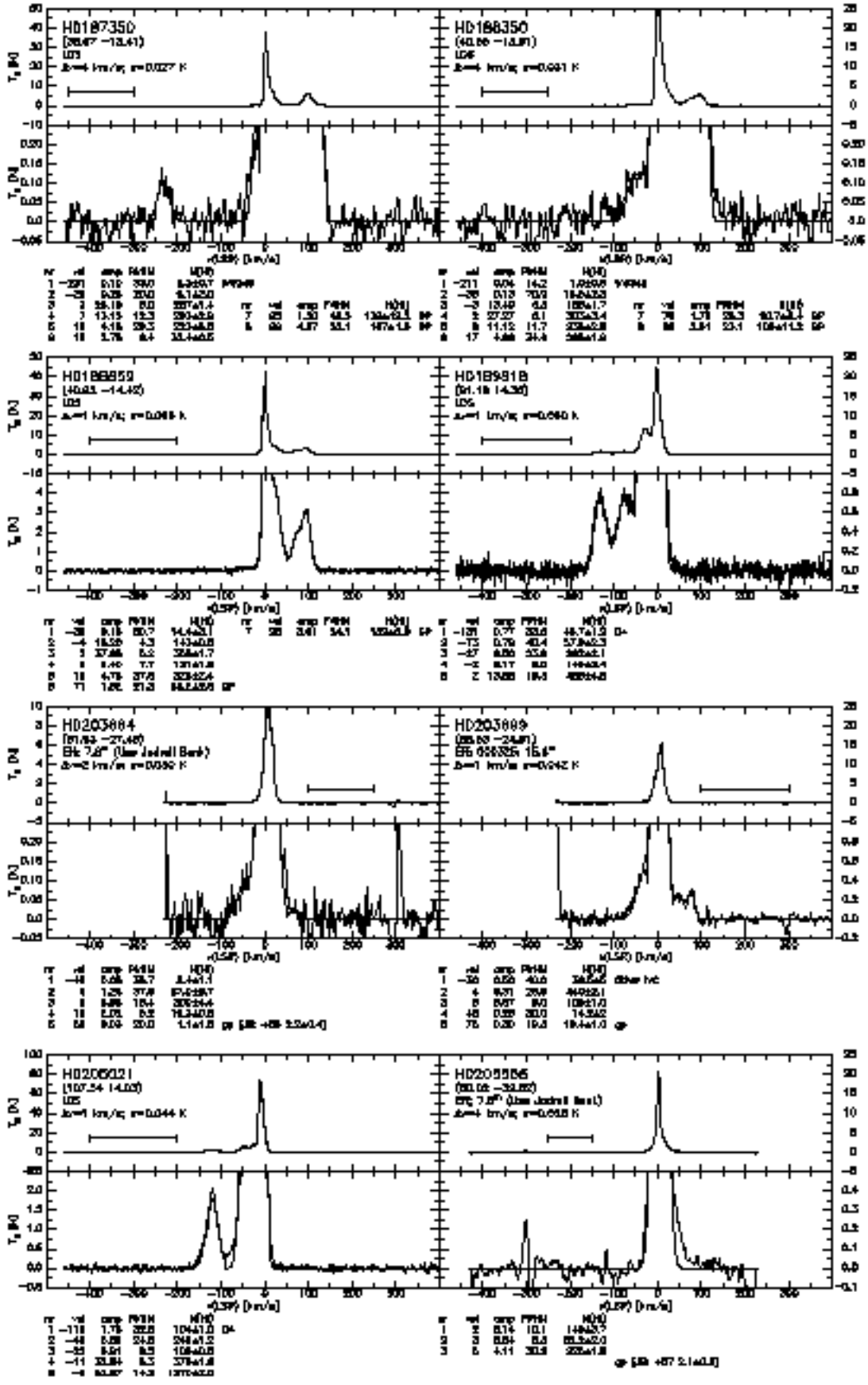
HD187350
HD188350
HD188959
HD189981B
HD203664
HD203699
HD205021
HD205554

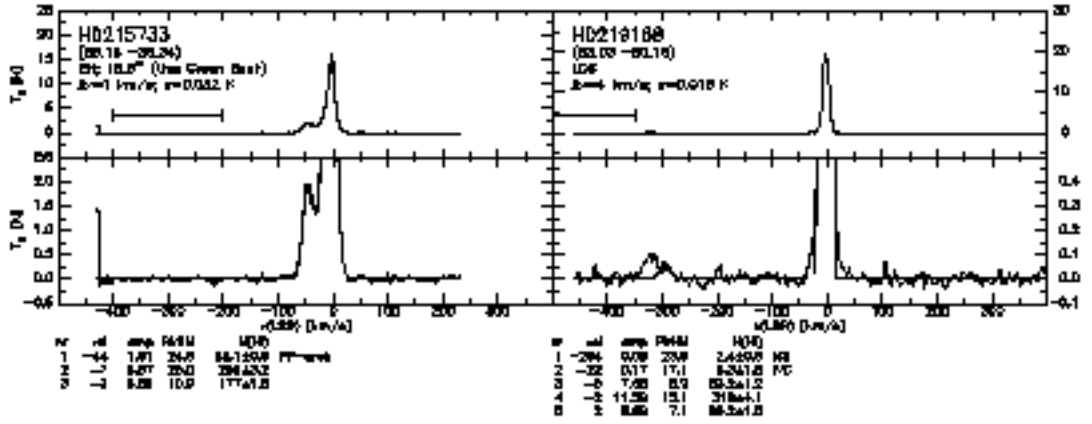
HD215733
HD219188
LDS

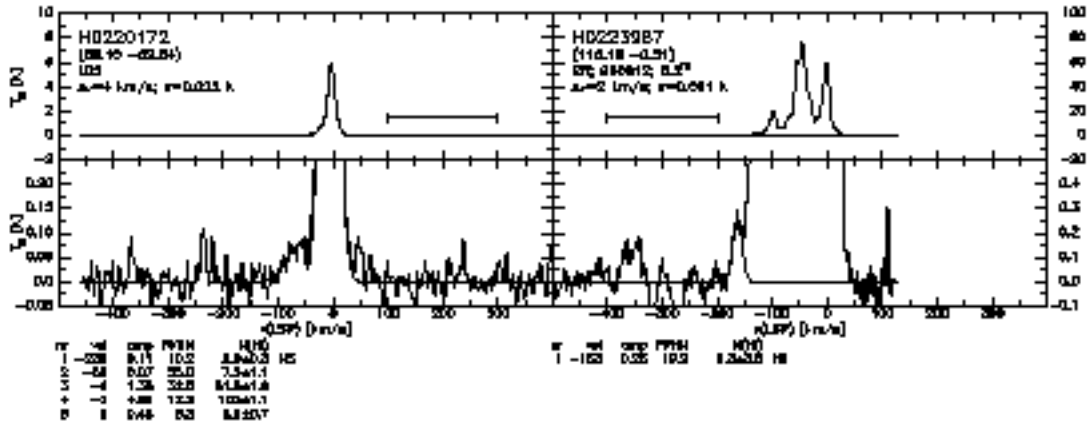
HD220172
HD223385
LDS

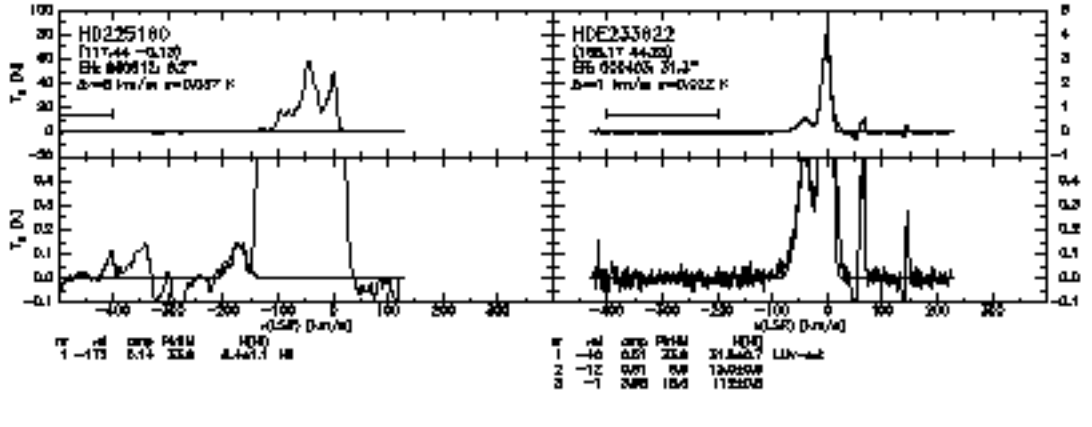
HD225160
HDE233622

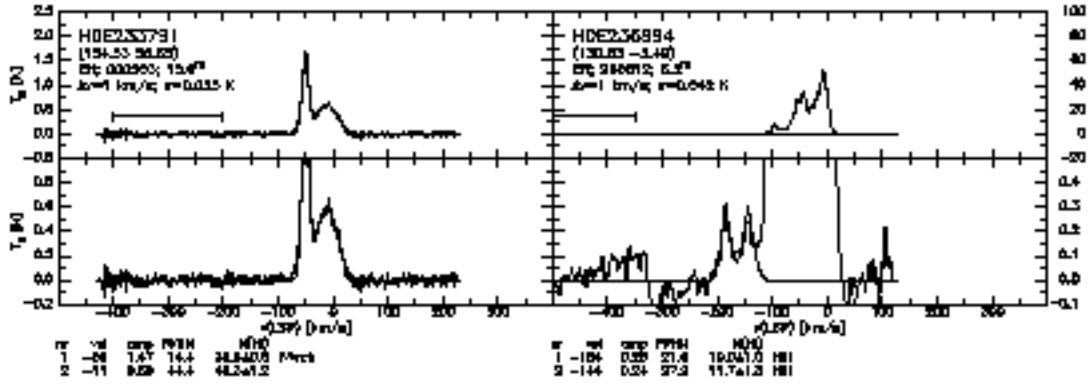
HDE233731
HDE236894

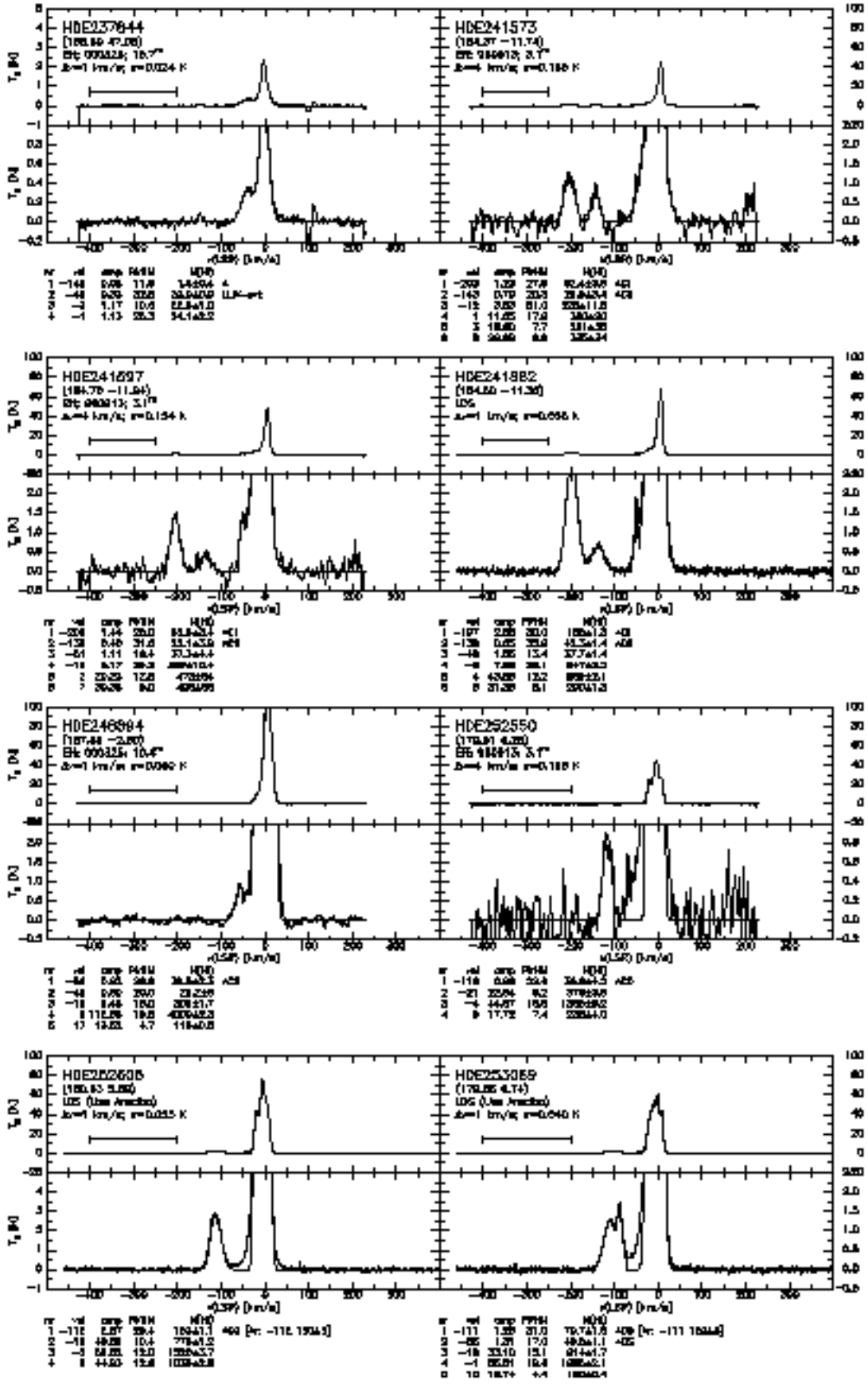
HDE237844
HDE241573
HDE241597
HDE241882
HDE246994
HDE252550
HDE252626
HDE253059

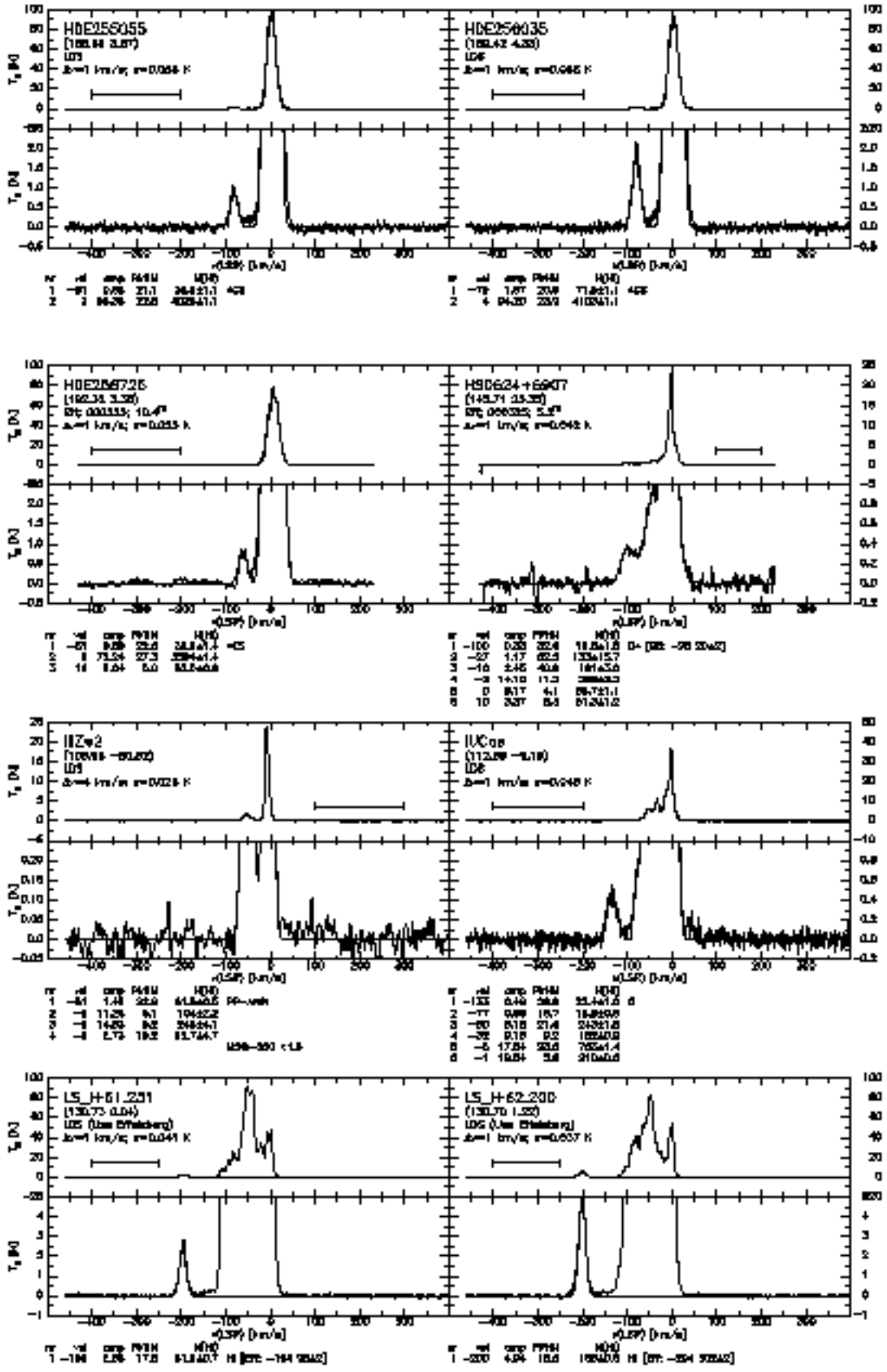
HDE259055
HDE259035
HDE259726
HD5624+69K7
IIZw2
IUCas
LS_H+61_231
LS_H+62_230

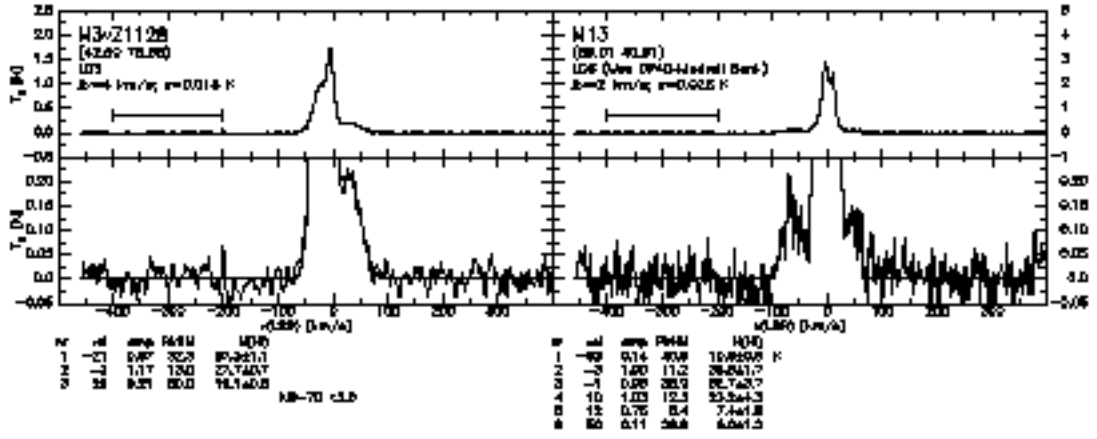
W3+Z1128
W13
v(LSR) [km/s]

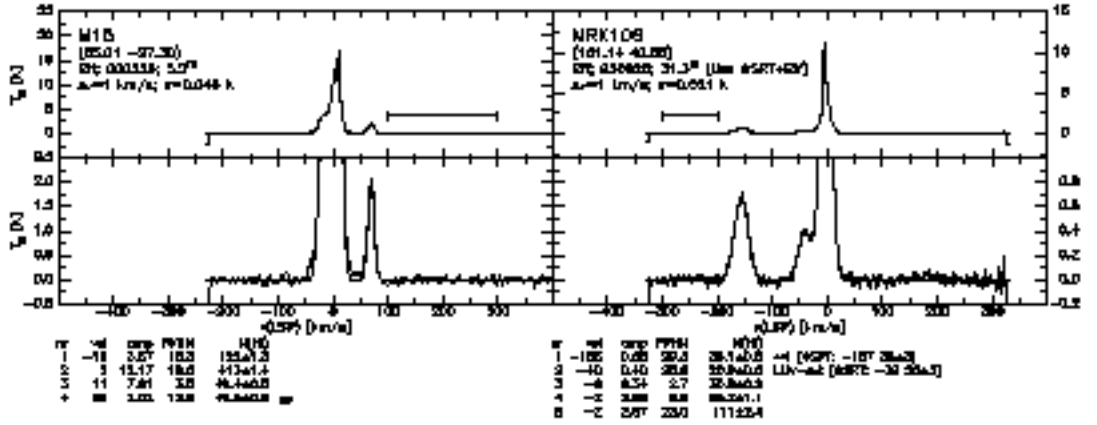
W15
MRK108
v(LSR) [km/s]

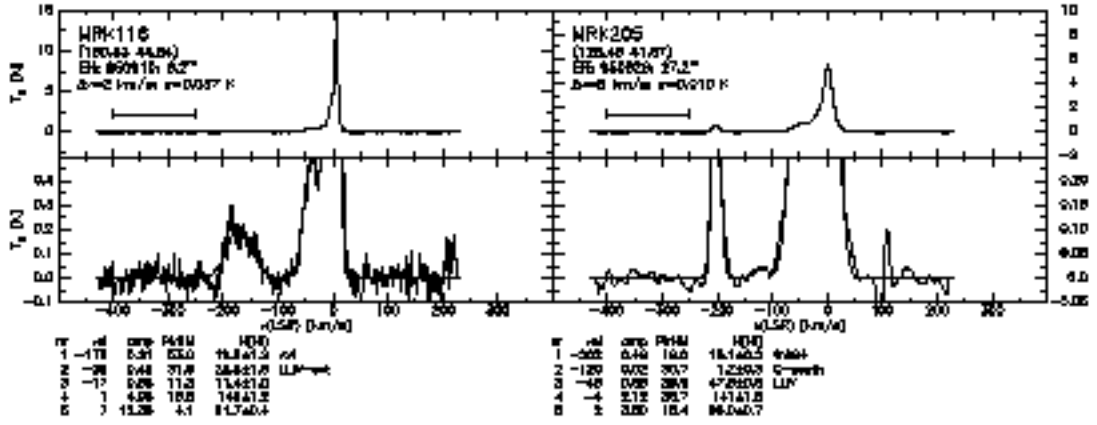
MRK116
MRK205
v(LSR) [km/s]

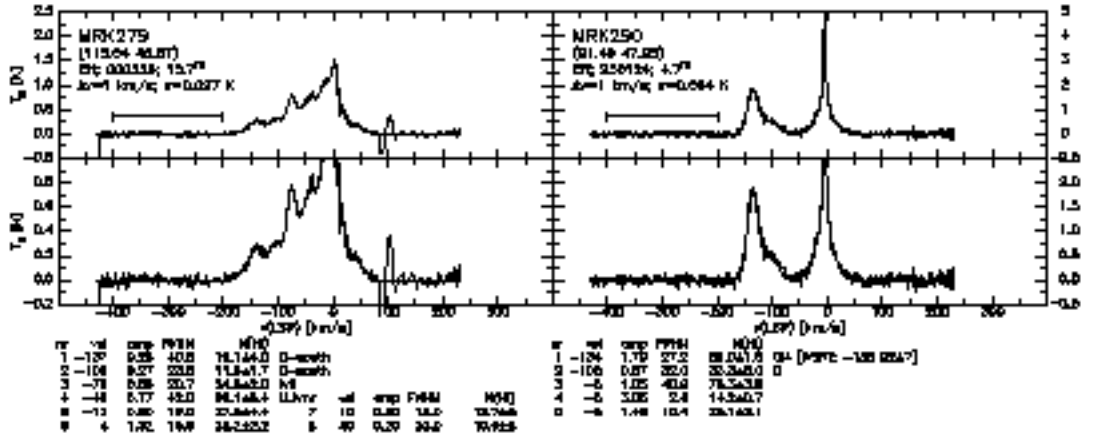
MRK279
MRK290
v(LSR) [km/s]

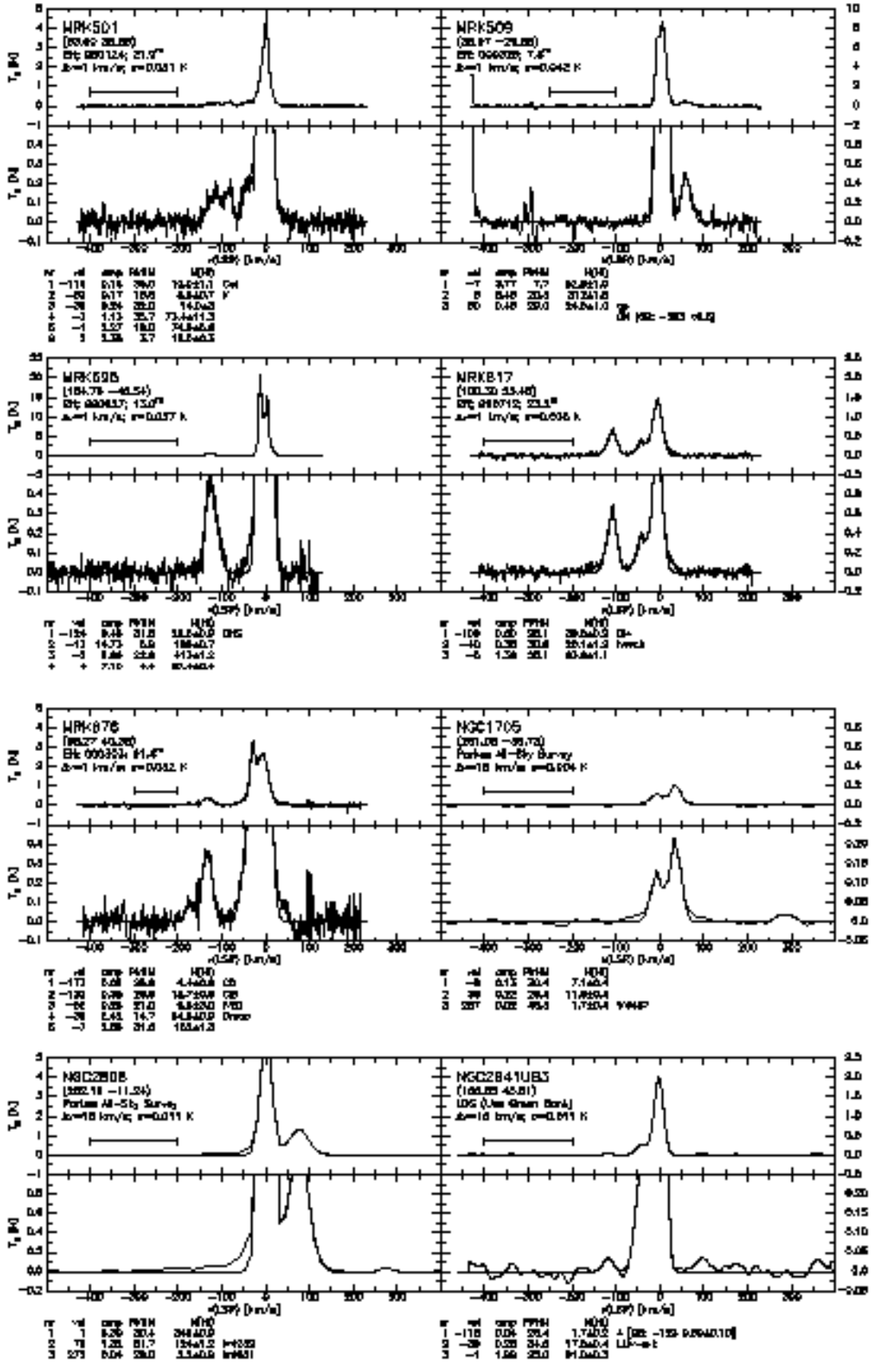
MRK501
MRK509
MRK595
MRK817
MRK876
NGC1705
NGC2808
NGC2841UB3

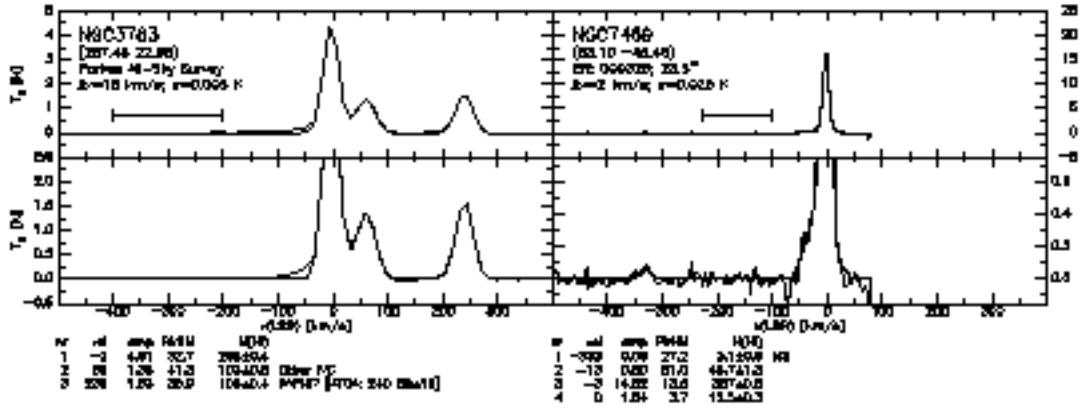
NGC3783
Parkes All-Sky Survey
NGC7469

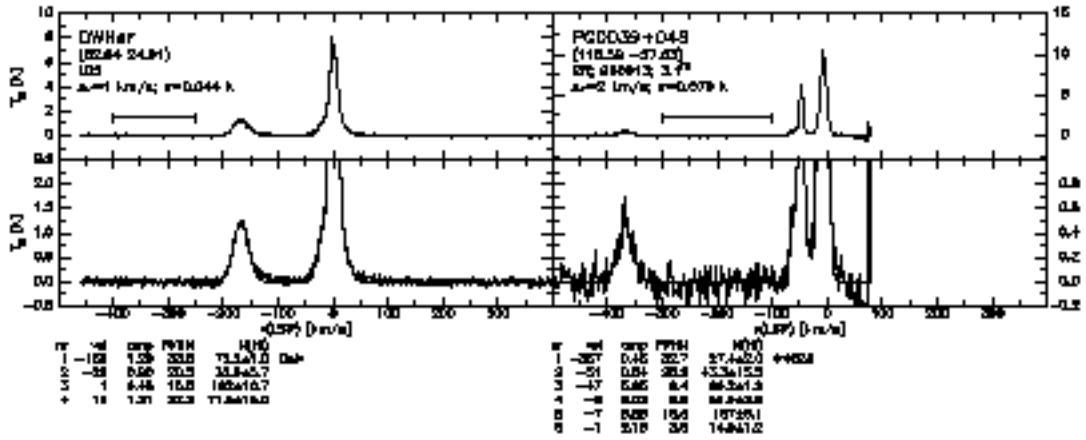
DWHer
LDS
PG0039+049

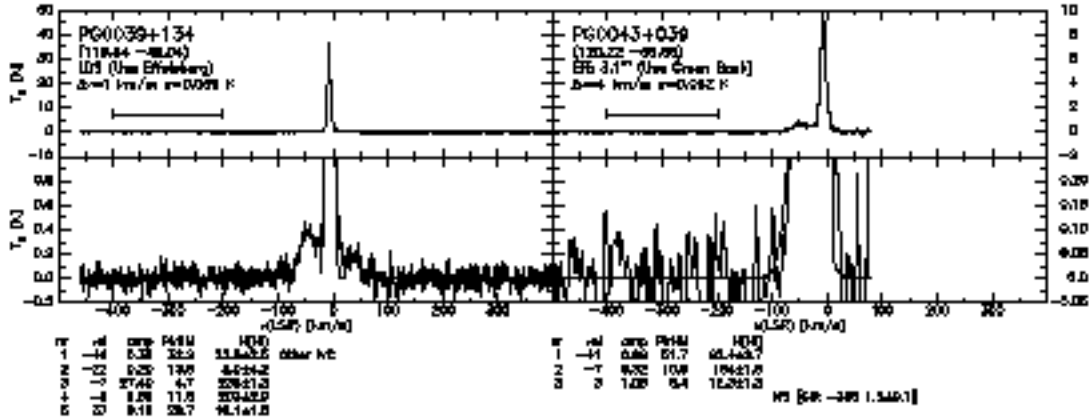
PG0039+134
LDS (Use Effelsberg)
PG0043+039

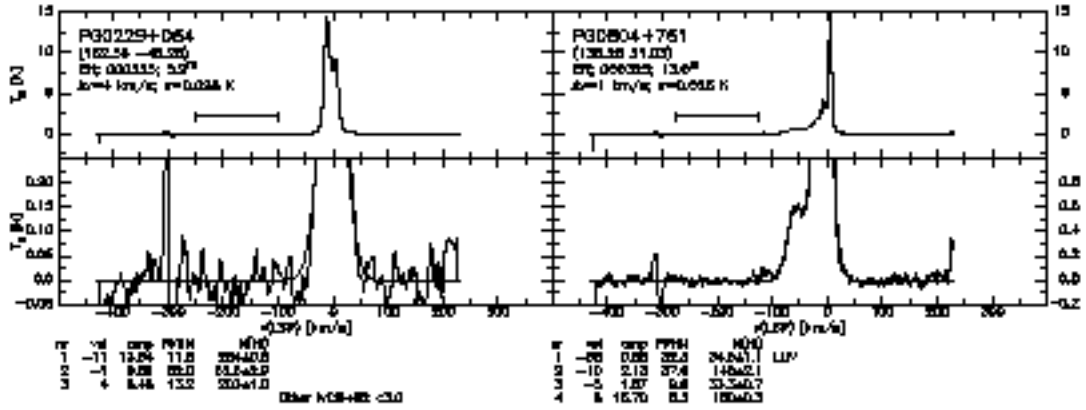
PG0229+064
PG0804+761

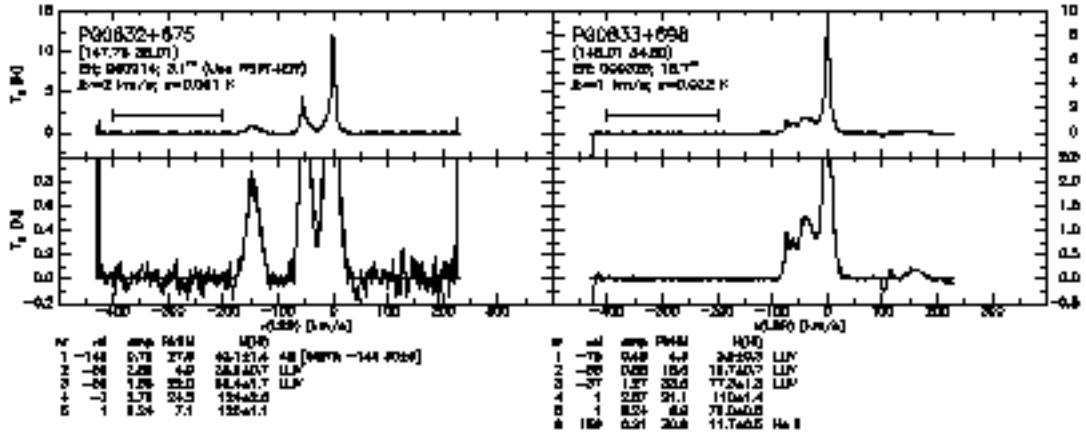
PG0832+675
PG0833+698

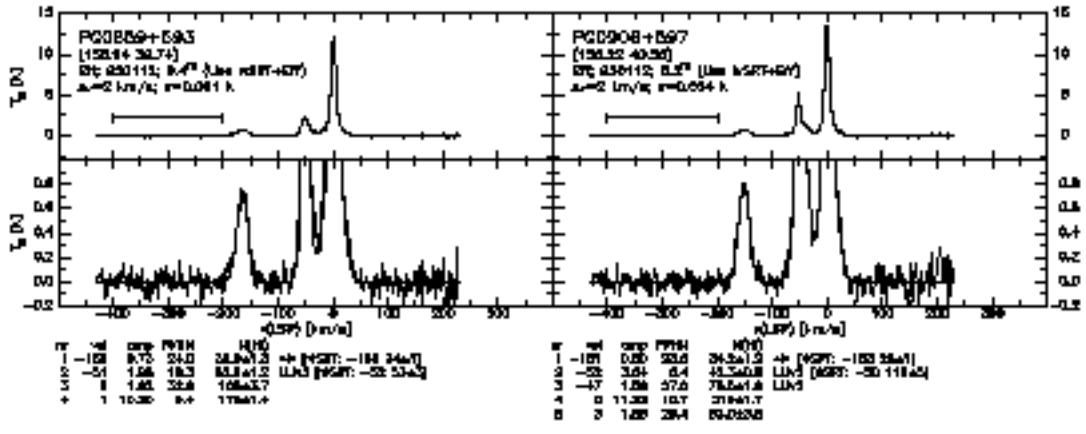
PG0859+593
PG0908+597

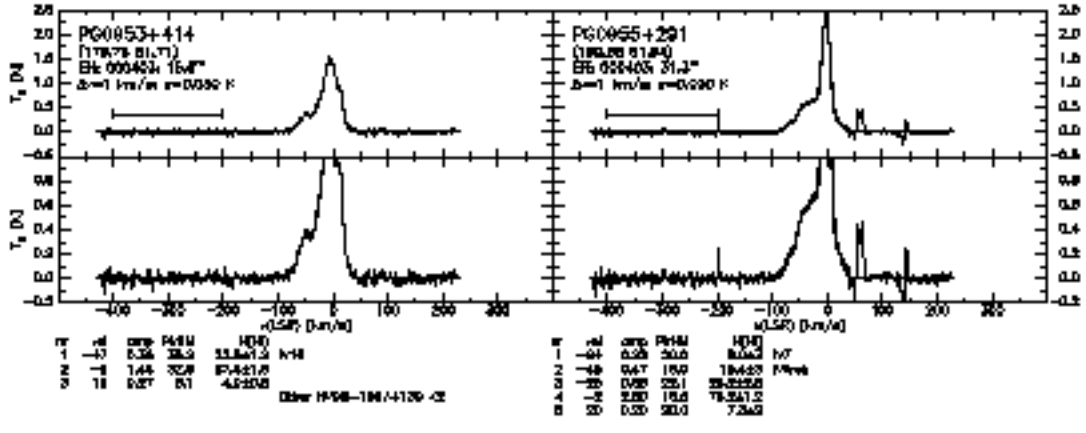
PG0953+414
PG0965+291

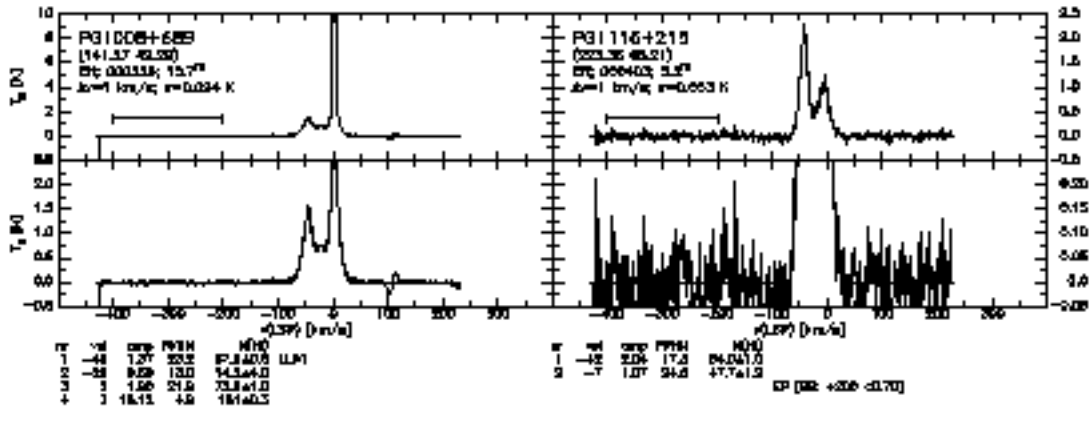
PG1008+689
PG1116+215

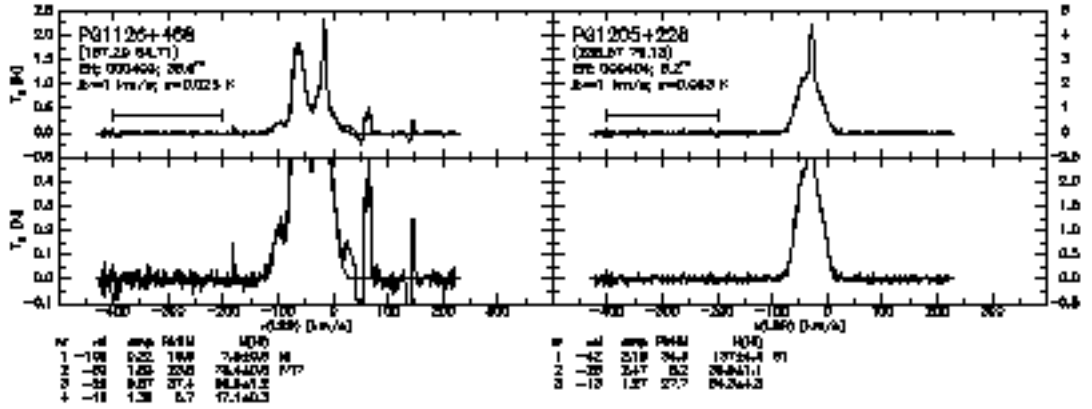
PG1126+468
PG1205+228

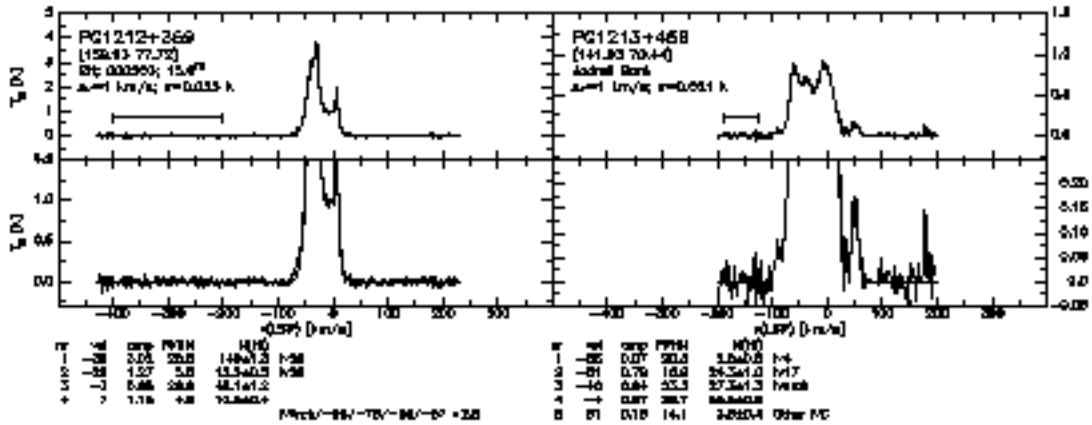
PG1212+269
PG1213+468

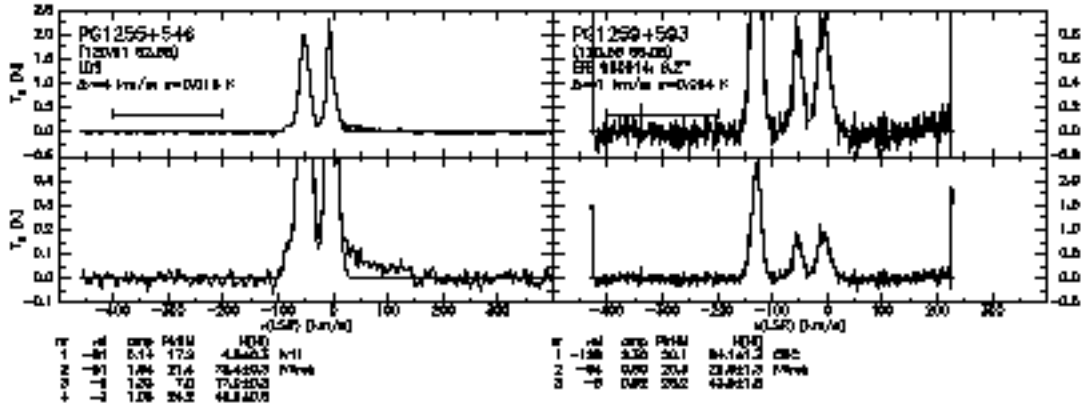
PG1256+546
PG1259+593

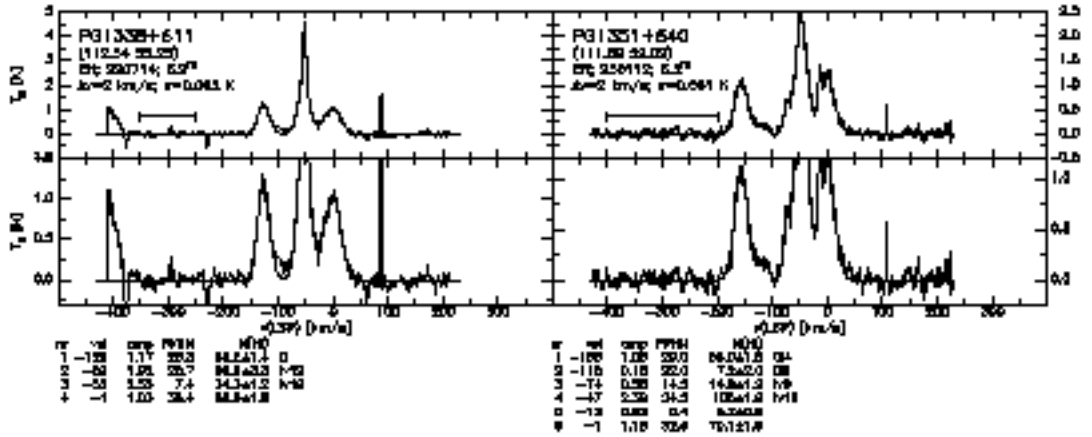
PG1338+611
PG1351+640

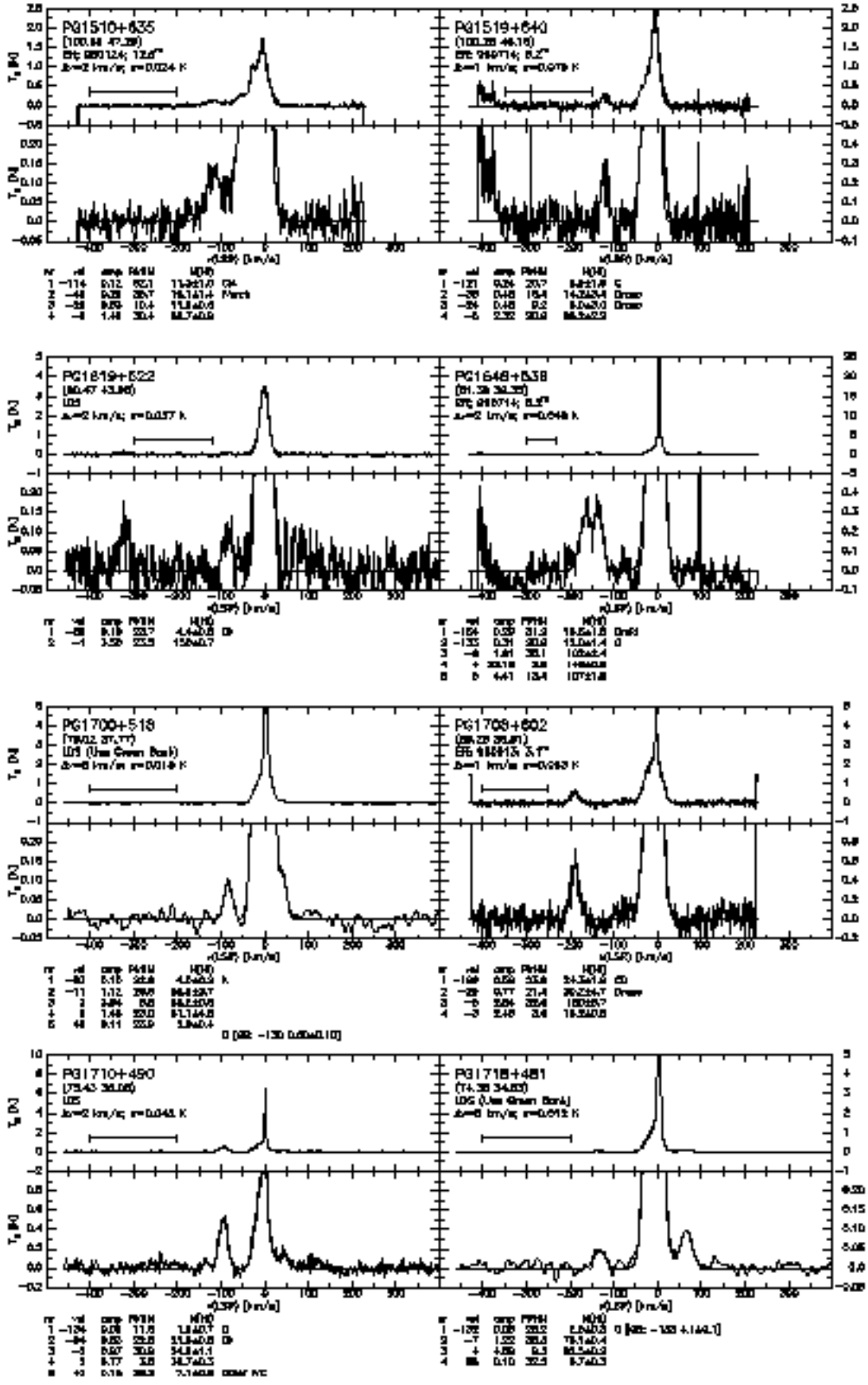
PG1510+635
PG1519+640
PG1619+522
PG1648+536
PG1700+518
PG1709+602
PG1710+490
PG1718+481

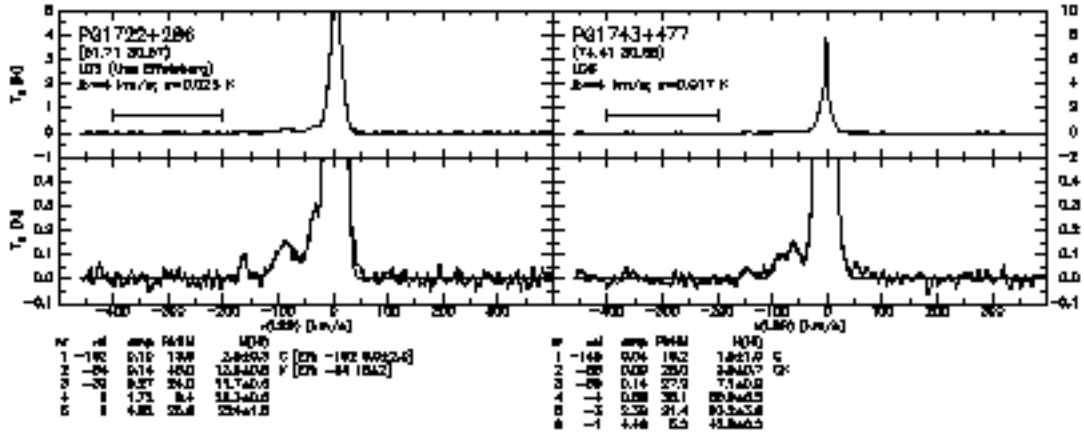
PG1722+286
PG1743+477

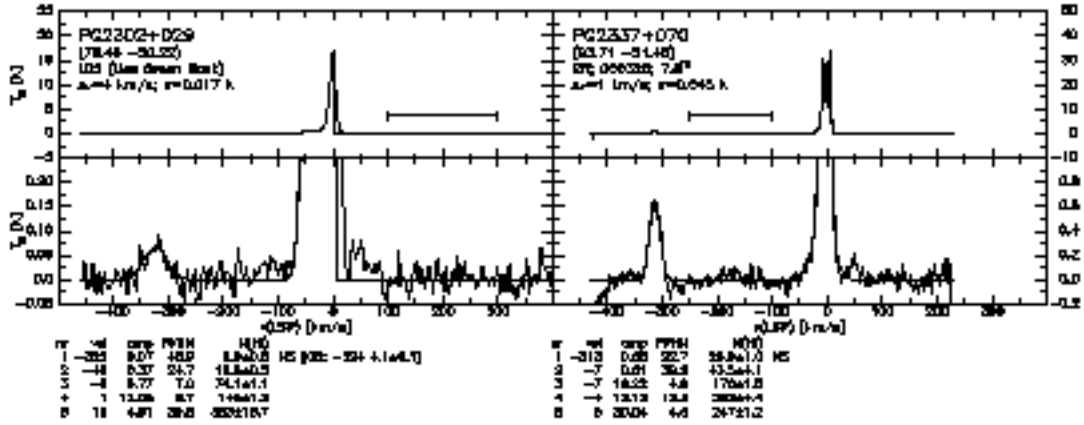
PG2202+029
PG2337+070

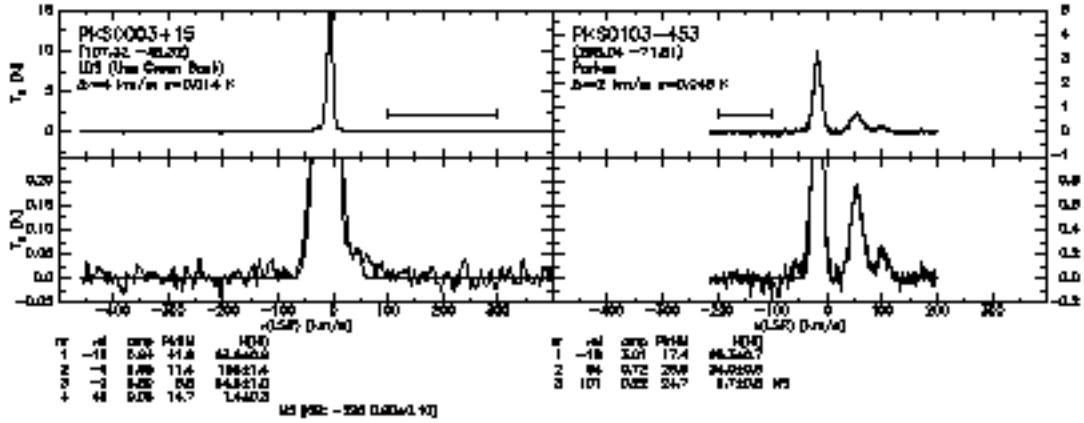
PKS0003+15
PKS0103−453

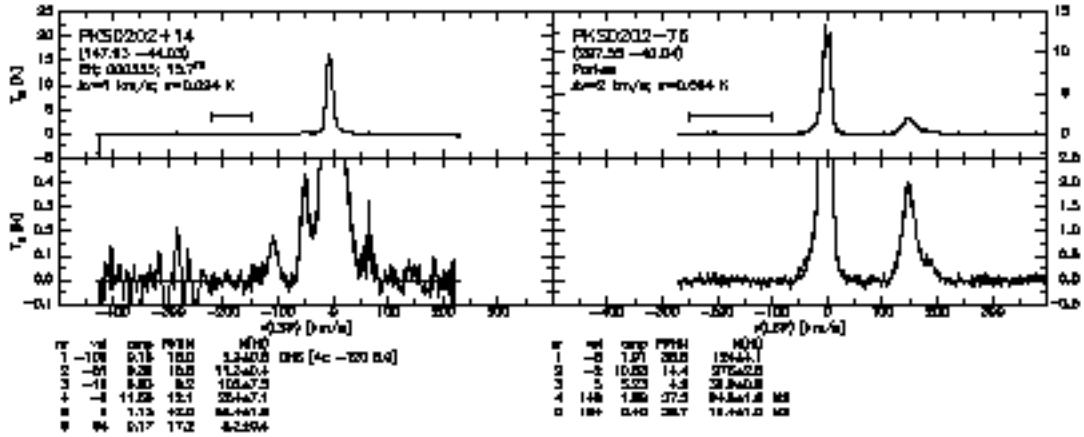
PKS0202+14
PKS0202−76

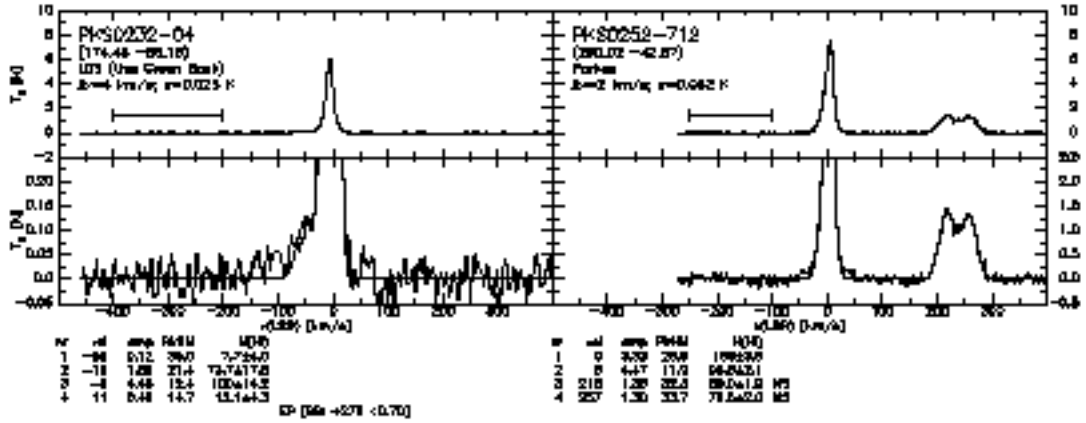
PKS0232−04
PKS0252−712
T_B [K]
T_B [K]
v(LSR) [km/s]
v(LSR) [km/s]

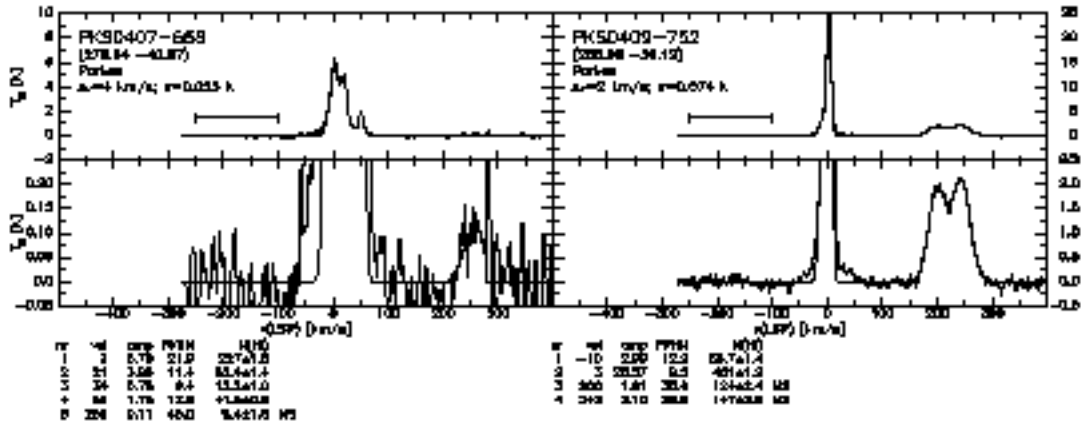
PKS0407−658
PKS0409−752
T_B [K]
T_B [K]
v(LSR) [km/s]
v(LSR) [km/s]

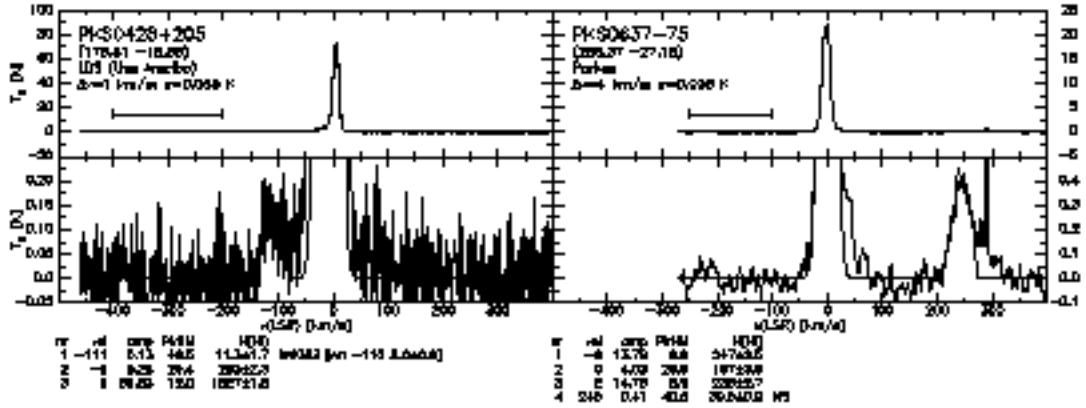
PKS0428+205
PKS0637−75
T_B [K]
T_B [K]
v(LSR) [km/s]
v(LSR) [km/s]

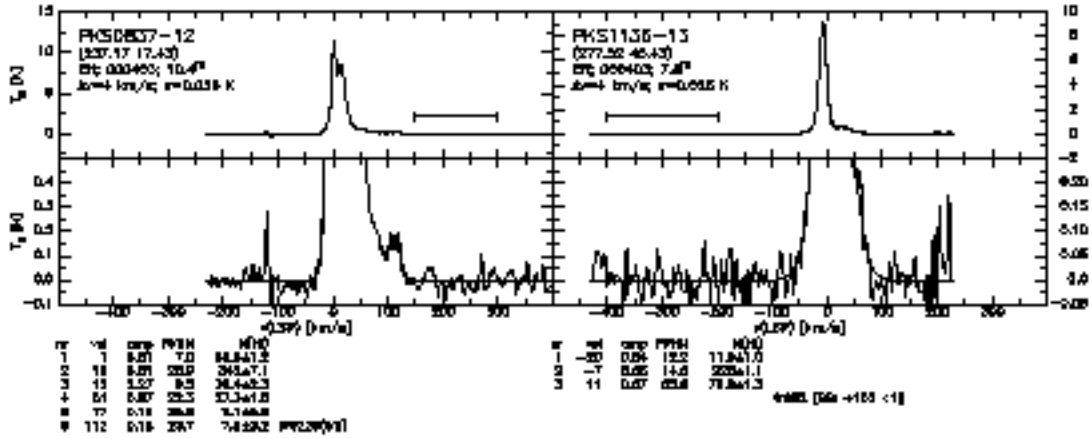
PKS0837−12
PKS1136−13
T_B [K]
T_B [K]
v(LSR) [km/s]
v(LSR) [km/s]

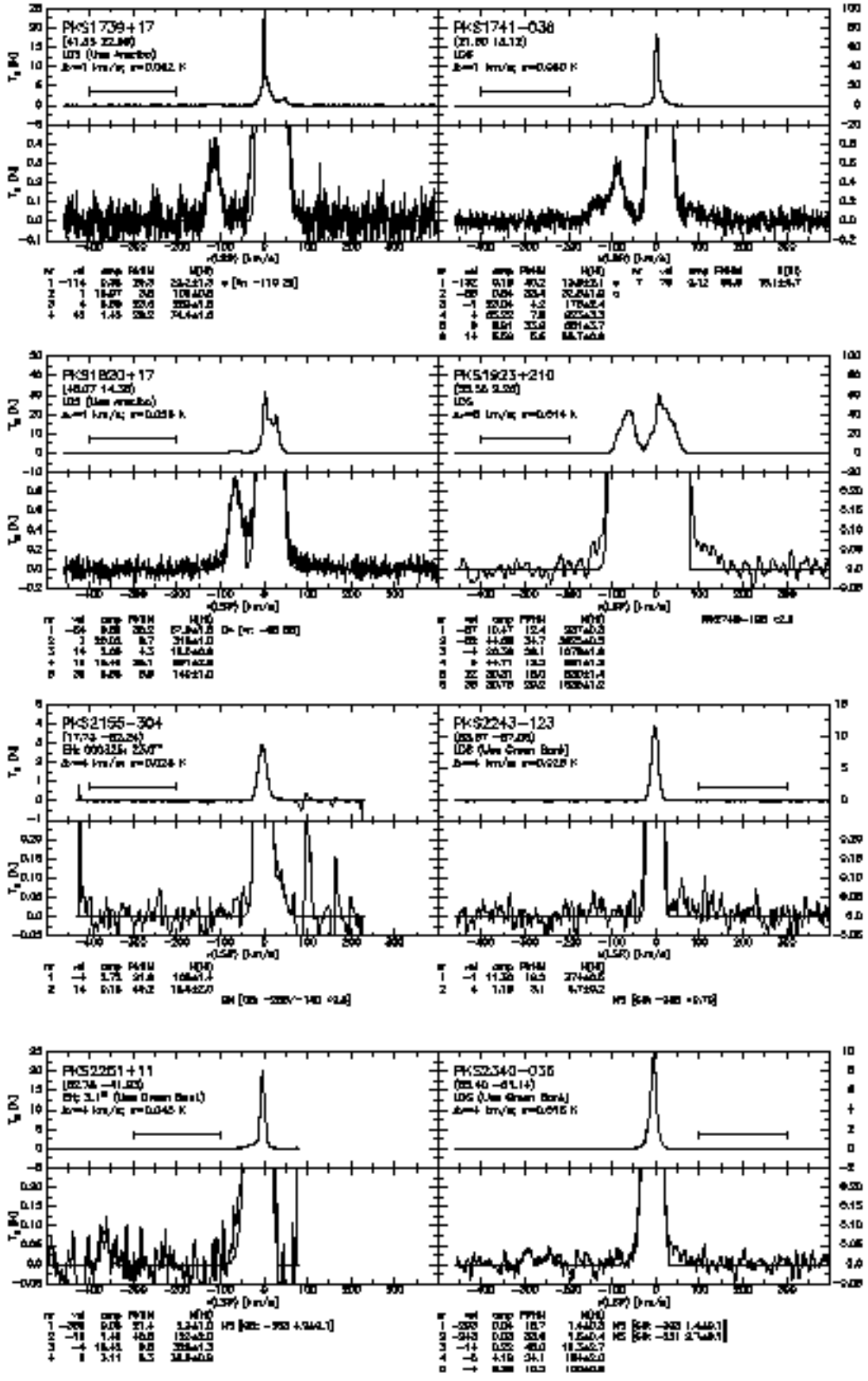
PKS1739+17
PKS1741−038
PKS1820+17
PKS1923+210
PKS2155−304
PKS2243−123
PKS2251+11
PKS2340−036

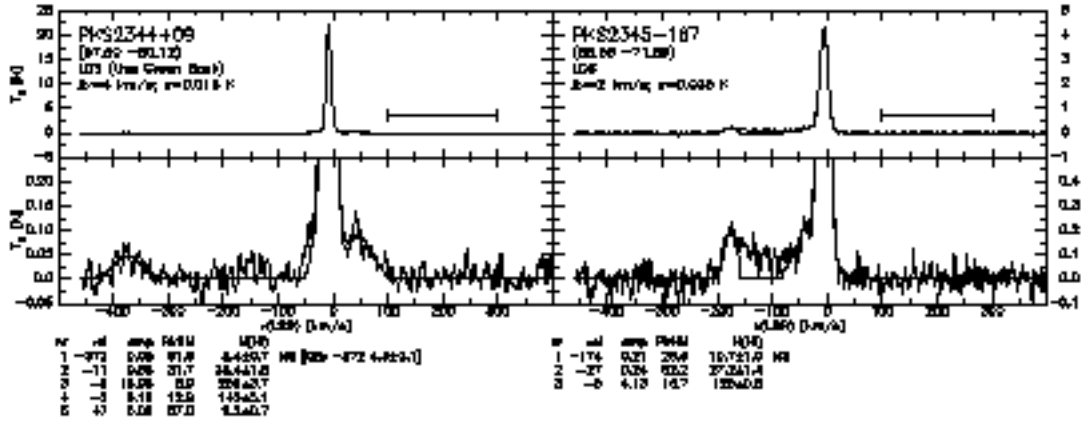
PKS2344+09
PKS2345−167
v(LSR) [km/s]

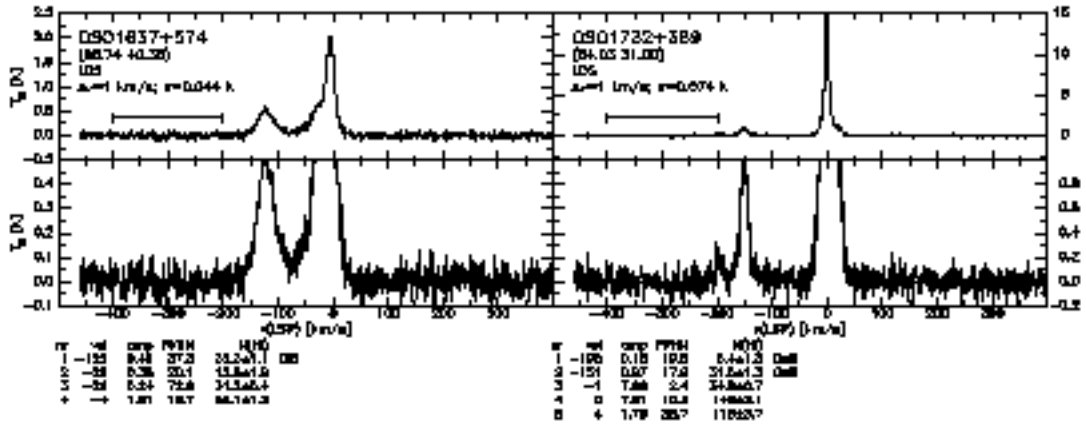
QSO1637+574
QSO1732+389
v(LSR) [km/s]

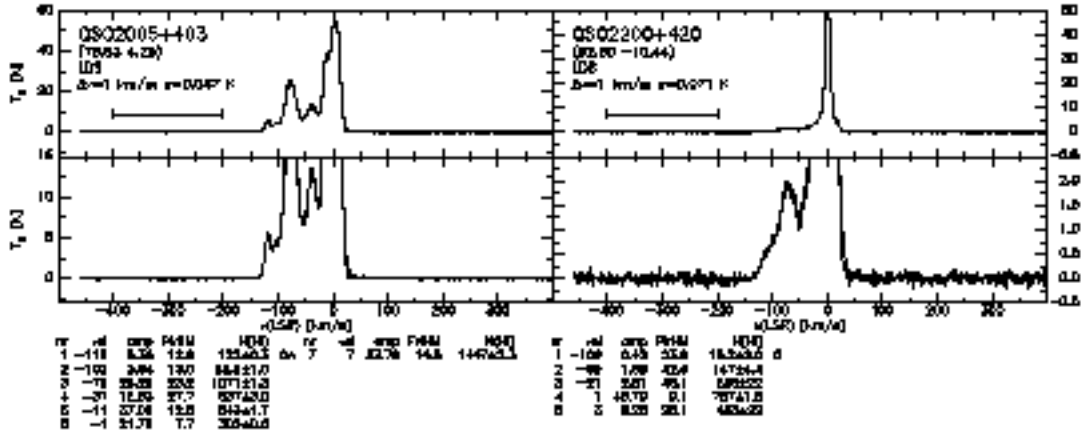
QSO2005+403
QSO2200+420
v(LSR) [km/s]

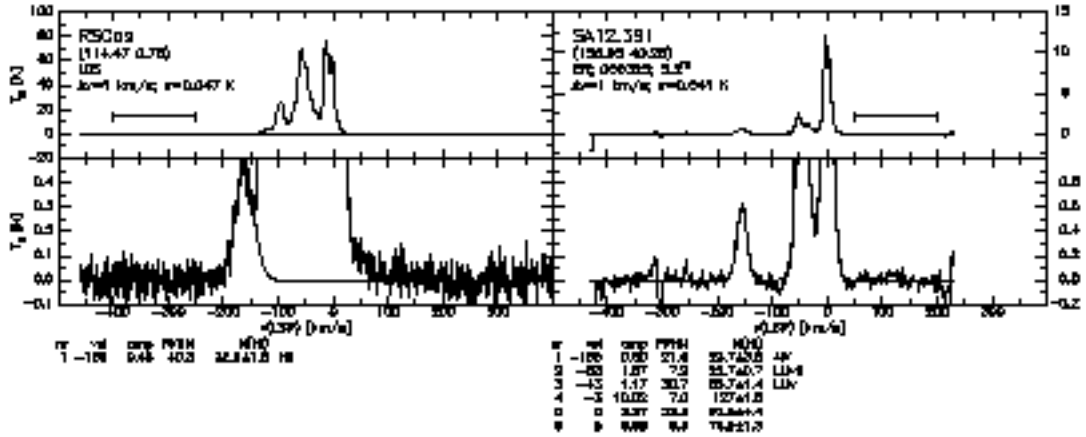
RSCas
SA12.391
v(LSR) [km/s]

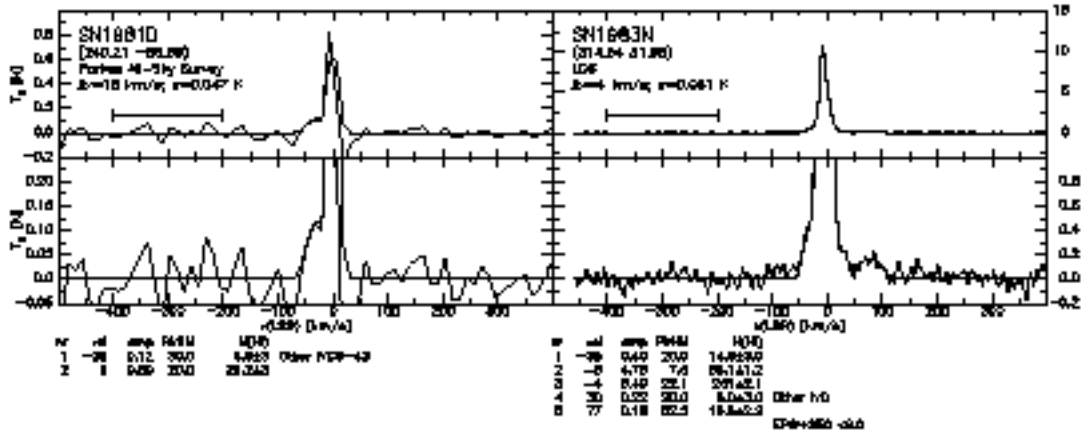
SN1981D
SN1983N
v(LSR) [km/s]

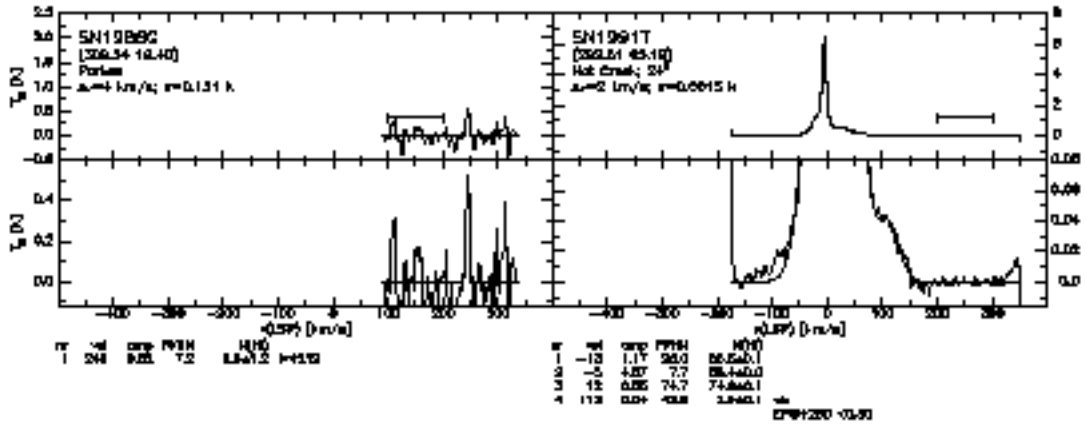
SN1989B
SN1991T
v(LSR) [km/s]

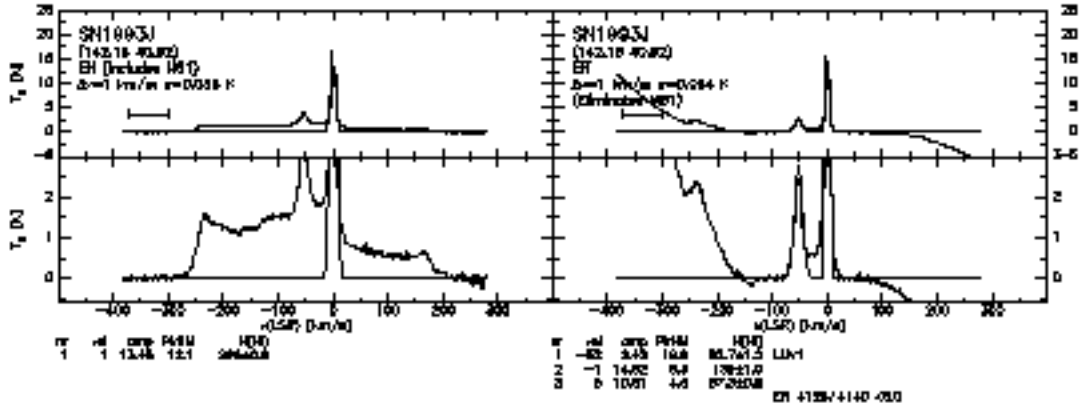
SN1993J
SN1993J
v(LSR) [km/s]

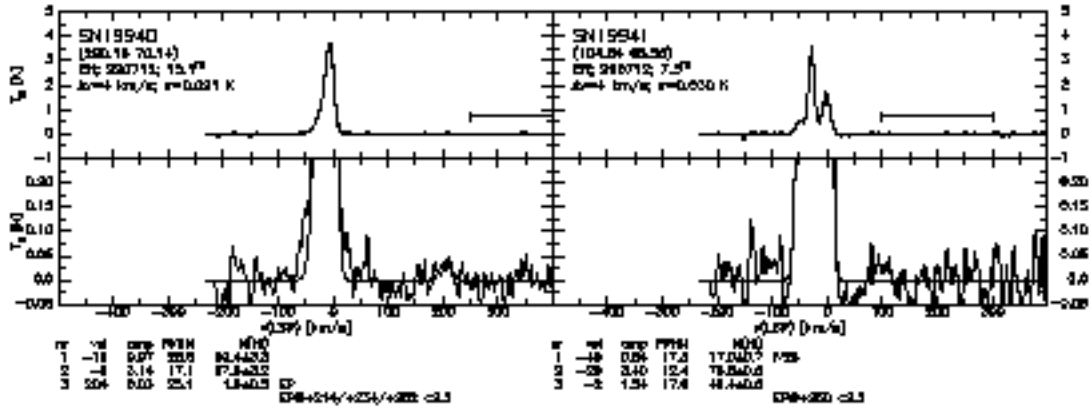
SN1994D
SN1994I
v(LSR) [km/s]

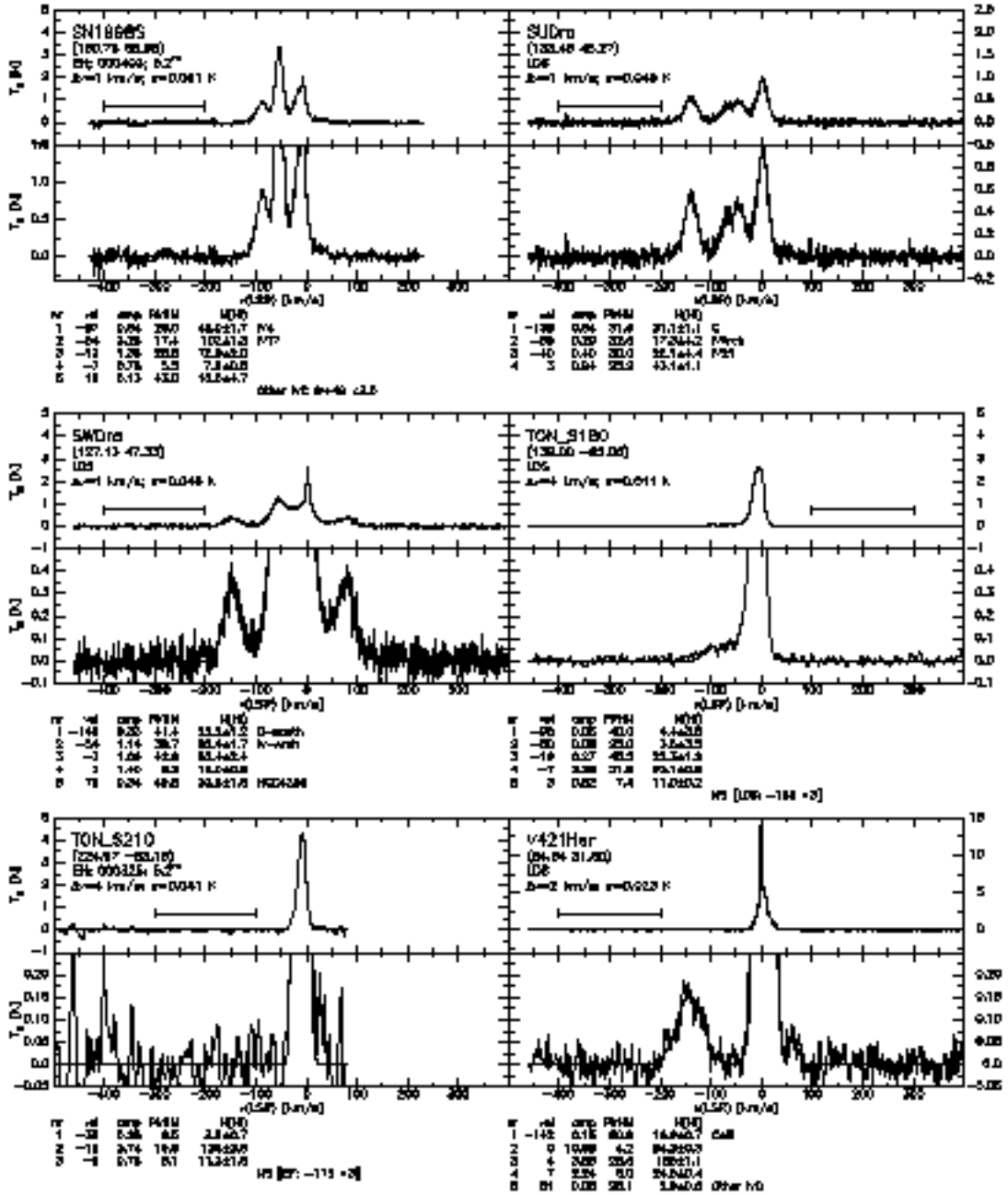
SN1986S
SUDra
SWDra
TON_S180
TON_S210
V421Her

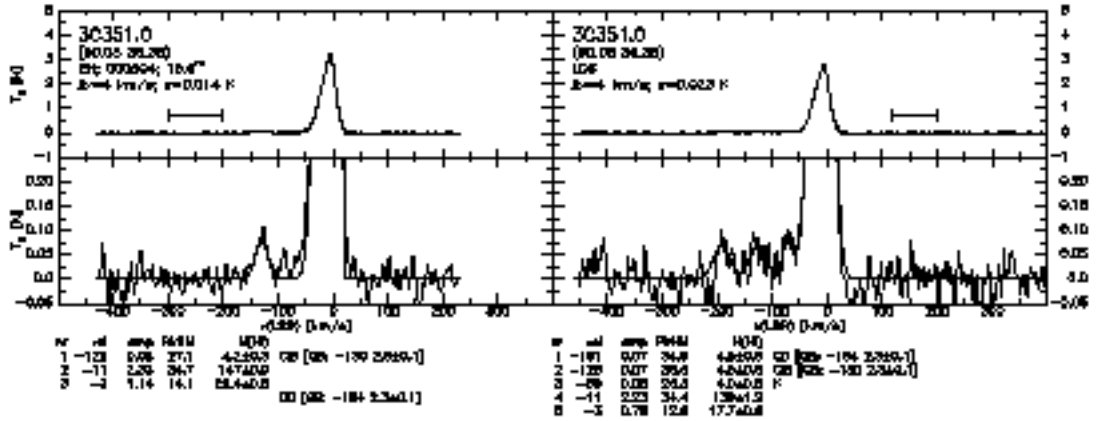
30351.0
30351.0
LDS

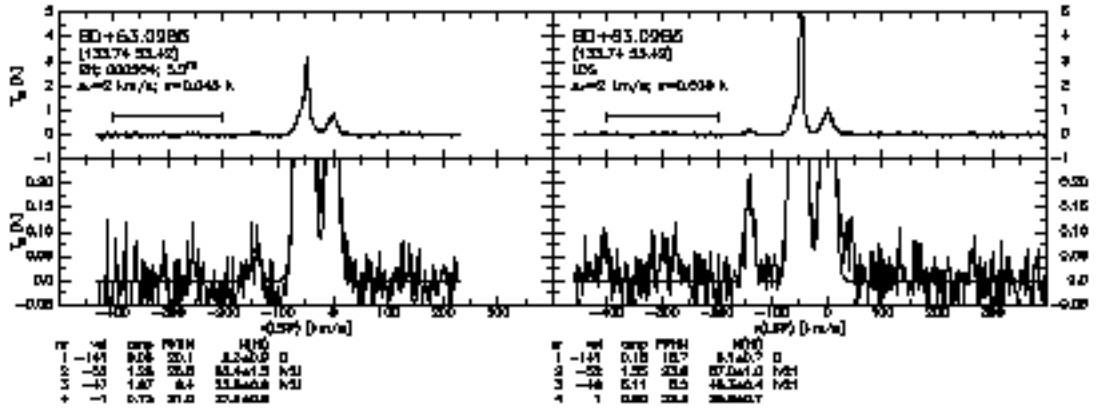
BD+63.0985
BD+63.0985
LDS

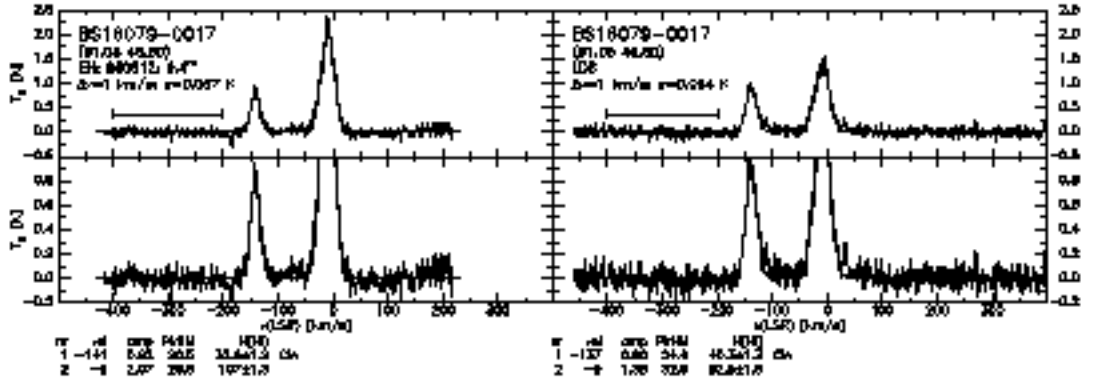
BS18079−0017
BS18079−0017
LDS

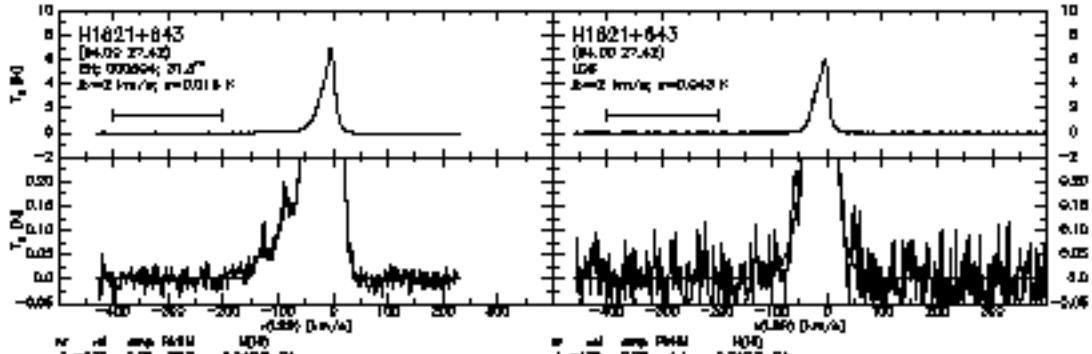
H1821+643
H1821+643
LDS

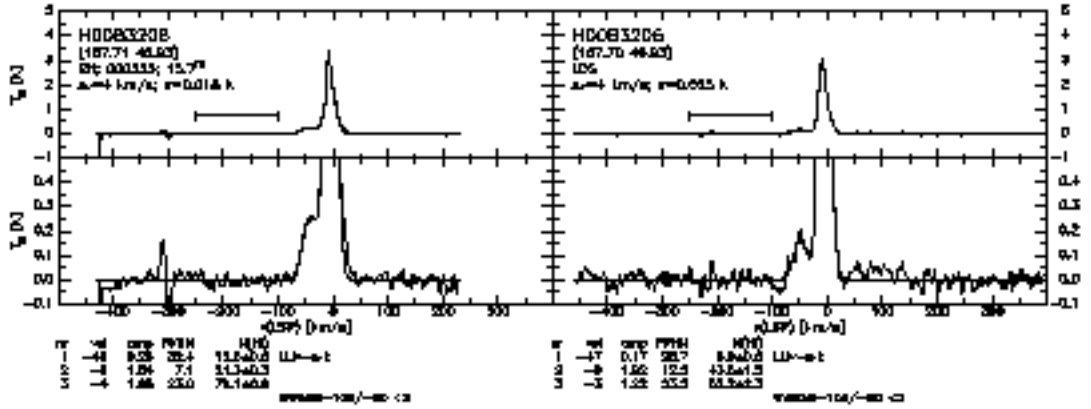
H0083206
H0083206
LDS

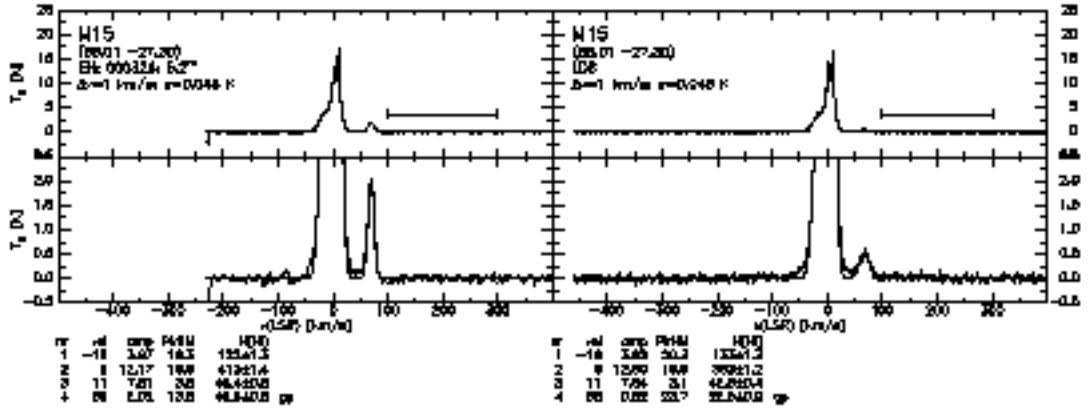
W15
W15
LDS

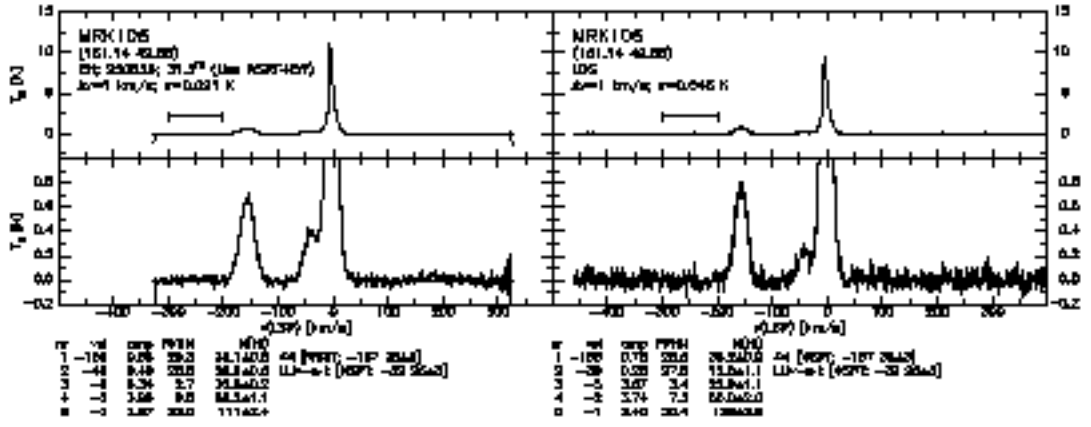
MRK1095
MRK1095
LDS

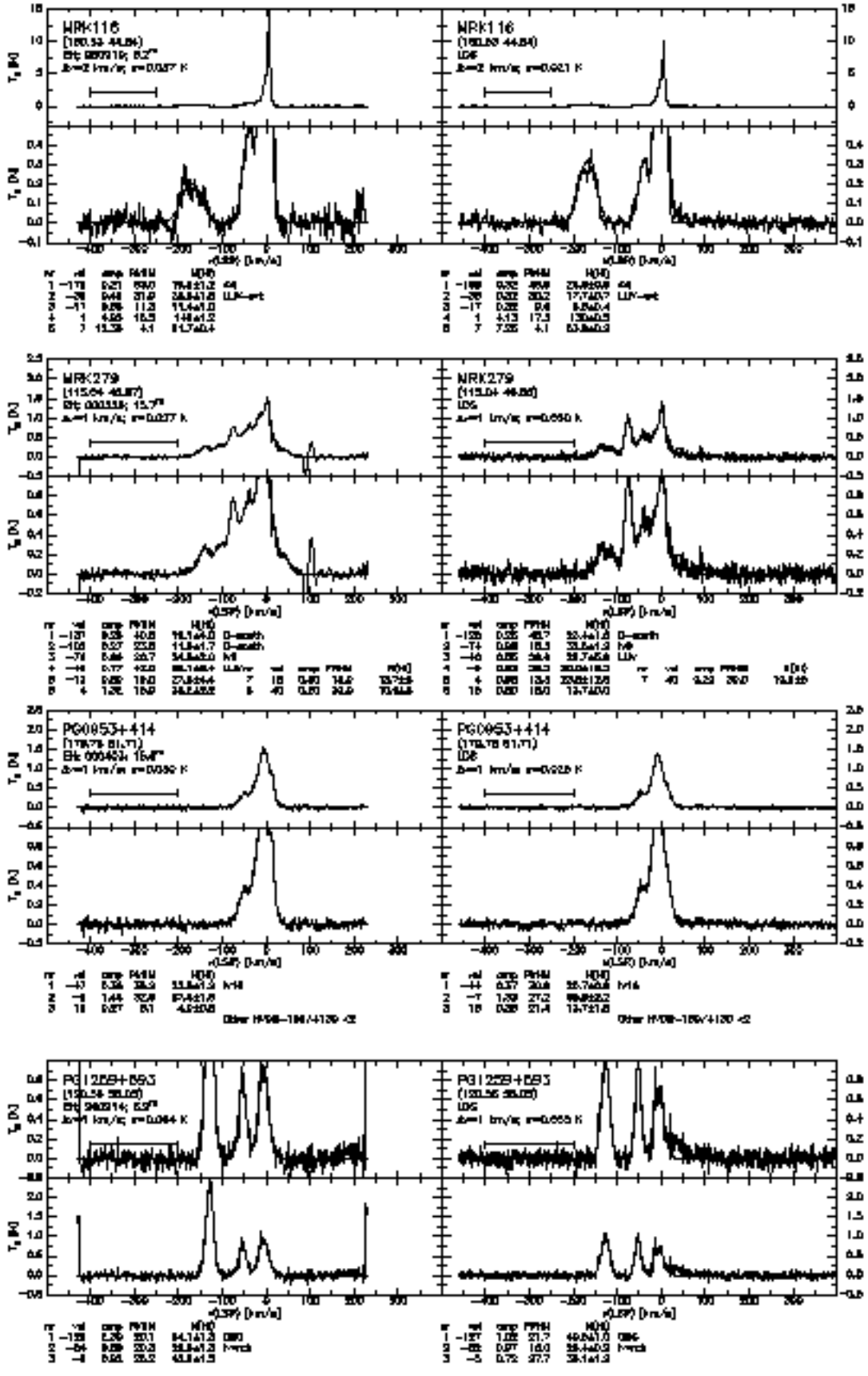
MRK116
MRK116
MRK279
MRK279
PG0953+414
PG0953+414
PG1259+593
PG1259+593

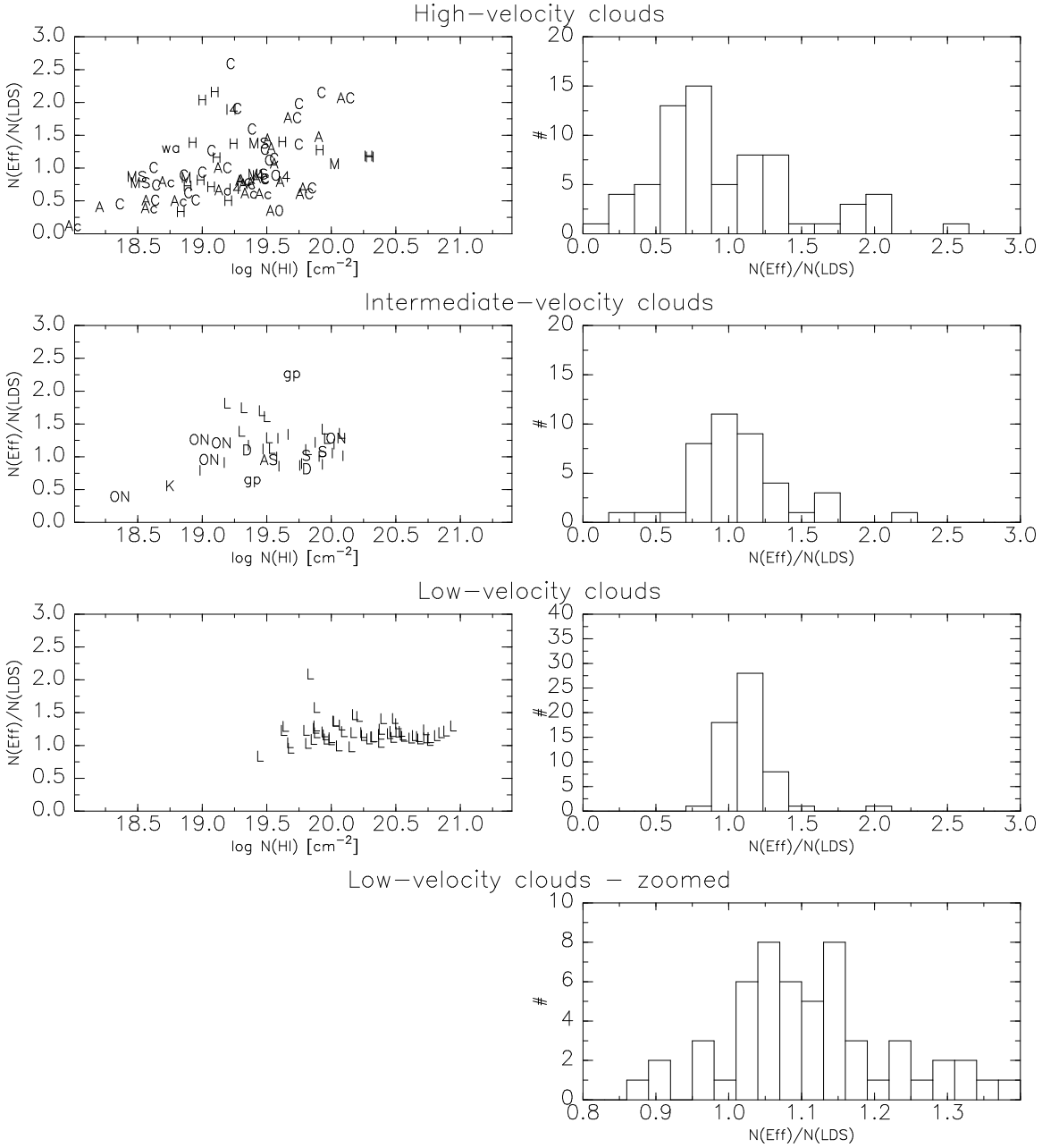

Figure 3. Distribution and histogram of the ratio of column density observed at Effelsberg and in the Leiden-Dwingeloo Survey. Top row: for high-velocity clouds; second row: for intermediate-velocity clouds; third and bottom row: for low-velocity gas. Left column: ratio N(H I-eff)/N(H I-LDS) vs N(H I-eff). Right column: histogram of the ratios. The letters in the plots indicate the HVC/IVC toward which the ratio of column densities was measured.

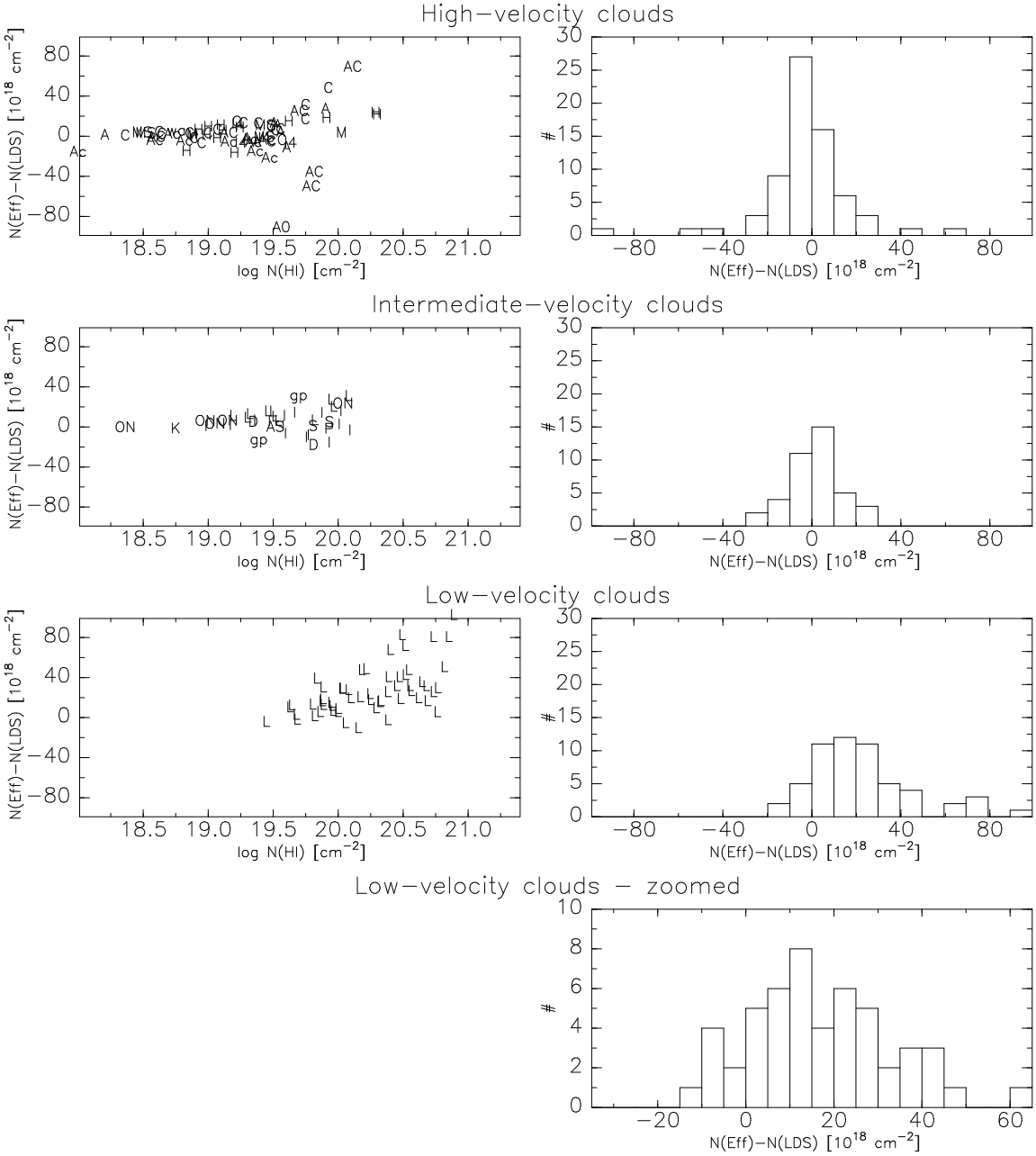

Figure 4. Distribution and histogram of the difference in column density observed at Effelsberg and in the Leiden-Dwingeloo Survey. Top row: for high-velocity clouds; second row: for intermediate-velocity clouds; third and bottom row: for low-velocity gas. Left column: difference N(H I-eff)−N(H I-LDS) vs N(H I-eff). Right column: histogram of the differences. The letters in the plots indicate the HVC/IVC toward which the ratio of column densities was measured.